Endogenous and exogenous hemodynamic signals in primary visual cortex of alert non-human primates

Mariana M. B. Cardoso

Dissertation presented to obtain the
Ph.D degree in Biology | Neuroscience

Instituto de Tecnologia Química e Biológica António Xavier | Universidade Nova de Lisboa

Oeiras,
May, 2016

INSTITUTO
DE TECNOLOGIA
QUÍMICA E BIOLÓGICA
ANTÓNIO XAVIER /UNL

Knowledge Creation

Endogenous and exogenous hemodynamic signals in primary visual cortex of alert non-human primates

Mariana Marcelino Belchior Cardoso

Dissertation presented to obtain the
Ph.D degree in Biology | Neuroscience

Instituto de Tecnologia Química e Biológica António Xavier | Universidade Nova de Lisboa

Research work coordinated by:

COLUMBIA UNIVERSITY
IN THE CITY OF NEW YORK

Champalimaud Foundation

FCT
Fundação para a Ciência e a Tecnologia
MINISTÉRIO DA CIÊNCIA, TECNOLOGIA E ENSINO SUPERIOR

FUNDAÇÃO CALOUSTE GULBENKIAN
Instituto Gulbenkian de Ciência

INSTITUTO
DE TECNOLOGIA
QUÍMICA E BIOLÓGICA
ANTÓNIO XAVIER /UNL
Knowledge Creation

Oeiras, May, 2016

Financial Support

Financial support for this thesis was provided by Fundação para a Ciência e Tecnologia and Fundo Social Europeu through the Quadro Comunitário de Apoio, doctoral fellowship: SFRH/BD/33276/2007.

Acknowledgements

Thank you to the super-nine PGCN/INDP-2007: Íris, Isabel, José, Margarida, Maria, Patrícia, Patrício, Pedro, Rodrigo: colleagues and friends, over the past several years (better not to name how many) were of impressive support in different forms and moments. Thank you in particular to Margarida without whom the “chapter thesis” would have been hard to imagine possible, and cleaning my tears over my poor writing. Thank you to Íris for her unconditional positivism. Thank you, Zé, for letting me learn to appreciate your wonderful imagination.

Thank you to my advisor, Aniruddha Das. Who kept his door open at all times. That hosted me in his laboratory for a very, very long time; and was always patient with my slow progress. Thank you for the opportunity of working in your laboratory and access to such rich setups and data.

Thank you especially to Bruss Lima and Maria (Masha) Bezlepkina. Bruss was the most patient teacher I could have wished for. With you, Bruss, I got to learn about electrophysiology and I wish I could say I had not learnt the sound of dying neurons. Masha kept me sane when that was far from a given, thank you for that and the friendship. Thank you to the other members in the lab, Yevgeniy, I have learned a lot by overlapping with you in the lab. Elena as well as Yana were wonderful ‘mothers’ when I arrived, thank you. Thank you as well to the wonderful veterinary team, in particular thank you to Dr. Girma Asfaw, Dr. Rodolfo Ricart and Dr. Amy Cassano.

In the thesis will not be included early work done with rodents, but there were a few critical inspiring people that should still be acknowledged here: Mark Andermann, Daniel W. Wesson, Tomas Hromadka, Dinu Florin Albeanu, Ashesh K. Dhawale. Also Marc Bucklin from Aniruddha Das’s lab, that was always ready for a challenge.

Thank you to wonderful Dorothée, and the awesome husband Arnaud, whose time and good hearing skills helped me keep focused on what my

priorities might be. Thank you, Angelie, with whom all is possible. Thank you Franco, if I had an old brother, I wish he would have been like you. Thank you to the early friends with whom I learned about the Big city: Gil, Joe, Yan and Renata: the first host. Thank to the friends that keep checking on me from afar, Mafalda, Fátima, Inês, Mónica, Pedro, Joana, Miguel, Lena.

Thank you, Zach, Rui, Marta, for creating this wonderful program and scientific environment and giving me the opportunity to be part of it.

Thank you to my thesis committee, Christian and Michael, who were always supportive, positive and encouraging.

Thank you to the hosting institution, Columbia University, and specifically to a few people that handled my process efficiently and with a smile, Fred Loweff and Alla Kerzhner. Thank you also to the Champalimaud structure and organization: for the great flexibility and ease of working with.

Thank you, Stephan, for support and patience through the least fun times.

Thank you to my family, Adelino, Isabel, Marta and Samuel, for the unconditional support (even financial), help, energy and trust!

Finally, thank you to the animals: not on the class of human primates, and not volunteer on this process, but without whom this project would have not been possible.

Resumo

O uso de técnicas de imagiologia cerebral (neuroimagem) em particular aquelas adequadas ao uso em humanos tem experienciado rápida disseminação. E tem havido grande crescimento nas áreas de investigação que estudam a correlação entre actividade neuronal e processos cognitivos. No entanto os fundamentos neuronais dos sinais resultantes de neuroimagem não estão ainda totalmente caracterizados; esta é ainda uma área de intensa investigação. E no contexto de tarefas comportamentais/cognitivas, a interpretação de neuroimagem é ainda mais complexa.

Em sistemas sensoriais primários, há a perspectiva de que as respostas de neuroimagem reflectem sobretudo informação sobre estímulos sensoriais externos. Há vasta investigação que se foca no mapeamento de estímulos e classes de estímulos no córtex. No entanto, mesmo sistemas sensoriais primários podem conter informação sobre comportamento, como por exemplo estádios de comportamento. Por exemplo, embora o córtex visual primário responda principalmente a estímulos visuais, também é modulado por respostas como atenção. A forma como estas respostas estão codificadas é fundamental para a interpretação de neuroimagem. Igualmente, compreender como diferentes aspectos das respostas de neuroimagem estão relacionados com a actividade neuronal subjacente é crucial para a interpretação de neuroimagem.

No laboratório tinha sido identificada uma resposta hemodinâmica relacionada com execução de tarefas (*task-related*), no córtex visual primário de primatas executando uma tarefa de fixação visual periódica. Este sinal foi observado na ausência de estimulação visual directa (não havendo portanto estímulo visual ou resposta visual a estímulos). Não se observaram alterações na quantidade de potenciais de acção dos neurónios na região de onde se reportou a actividade hemodinâmica. No entanto, nestas tarefas a resposta hemodinâmica relacionada com a tarefa é robusta e esta

resposta ajusta-se à duração da tarefa. Esta resposta confirma a presença de uma resposta endógena numa área sensorial primária. A ausência de correlação com a activitade neuronal (medida como alterações na frequência de potenciais de acção) reinforça a importância de compreender os mecanismos que estão na base da resposta hemodinâmica.

O trabalho apresentado nesta tese tem como objectivo auxiliar a interpretação de neuroimagem, em particular tenta distinguir contribuições endógenas e exógenas. Seguimos dois caminhos experimentais: um que tenta caracterizar as respostas hemodinâmicas relacionas com a apresentação de estímulos, e outra cujo objectivo é de compreender contribuições endógenas para o sinal. Em ambas as circunstâncias, para além de neuroimagem, foi medida actividade neuronal (na forma de potenciais de acção locais, *LFP*, ou frequência de potenciais de acção neuronais locais).

Gravámos simultaneamente actividade de neuroimagem bem como de eletrofisiologia em primatas a executar tarefas periódicas. A técnica de neuroimagem utilizada, imagiologia óptica de sinais intrínsecos, baseia-se na absorção preferencial de luz visível pela hemoglobina presente em tecidos; trata-se portanto uma medida indirecta de metabolismo. Recolhemos dados no córtex visual primário, uma região cortical bem conhecida, com respostas neuronais a estímulos bem caracterizada e que anatomicamente se localiza na superfície do cérebro, portanto ajustada ao uso de imagem óptica intrínseca.

Dada a montagem experimental disponível no laboratório, há a possibilidade de comparar dados de neuroimagem e electrofisiologia adquiridos simultaneamante (não típico aquando o uso de outras técnicas de neuroimagem) o que nos coloca numa posição priveligiada para avaliar a relação entre neuroimagem e actividade neuronal. Utilizámos uma tarefa periódica com a apresentação de estímulos visuais com uma relação bem estabelecida entre propriedades do estímulo e actividade neuronal: usámos contraste do estímulo para testar uma gama de intensidades de actividade neuronal. Contraste e actividade electrofisiológica têm uma relação monotó-

nica: aumentos no contraste estão associados a aumentos na frequência de potenciais de acção (obedecendo uma função hiperbólica). Ao utilizármos contraste para induzir alterações previsíveis em actividade neuronal, observámos que numa tarefa periódica a resposta de neuroimagem reflecte a soma linear de uma componente exógena (relacionada com o estímulo) e outra endógena (relacionada com a tarefa). A componente relacionada com o estímulo tem uma relação linear com a actividade neuronal local (medida como alterações na frequência de potenciais de acção).

Finalmente, queriamos também avaliar potenciais contribuições para a factores da resposta endógena (independente do estímulo) que possam contribuir para o sinal de neuroimagem. Usámos a mesma tarefa já antes utilizada do laboratório: fixação na ausência de estimulação visual (para além do ponto de fixação), observámos períodos em que o animal não estava envolvido na tarefa estavam associados com alterações *lentas* na resposta hemodinâmica. Para além da já mencionada resposta hemodinâmica relacionada com execução de tarefas (*task-related*), propomos que o envolvimento (*engagement*) numa tarefa tem uma contribuição significativa para alterações lentas no nosso sinal de neuroimagem. Observámos aumentos na resposta hemodinâmica acompanhados de diminuição do batimento cardíaco e ligeira diminuição na frequência dos potenciais de acção, no córtex visual primário. As alterações na resposta hemodinâmica são significativas em magnitude. O trabalho apresentado nesta tese avança assim a nossa compreensão da natureza da neuroimagem.

Abstract

The advent of neuroimaging techniques in particular the ones suitable for studies in alert humans has disseminated fast. Research in fields involving neuro-correlates of cognitive processes has flourished. Still the neural underpinnings of the neuroimaging signals remain to be fully characterized; this field is an active topic of research. In the context of behavior/cognition, the interpretation of neuroimaging signals is even more intricate.

In early sensory systems, neuroimaging signals are thought to primarily carry information about sensory inputs; there is significant research focused on mapping evermore specific stimuli and stimulus classes to cortical regions. Nevertheless even early sensory systems can relay information on behavior, like brain states. For example, it is known that visual cortex even though primarily responding to visual stimuli, is also sensitive to such signals as attention. The way these signals are differentially encoded is critical in trying to interpret neuroimaging signals. Also how the different aspects of neuroimaging signals related to underlying neuronal activity is critical for neuroimaging interpretation.

Earlier the lab showed the existence of a hemodynamic task-related signal, in primary visual cortex of alert non-human primates performing a periodic fixation task. This signal was observed in the absence of direct visual stimulation (there was no stimulus present or a stimulus response). In the vicinity of the recorded hemodynamic response, there were no changes in the spiking rates of neurons, which could predict the homodynamic task-related signal. Nevertheless there was a robust task-related hemodynamic response, which entrains to trial schedule. It confirms the presence of an endogenous response in an early sensory area. The lack of a local neuronal correlate (as changes in firing rate) further emphasizes the importance of understanding the mechanisms underlying the hemodynamic signals.

The work presented in this thesis aims helping our understanding of neuroimaging, namely by trying to disambiguate endogenous from exogenous contributions to the imaging signal. We followed two lines of experiments: one aiming to characterize stimulus-related hemodynamic responses and other aiming to understand endogenous contributions to the signal. In both instances we also measured local neuronal activity (in the form of spikes and local field potentials).

We recorded simultaneously neuroimaging and electrophysiology signals from alert behaving monkeys trained to perform periodic tasks. We used intrinsic signal optical imaging techniques, which harvest the preferential absorption of visible light by hemoglobin in tissue, and are therefore an indirect measure of metabolism. We recorded activity from primary visual cortex; a cortical region with well characterized neural representations to external stimuli, anatomically on the brain surface allowing the use of intrinsic signal optical imaging.

Our ability to compare simultaneously acquired neuroimaging and electrophysiological signals (not trivial when using other imagining techniques) places us in a privileged position to evaluate the relationship of neuroimaging to underlying neuronal activity. We used a periodic task with visual stimuli present with known relationship to electrophysiological activity: we used contrast to test a range of different intensities of changes in neuronal activity. Contrast and neuronal activity have a monotonic relationship: increases in contrast are associated with increases in spiking (following a hyperbolic function). Using contrast as a way of inducing controlled changes in electrophysiological activity, we observed that in a periodic task the imaging response reflects a linear sum of exogenous (stimulus-related) and endogenous (task-related) components. Moreover the stimulus-related component had a linear relationship with local neuronal activity (as evaluated by changes in firing rates).

Finally, we wanted to investigate potential contributors to the endogenous factors (stimulus-independent) influencing the resulting neuroimaging signal.

In the same task previously used in the laboratory: fixation in the absence of visual stimulus (other than the fixation point), we observed that periods where the animal was disengaged from the task were associated with a *slow* hemodynamic response change. Other than the aforementioned task-related hemodynamic response, we propose that engagement in a task has a significant contribution to *slow* changes in our imaging signal. We observed an increase in the hemodynamic response, accompanied by a decrease in heart rate and a modest decrease in firing rates, in primary visual cortex. The changes in hemodynamic response were of significant magnitude. The work presented in this thesis advances the understanding of the nature of the neuroimaging signals.

Publications

Publication included in this thesis (Chapter 2 is a full reprint of the publication below)

Cardoso M*, Sirotin YB *, Lima B, Glushenkova E and Das A (2012). The Neuroimaging Signal is a Linear Sum of Neurally Distinct Stimulus- and Task- Related Components. Nat. Neurosci. 15(9): 1298-306. (*Equal contribution.)

Publications not included in this thesis

Lima B, **Cardoso M**, Sirotin YB and Das A (2014). Stimulus-related neuroimaging in task-engaged subjects is best predicted by concurrent spiking. J. Neurosci., 34(42): 13878-91.

Sirotin YB, **Cardoso M**, Lima B and Das A (2012). Spatial homogeneity and task-synchrony of the trial-related signal. Neuroimage. 59: 2783-2797.

Publication in preparation (Chapter 4)

Cardoso M, Lima B and Das A. Slow drifts in brain blood volume are associated with behavioral changes in primate V1.

Author Contributions

Chapter 2

Mariana Cardoso (MC) conducted the bulk of the experiments, data analysis and wrote the manuscript. Yevgeniy B Sirotin (YBS) designed the experiments, conducted the initial experiments, analyzed data and wrote the manuscript. Bruss Lima (BL) conducted the bulk of the experiments, contributed to analysis and wrote the manuscript. Elena Glushenkova (EG) contributed to the experiments. Aniruddha Das (AD) designed the experiments, analyzed the data, wrote the manuscript and supervised the project.

Remaining chapters

MC and AD designed the bulk of the experiments with assistance from BL and YBS. MC and BL trained the animals and collected the data with assistance from EG and Maria Bezlepkina (MB). MC analyzed the bulk of the data and wrote the associated text.

Abbreviations

ARI	arousal related index
BOLD	blood-oxygen level dependent
CCD	charge-coupled device
COX-2	cyclooxygenase-2
DMN	default mode network
EEG	electroencephalography
fMRI	functional magnetic resonance imaging
HbO	oxyhemoglobin
HbT	total hemoglobin
HbR	deoxyhemoglobin
LC	locus coeurulus
LED	light-emitting diode
LFP	local field potentials
MUA	multi-unit activity
NA	norepinephrine
NMDA	N-methyl-D-aspartate receptor
OIIS	optical imaging of intrinsic signals
TTX	tetrodotoxin
V1	primary visual cortex

Table of Contents

1. Introduction

1.1 Hemodynamic responses in the brain

Understanding the functioning of the brain has captured our fascination for a long time. In the quest to understand the inner workings of the brain, several techniques have been developed. These range immensely in application and scope. In this thesis we used a combination of neuroimaging and electrophysiology to probe questions pertaining to the behaving brain.

The space of questions that can be answered using neuroimaging in alert subjects is extremely vast. The questions addressed here have as seed the results found previously in the lab (Sirotin & Das 2009), where a task-related hemodynamic signal was described in alert non-human primates, when animals were engaged in a periodic fixation task. This hemodynamic task-related signal was observed in the absence of concurrent changes in local neuronal activity. In this thesis we aimed at understanding, firstly if the hemodynamic responses to external stimuli have a comprehensive relationship to underlying changes in spiking activity. Furthermore, we wanted to understand the correlations, if any, between the hemodynamic response and the behavior of the subjects; thus exploring also endogenous responses and not only responses to external sensory stimuli.

To address these questions, we studied alert non-human primates (as in the original study, Sirotin & Das 2009). Interestingly, such signals were also observed in humans (Jack et al. 2006, Sylvester et al. 2007, Donner et al. 2008). It is worth noting, these recordings in human subjects comprised only neuroimaging. The recording of electrophysiologycal activity in human subjects tends to rely on techniques like EEG; those were not used in mentioned human studies. Moreover, EEG recordings might not reflect unubiquitous spiking activity (Saltzberg et al. 1971). Electrophysiological

techniques aiming to record spiking activity tend to be still intrusive techniques not routinely performed in human subjects.

We recorded activity from the primary visual cortex (V1), which is the entry point of visual information into cortex. This is a structure on the cortical surface, which has been very well characterized in terms of its neural responses. Known properties of V1 date back to the seminal work by Hubel and Wiesel (Hubel & Wiesel 1968). V1 has a retinotopic organization, and not only is position relative to the fovea encoded in its responses, there are also several known properties of visual stimuli that can be differentially encoded in V1, as contrast, direction, orientation, spatial or temporal frequency. By combining optical imaging of intrinsic signals (OIIS) with simultaneous multi-unit electrophysiological activity (MUA) in V1, it is possible to address questions pertaining to the neural underpinnings of the neuroimaging response, as well as to improve our understanding of the signals encoded in visual cortex.

Finally, V1 is a cortical region dedicated to vision, but that receives modulatory input from multiple structures in the brain. It is known to be influenced by endogenous variables such as attention (Bashinski & Bacharach 1980) or the timing of reward delivery (Shuler & Bear 2006, this is work with rodents). V1 is therefore particularly well positioned to study the contributions of endogenous and exogenous signals into the hemodynamic responses and their neural correlates.

1.2 Neuroimaging: intrinsic signal optical imaging

Intrinsic signal optical imaging techniques were developed in the 80's by Amiram Grinvald's group (Grinvald et al. 1986). Optical imaging of intrinsic signals (OIIS) techniques measure changes in the intensity of light reflected off cortical tissue. If one illuminates cortex with visible light the largest absorber of light in tissue is hemoglobin. Thus this form of imaging allows the monitoring of changes in hemoglobin tissue concentration; analogous to

how one can identify vasculature in tissue, i.e., distinguishing arteries and veins below the skin, by visual inspection.

At different wavelengths, hemoglobin absorbs light differently. Depending on hemoglobin's redox state light is also absorbed differently (e. g. Zijlstra & Buursma 1997), hence it allows to distinguish changes in oxy-hemoglobin (HbO), deoxy-hemoglobin (HbR) and total blood volume (HbT; the sum of oxy- and deoxy-hemoglobin). OIIS at wavelengths equally absorbed by oxy- and deoxy-hemoglobin (isosbestic points, wavelengths of overlap of the absorption spectra) provides information about HbT. 530 nm is an isosbestic point. Another relevant wavelength is around 605 nm; at this wavelength HbR absorbs light around 5 fold more strongly than HbO. The combined imaging at the two wavelengths allows us to decompose the net response into HbO and HbR components (Sirotin et al. 2009); or, into blood volume and blood oxygenation components. Blood oxygenation is what is typically measured in functional magnetic resonance imaging (fMRI), blood-oxygen level dependent (BOLD) (Ogawa et al. 1990). Parenthetically, simultaneous recording of fMRI and OIIS signals show a good agreement between the two techniques, e.g. Jezzard et al. 1994, Fukuda et al. 2006 (in this latter study they used an isosbestic point, wavelength of 570 nm).

The data presented in this thesis was acquired at 530 nm (isosbestic point; green wavelength). This wavelength provides a larger percent signal change than say the 605 nm ("deoxy-hemoglobin signal"), and is a signal with a known relationship between hemoglobin species (Sirotin et al. 2009). At this wavelength the hemodynamic signal is a proxy for changes in total blood volume.

When the cortical surface is illuminated with visible light, light is preferentially absorbed by the vasculature, as mentioned above. Acquired images are darker where vasculature lies. Depending on image quality and magnification one can identify blood vessels. Capillaries too small to be resolved in the images comprise the capillary bed and parenchyma and they also contribute to changes in the imaging signal. There are a number of other

aspects that can contribute to the global OIIS, as light scattering. In the intact brain, heart rate or breathing should also be taken into account, as there is evidence of their influence in the BOLD signal (Chang et al. 2009, Birn et al. 2008).

By using two different wavelengths in the same experiment (530, and 605 nm), we can distinguish arteries and veins. Arteries have low contrast when imaged at 605 nm, but veins have high contrast. At 530 nm, both arteries and veins should have similar contrast; hence comparing images acquired at these wavelengths permits distinguishing arteries from veins. Even though the results included on this thesis reflect changes measured with the 530 nm illumination wavelength, some measures were made using both 530 and 605 nm.

The intensity value resulting from the OIIS (light intensity from a CCD camera) is in arbitrary units; its absolute value is not informative, but differential analysis can inform about changes in the hemodynamic species' concentration.

Bonhoeffer and Grinvald (Bonhoeffer & Grinvald 1991) presented subtraction and division methods for analysis of this type of data; they found similar results with either approach. In the experiments included in this thesis we used fractional changes of the light intensity reflected off the cortical surface, relative to the mean (light reflected), as a proxy for changes in concentration of total blood volume. In Chapter 2 we used fractional changes in the intensity of light reflected off the cortical surface, here increases in blood volume are reflected as decreases in the fractional changes, but Chapters 3 and 4 use the negative of this change, in this case increases in blood volume are reflected as increases in the signal's fractional change (this difference reflects publication history).

The experimental setup was composed of a CCD camera, an ensemble of lenses focusing the imaging plane in the cortical surface, taking pictures of the brain surface. Attached to the recording chamber is the illuminator (a ring like structure holding optical fibers; each fiber is coupled to a LED) as

well as the electrode holder (another ring like structure with the capacity to hold one or two electrodes connected to electrode micro drivers). The imaging region is kept under sterile conditions and separated from contact with outside air (a titanium chamber encloses a clear glass, sealing the chamber). To ensure optical clarity the imaging chamber it is filled with a clear solution of agarose. A schematic of the setup can be found in Figure 1.1. In Figure 1.1a, one can see the edge of the imaging lenses, as well as the electrode holder (metal piece attached to recording chamber). The illumination system is composed of optical fibers coupled to LEDs, it produces a uniform illumination profile as in Figure 1.1a. In Figure 1.1b is a close-up picture of the recording chamber, where can be noticed an aperture (through a silicon-coated glass, sealing the chamber) for one recording electrode.

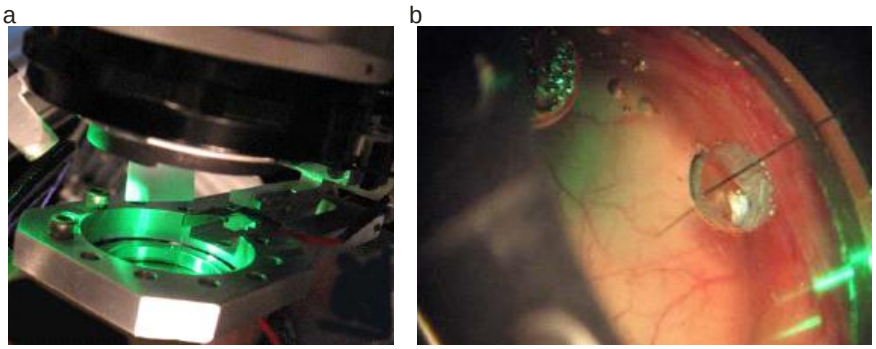

Figure 1.1 – The experimental setup. **(a)** Picture of the setup illustrating: imaging arrangement, with LED illumination of 530nm. **(b)**. Picture of the imaging region with single electrode.

Images were acquired at 15 Hz (or 7.5 Hz, if two wavelengths were used). Below is a typical image (Figure 1.2a, b) from one of our experiments. Here it can be noticed the artery that comes on gray on Figure 1.2a and is dark in Figure 1.2b, has a different profile from veins (visible and dark on both images). When looking at the time series, at this imaging frequency, one can clearly notice the effect of the brain's pulsation (heart beat driven

palpitation) (Figure 1.2d). Pulsation can be removed by subtracting a high-pass filtered version of the imaging signal (Figure 1.2c). From this pulsation one can estimate heart rate.

The use of neuroimaging techniques ultimately aims at estimating neural activity, but neither OIIS nor BOLD fMRI, are direct measures of neural activity (review on BOLD interpretation, e.g. Logothetis & Wandell 2004).

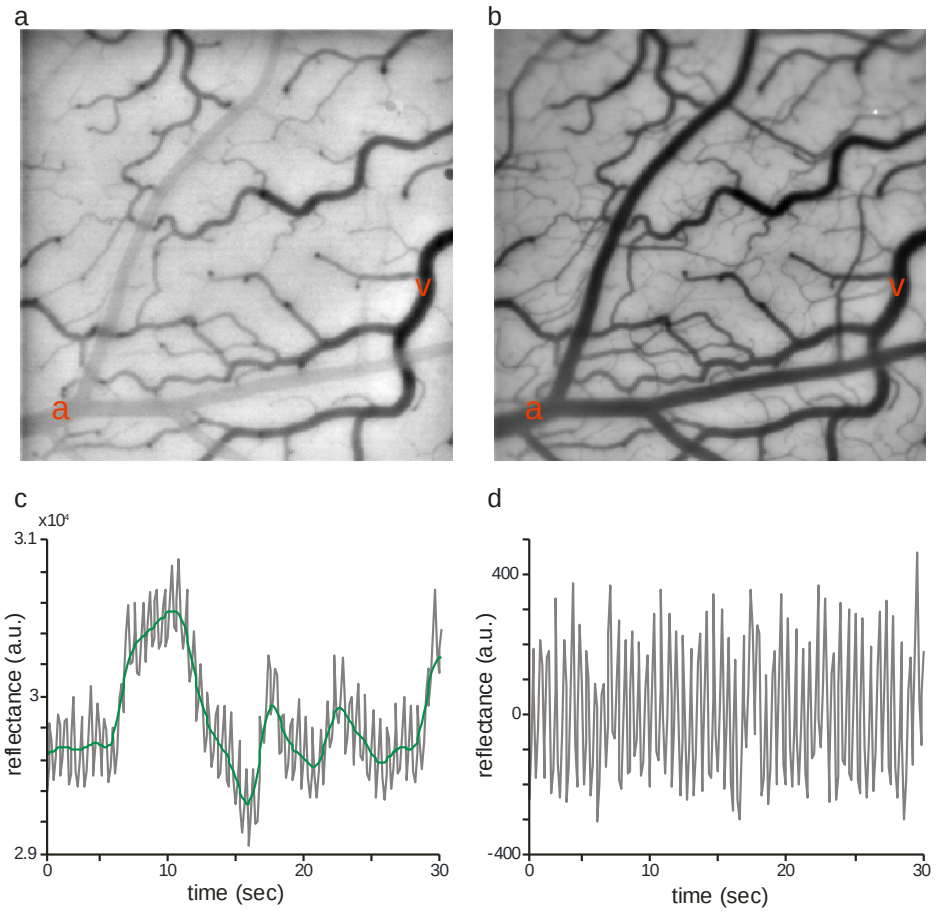

Figure 1.2 Intrinsic signal optical imaging in V1. **(a)** Reflectance of cortical surface with incident light of 605 nm. **(b)** Similar to **a**, but incident light of 530 nm. The letters in red: a – artery, v – vein. **(c)** Average reflectance for the first 30 s of imaging (wavelength: 530 nm), in gray is raw signal and in green is the signal without the high frequency pulsation (low-pass filtered version of the raw signal). **(d)** Pulsation signal observed at 530 nm on the first 30 s of imaging.

1.3 Neural basis of intrinsic signal optical imaging

In this section, I aim to bring attention to the complexity of the neuroimaging signals and their respective interpretations.

Spiking activity is an energetically demanding process for the brain, with several components of neural activity weighing in (Laughlin et al. 1998, Attwell & Laughlin 2001). Metabolic demand in the brain is mostly replenished by the blood supply, as neurons do not have significant energy reserves. Therefore, if the relationship between neuronal activity and metabolic demand, and between metabolic demand and blood supply was linear, neuroimaging would have a clear relationship with underlying neuronal activity. However, there is ample evidence of a more complex relationship. Thus, understanding the *neuro-vascular coupling,* the coupling of spiking activity to metabolism and from metabolism to blood supply, will help interpret neuroimaging.

The main metabolic substrates of the brain are glucose and oxygen; both reach the brain through blood circulation. There is considerable research into the metabolic cost of spiking (for estimations of metabolic neural cost in the rodent brain see: Attwell & Laughlin 2001). The development of autoradiography allowed measuring local glucose consumption in alert and anesthetized rodents using a radioactive analogue of glucose, which permits monitoring of metabolic rate (Sokoloff et al. 1977). The development of positron emission tomography permitted a better temporal and spatial mapping of radioactive species (a broad perspective of the field is presented in Raichle 1979). More relevant to the work presented in this thesis: metabolic measures have been used in primary visual cortex of alert humans undergoing physiological visual stimulation. These confirmed an increased metabolic rate with visual simulation, using nuclear magnetic resonance spectroscopy (Prichard et al. 1991). Finally when considering oxygen consumption, there have been reported increases in oxygen rate of

consumption in response to electric pulses (in rabbits' isolated neurons, Ritchie 1967). Both glucose and oxygen consumption increase in response to neuronal activation, therefore measures of metabolism can be appropriate proxies for monitoring changes in neural activity. Ultimately, if hemodynamic changes reflect metabolism, then the hemodynamic response can be an attractive proxy for changes in neural activity.

Given the advent of techniques, such as fMRI that allows monitoring large portions of brain (virtually non-intrusively) make those increasingly relevant. It should be noted that OIIS requires the imaged surface to be exposed, making it an intrusive technique. The use of neuroimaging techniques should however be combined with research efforts on its interpretation.

Intrinsic signal optical imaging also reflects light scattering from neuropil activation. Early work in isolated nerve cells showed that action potentials in unmyelinated isolated fibers cause birefringence changes as well as light scattering, in the visible light spectrum (Cohen et al. 1968). There is also evidence from work done in hippocampal slices, where transmitted and reflected light profiles were observed to be, on average, symmetric and opposite in sign. This suggests a bigger role for light scattering than light absorption with intrinsic signal optical imaging (Aitken et al. 1999). Work with intrinsic signal optical imaging in the olfactory bulb of anesthetized rodents used multiple imaging wavelengths to address whether the response to stimulating odors in olfactory glomeruli results more from light scattering in tissue with neuronal activation or from changes in HbO/HbR concentration in blood. In their case, they concluded that light scattering is in the origin of the imaging response (Meister & Bonhoeffer 2001).

Neuronal activity is responsible for other changes that can be accessed by looking at hemodynamic responses, other than direct light scattering changes Functional hyperemia – increased blood flow in response to neuronal activity – also contributes to hemodynamic changes. Astrocytes that have a privileged relationships with blood vessels are known to play an important role in mediating hyperemia (for a review see Iadecola &

Nedergaard 2007 and Attwell et al. 2010). Other than acting as a 'relay-system' of neurons' metabolic needs to the vasculature, there is also evidence that astrocytes also incur in metabolic cost following neuronal activity (Kasischke et al. 2004). This suggests that neurons are not the sole determinants of functional hyperemia.

Experiments in the olfactory bulb of anesthetized rodents have shown changes in blood flow that are directly related to responses to odors in olfactory glomeruli (Chaigneau et al. 2003, Chaigneau et al. 2007). Once more, it points to a direct involvement of neuroral activity into functional hyperemia. OIIS not only does not reflect exclusively metabolism, as metabolism itself has a somewhat complex relationship with spiking activity. Indeed, OIIS signals have been shown to be related to presynaptic activation more than with postsynaptic activity: Gurden and colleagues did experiments in the olfactory bulb of anesthetized rodents showing that blocking spiking activity with TTX suppressed the imaging signal, as well as when glutamate reuptake by astrocytes was inhibited. On the other hand, when they used postsynaptic antagonists they saw no changes in the imaging response (Gurden et al. 2006). It should be noted, however, that data collected in the olfactory bulb of mice but using glutamate receptor antagonists, showed that blood flow responses were blocked; suggesting a role of postsynaptic activity in functional hyperemia (Chaigneau et al. 2007). More recent work in sensorimotor cortex, looking at both OIIS and blood flow changes (using laser speckle contrast imaging) can be elicited by optogenetic stimulation of deep layer cortical pyramidal neurons even with postsynaptic activity pharmacologically blocked (Scott & Murphy 2012).

Aiming to address the possibility of neurons eliciting hyperemia without the direct involvement of astrocytes, it has been shown in rodents, that application of NMDA can induce vasodilation, and corresponding hemodynamic response, that involved COX-2 activation originating on pyramiddal cells (Lacroix et al. 2015)

There is also recent evidence relating specific cell activation and different neuronal pathways to BOLD fMRI. In Kahn et al. 2011, they used optogenetic techniques in alert rodents and directly activated layer V neocortical pyramidal cells which resulted in an increase in BOLD response at the stimulated location, similar results were previously observed by other research group (Lee et al. 2010). In Kahn et al. 2013, they were able to relate that stimulation to spiking activity better than changes in local field potentials.

In summary, the hemodynamic responses are complex, reflecting metabolic and non-metabolic changes as well as hyperemia responses due to direct neuronal activity and changes observed in astrocytes. It is hard to interpret these responses; nevertheless its study is critical to the neuroimaging community. There are many questions that have not been fully answered and that will potentially change the current understanding of neuro-vascular coupling. Some of those are: how local is the hemodynamic response relative to the underlying neural activity? Are there specific hemodynamic responses that can help disambiguate the contribution of different cell types (e.g., excitatory neurons, inhibitory neurons, astrocytes)? Is the metabolic rate similar all across the brain? Is the vascular response similar for different brain areas? What are the effects of vasodilatation or constriction to flow in regions away from the focus of neural activity? What is the temporal relationship between neural activity and the ultimate hemodynamic response? Can non-glutamatergic neurotransmitters also influence vasodilation and constriction?

Plenty of research in this topic has been done in anesthetized animals, slices and isolated neurons, but there is also research in alert animals. A significant body of research using intrinsic signal optical imaging in animals as contributed to a better understanding of the technique (with multiple research groups focusing on these questions, e.g., anesthetized rodents: Mayhew et al. 1996, Devor et al. 2003, Sheth et al. 2004, Weber et al. 2004, Devor et al. 2007, Chen et al. 2011, alert rodents: Martin et al. 2002,

anesthetized non-human primates: Grinvald et al. 1986, Lu & Roe 2007, behaving non-human primates: Shtoyerman et al. 2000, Sirotin & Das 2009). This thesis aims at adding information on this body of research.

1.4 Thesis's scope

The present thesis is focused on two main points. First, explore the relationship between stimulus-related hemodynamic responses and underlying spiking activity. Second, further characterize endogenous contributions to the hemodynamic signal. This part is divided in two sections; the first is focused on the hemodynamic task-related response. Here is included data of several experimental manipulations of the original task where the hemodynamic task-related response was described (Sirotin & Das 2009). The second and final section looks at changes in the hemodynamic signal with engagement.

2 The neuroimaging signal is a linear sum of neurally distinct stimulus- and task-related components.

2.1 Abstract

Neuroimaging (for example, functional magnetic resonance imaging) signals are taken as a uniform proxy for local neural activity. By simultaneously recording electrode and neuroimaging (intrinsic signal optical imaging) signals in alert, task-engaged macaque visual cortex, we recently observed a large anticipatory trial-related neuroimaging signal that was poorly related to local spiking or field potentials. We used these same techniques to study the interactions of this trial-related signal with stimulus-evoked responses over the full range of stimulus intensities, including total darkness. We found that the two signals could be separated, and added linearly over this full range. The stimulus-evoked component was related linearly to local spiking and, consequently, could be used to obtain precise and reliable estimates of local neural activity. The trial-related signal likely has a distinct neural mechanism, however, and failure to account for it properly could lead to substantial errors when estimating local neural spiking from the neuroimaging signal.

2.2 Introduction

The hemodynamic signals forming the basis of functional neuroimaging techniques such as functional magnetic resonance imaging (fMRI) are typically assumed to linearly reflect changes in local neural activity (Boynton et al. 1996) (specifically spikes Heeger et al. 2000; Rees et al. 2000; for a review, see ref. Heeger & Ress 2002). In particular, the neuroimaging signal is often modeled as a linear convolution of a presumed underlying neural time course with some standard hemodynamic response function (HRF) (Boynton et al. 1996; Friston et al. 1994; Josephs et al. 1997; Dale & Buckner 1997; Cohen 1997; Pestilli et al. 2011). A considerable body of

evidence suggests that such a linear relationship reliably models the imaged responses to exogenous stimuli (Boynton et al. 1996; Engel et al. 1997; Buckner et al. 1998; Boynton et al. 1999; Grill-Spector & Malach 2001; Logothetis et al. 2001; Mukamel et al. 2005; Gardner et al. 2005; Boynton 2011). In alert, task-engaged subjects, however, the exogenous stimulus alone poorly predicts the full recorded neuroimaging signal. This mismatch is taken as evidence for additional endogenous non-sensory signals related to anticipation, attention and task structure (Jack et al. 2006; Sylvester et al. 2007; Donner et al. 2008). The neural mechanisms underlying these endogenous signals have been proposed to be distinct from stimulus-evoked neural activity Jack et al. 2006; Sylvester et al. 2007; Donner et al. 2008. However, the neurovascular origins of these endogenous hemodynamic signals have not been directly investigated or compared with those of exogenous sensory signals, such as with extracellular electrode recordings, as most neuroimaging studies of alert, task-engaged individuals involve human subjects (but see refs. Mukamel et al. 2005; Maier et al. 2008).

We recently Sirotin & Das 2009 compared the neural correlates of stimulus-evoked and endogenous hemodynamic signals directly in alert macaque primary visual cortex (V1) by combining electrode recordings with simultaneous intrinsic-signal optical imaging (Bonhoeffer & Grinvald 1996 Shtoyerman et al. 2000) (a high-resolution optical analog (Fukuda et al. 2006; Kennerley et al. 2009) of fMRI that visualizes local changes in blood volume and oxygenation (Bonhoeffer & Grinvald 1996, Sirotin et al. 2009)). When the animals performed a periodic visual fixation task, their V1 hemodynamic response revealed a particular anticipatory endogenous signal (hereafter referred to as the trial-related hemodynamic signal, *T*) that entrained robustly to predicted trial onsets even in the absence of visual input. Notably, this trial-related signal could not be predicted from local multi-unit activity (MUA) or local field potentials (LFP) down to 2 Hz, unlike the visually evoked hemodynamics that could be reliably predicted from local MUA or gamma-band LFP using a standard HRF (Sirotin & Das 2009).

In our earlier work (Sirotin & Das 2009), we only compared brain signals at the two extremes of visual drive. To measure stimulus-evoked signals, we used near-maximal stimulus intensities at which the visual input dominated; meanwhile, we characterized the trial-related signal only in essentially complete darkness. A question not explored in the earlier work was how these signals would interact when presented together in different proportions in routine visual tasks involving stimuli of varied intensities, and how this admixture of signals would affect the interpretation of brain images.

We addressed these questions using our technique of simultaneous optical imaging and electrode recording in alert, task-engaged macaques. Here, however, we presented visual stimuli over the full contrast range (0% to 100%); for some experiments, we also included trials in complete darkness. This allowed us to test whether the net imaging signal could be separated into stimulus-evoked (that is, correlated with stimulus contrast and evoked neural spiking) and trial-related components (dependent on task structure, but not stimulation or local spiking) over a full range of V1 spiking and hemodynamics. Furthermore, as the primary use of neuroimaging is to estimate local neural activity (often done implicitly, but also quantitatively by deconvolving the imaging signal using an HRF (Glover 1999)), we examined the accuracy of this estimate with and without correcting for the trial-related signal.

2.3 Methods

2.3.1 Summary

Simultaneous intrinsic-signal optical imaging and electrophysiology were acquired from alert macaques engaged in passive fixation tasks (n = 34 sites, 5 hemispheres in 3 monkeys, plus 14 additional experiments) using methods developed previously (Bonhoeffer & Grinvald 1996, Sirotin & Das 2009; Shtoyerman et al. 2000). All experimental procedures were performed

in accordance with the US National Institutes of Health Guide for the Care and Use of Laboratory Animals and were approved by the Institutional Animal Care and Use Committees of Columbia University and the New York State Psychiatric Institute.

2.3.2 Behavior and stimuli

Animals held fixation periodically for juice reward, cued by the color of a fixation spot (fixation window, 1.0–3.5 degrees in diameter; monitor distance, 133 cm; fixation duration, 3–4 s; trial duration, 10–20 s). For experiments with visual stimulation, stimuli consisted of sine-wave gratings (contrasts, 0% (blank), 6.25%, 12.5%, 25%, 50% and 100%; mean luminance = background luminance = 46 cd m^{-2}; spatial frequency, 2 cycles per degree; drift speed, 4 degrees per s; diameter, 2–4 degrees; orientation optimized for the electrode recording site). Trials typically comprised single fixations, with stimulus presented during fixation. For some experiments (Figure 2.5), trials comprised sequences of two or three fixations with the stimulus presented only on the first fixation. Stimuli were block randomized, that is, presented in blocks each containing a single full set of contrasts in random order. In the block, stimuli were repeated following errors (incorrect fixation) until the animal had a correct trial for each stimulus in a block (for multi-fixation trials, all fixations had to be correct for a trial to be correct). Some experiments included 3.125% contrast for finer resolution at low contrasts; some others used a reduced set of contrasts to increase the number of trials per condition. Dark-room experiments were performed in a completely dark room with the monitor covered and the fixation point behind a pinhole (as described in ref. Sirotin & Das 2009). Eye fixation and pupil diameter were recorded using an infrared eye tracker (Matsuda et al. 2000).

2.3.3 Surgery, recording chambers and artificial dura

After the monkeys were trained on visual fixation tasks, craniotomies were performed over the animals' V1 and glass-windowed stainless steel recording chambers were implanted, under surgical anesthesia, using standard sterile procedures (Shtoyerman et al. 2000), to image a ~ 79mm^2 area of V1 covering visual eccentricities from ~1 to 5°. The exposed dura was resected and replaced with a soft, clear silicone artificial dura. After the animals had recovered from surgery, their V1 was optically imaged, routinely, while they engaged in the fixation task. Recording chambers and artificial dura were fabricated in our laboratory using published methods (Arieli et al. 2002).

2.3.4 Hardware

Camera, Dalsa 1M30P (binned to 256 × 256 pixels, 7.5 or 15 frames per s); frame grabber, Optical PCI Bus Digital (Coreco Imaging). Software was developed in our laboratory based on a previously described system (Kalatsky & Stryker 2003). Illumination, high-intensity LEDs (Agilent Technologies, Purdy Technologies) with emission wavelength centered at 530 nm (green, equally absorbed in oxy- and deoxyhemoglobin). Lens, macroscope of back-to-back camera lenses focused on the cortical surface. Imaging, trial data (trial onset, stimulus onset, identity and duration, etc.) and behavioral data (eye position, pupil size, timing of fixation breaks, fixation acquisitions, trial outcome) were acquired continuously. Data analyses were performed offline using custom software in MATLAB (MathWorks).

2.3.5 Image pre-processing

Prior to analysis, acquired images were (if necessary) motion corrected by aligning each frame to the first frame by shifting and rotating the images using the blood vessels as a reference (Lucas & Kanade 1981). Slow temporal drifts (>30 s) were removed with high-pass filtering, and cortical pulsations with low-pass filtering using the Chronux MATLAB Toolbox

function runline.m (typical heart rates were ~2–3 Hz, much faster than the typical hemodynamic response frequencies of ~<0.5 Hz).

2.3.6 Electrophysiology

Electrode recordings were made simultaneously with optical imaging. Recording electrodes (FHC, AlphaOmega; typical impedances were ~600–1,000 kΩ) were advanced into the recording chamber through a silicone-covered hole in the external glass window, using a custom-made low-profile microdrive. Recording sites were mostly, but not exclusively, confined to upper layers. Signals were recorded and amplified using a Plexon recording system. The electrode signal was split into spiking (100 Hz to 8 kHz band-pass) and LFP (0.7–170 Hz); LFP data not shown. No attempt was made at isolating single units and all measured spiking was MUA (defined as each negative-going crossing of a threshold = ~4× the r.m.s. of the baseline obtained while the animal looked at a grey screen (Sirotin & Das 2009)). The MUA signals were then high-pass filtered to remove slow drifts (>30 s), down sampled to the imaging frame rate (7.5 or 15 samples per s) and aligned offline with the images.

2.3.7 HRF kernel fitting

Each HRF was modeled as a gamma-variate function kernel of the form

$$HRF(t,T,W,A) = A * \left(\frac{t}{T}\right)^{\alpha} * exp\left(\frac{t-T}{-\beta}\right)$$

where $\alpha = (T/W)^2 * 8.0 * \log(2.0)$, $\beta = W^2/(T * 8.0 * \log(2.0))$, A is the amplitude, T is the time to peak and W is the full width at half maximum (Cohen 1997; Sirotin & Das 2009; Madsen 1992). This functional form allows for parametrically varying kernel amplitude, latency and width. For fitting, we used a downhill simplex algorithm (fminsearch, MATLAB) minimizing the sum square difference between measured and predicted hemodynamics. All fits used periodic functions (30 repetitions) constructed from means of the

relevant signals across contrasts, aligned to trial onsets, for correct trials alone. Thus, HRF_{STIM} was obtained by fitting a periodic pattern of the mean S_{STIM} to the mean H_{STIM}, the HRF_{NULL} by fitting the mean S to the mean H (over correct trials alone), the HRF_{BLANK} by fitting the mean S_{BLANK} to the mean H_{BLANK}, and the HRF_{DARK} by fitting the mean S_{DARK} to the mean H_{DARK}.

2.3.8 Goodness of fit of predicted hemodynamics

Fit was quantified as R^2 = 1 − (variance of the residual error)/(variance of measured hemodynamics) (Supplementary Note, equation (10)), expressed either separately for each contrast or as mean R^2, that is, calculated for the mean signals averaged across all contrasts. For all fits other than of the blank signal, predictions (and residual errors) were calculated by convolving the full raw measured spike trace with the relevant HRF and then separating later into correct trials by contrast, or averaging across contrasts. This is more reliable than convolving synthetic periodic functions constructed from mean signals because with periodic functions there is a risk of getting a match, not with the true signal, but with a signal phase-shifted by a fraction of a trial period (Das & Sirotin 2011). Such mismatches are highly unlikely in the measured signal with its random sequence of stimulus intensities and corresponding evoked hemodynamics (Das & Sirotin 2011). The blank signal fit using HRF_{BLANK} was tested using periodic functions, as in this case we were testing the fit using a kernel that specifically did not fit the full stimulated spike sequence.

2.3.9 Bootstrapping to get confidence limits on R^2

For each experiment, 200 bootstrap data sets were constructed, each with the same number of trials as the original, using random resampling with replacement (Supplementary Figure 2.10). The resampled hemodynamic and spike trials were then fitted against each other separately for both models (MLM and null) and R^2 values were calculated as before (Supple-

mentary Note, equation (10)). The 95% confidence limits were obtained by taking the 2.5th to the 97.5th percentiles; similarly, 80% confidence limits by taking the 10th to the 90th percentile. Random reselection was done separately by contrast to have the same number of trials per contrast. However, each contrast used the same random number set to maintain stimulus blocks and reduce variability resulting from long-term drifts in physiology or recording stability. This was particularly necessary for the MLM, which involves subtracting the mean blank signals H_{BLANK} and S_{BLANK} from all other contrasts; if blocks are not maintained, this subtraction leads to a number of noisy outliers in the bootstrap estimate when a set of blanks trials dominated by one epoch of a session (for example, high signal) is subtracted from nonblank trials dominated by a different epoch (for example, low signal).

2.3.10 Cross-validation of HRF_{STIM} kernels across sessions

For each session, we created a leave-one-out mean HRF_{STIM} kernel by averaging the two timing parameters (peak latency and width) across all kernels excluding the given one. Kernel amplitude was obtained by fitting, using this mean kernel to fit the given session's data (HRF_{STIM} amplitude depends on an arbitrary scale factor in electrode recording; Supplementary Figure 2.11). This leave-one-out mean kernel with the best fitted amplitude was then used to obtain the cross-validation prediction and corresponding R^2. Cross-validation was performed either across all animals or restricting the leave-one-out averaging to other kernels for the given animal.

2.3.11 Deconvolution

The spike trace estimated by deconvolution was defined as

$$D = F^{-1}\left\{\frac{F(H)}{F(HRF)}\right\}$$

where H is the relevant hemodynamic signal, HRF is the corresponding optimal HRF kernel and F and F^{-1} indicate forward and inverse (fast) Fourier

transforms, respectively. Given that $F(HRF)$ has low power at high frequencies, reflecting the slow hemodynamic response, we filtered using a Hamming window with a 0.5-Hz cutoff in frequency space. This avoided high-frequency noise in the hemodynamic signal from being amplified during deconvolution. The same filter was used to discount high frequencies in the measured spike rate before correlating with the deconvolved estimate.

2.3.12 Checking the stability of our primary findings against variability in electrode recordings

If measured spiking S is a veridical scaled sample of the true spiking s of our models despite measurement variability across experiments (different electrodes, different thresholds for spike detection for MUA), then the amplitude of the fitted *HRF* should simply scale inversely with measured spiking for a given experiment (Supplementary Figure 2.11 and Supplementary Note, equation (7))

$$HRF_{STIM} \otimes S_{STIM} \approx hrf \otimes s_{STIM} \approx H_{STIM}$$

The scale factor (between the measured S and the true s) will cancel out in all equations for a given experiment, leaving model features unchanged (that is, kernel shape, trial-related signal T and R^2). We tested for this in two ways. First, we tested the effect of varying spike detection thresholds. In five experiments, we recorded the electrode signal at a low threshold and then rethresholded off-line to generate multiple sets of spiking data S for the same imaging data (for example, peak spike rates from about 300 s^{-1} to about 10 s^{-1} for progressively higher thresholds; Supplementary Figure 2.11a,b). These rethresholded spike data were then fitted separately against the common imaging signal (Supplementary Figure 2.11c–g). In a second test, we checked the linearity of the relation linking HRF_{STIM} amplitude against the inverse of the S_{STIM} amplitude over our full data set (integration window for mean S_{STIM} coextensive with stimulus duration as in Figure 2.2a; Supplementary Figure 2.11h).

2.4 Results

For these experiments, we used three rhesus macaques (monkeys Y, T and S; *n* = 34 recording sites across five hemispheres; monkey S was also used previously (Sirotin & Das 2009)). The animals' task, which was cued by the color of a fixation spot, involved fixating and relaxing (that is, free viewing) periodically for a juice reward. This task is known to evoke robust trial-related signals in V1 (ref. Sirotin & Das 2009). A trial typically comprised a single fixation, with fixed trial periodicity of 10–20 s. For one set of experiments, trials consisted of sequences of two or three fixations, each rewarded for correct fixation. Visual stimuli comprised drifting sine-wave gratings that were presented passively while the animal fixated. The grating contrast was typically varied in five log2 steps plus a blank, presented in randomized order; the contrasts varied in some experiments and grating orientation was optimized for each electrode recording site. In addition, to compare with our earlier results (Sirotin & Das 2009), we performed a set of experiments in darkness (see Online Methods).

We recorded concurrent MUA and hemodynamics from V1. For hemodynamics, we used intrinsic-signal optical imaging, a high-resolution optical analog of fMRI that deduces cortical hemodynamics by measuring fractional changes in the intensity of light reflected off the cortical surface at wavelengths absorbed by hemoglobin (Bonhoeffer & Grinvald 1996 Sirotin & Das 2009; Sirotin et al. 2009). We specifically used the blood volume signal imaged at 530 nm (green), as it directly measures changes in total local tissue hemoglobin concentration, and thus in local blood volume (Sirotin & Das 2009; Devor et al. 2003; Sheth et al. 2004; Nemoto et al. 2004). Furthermore, it matches corresponding fMRI signals (Fukuda et al. 2006). A particular advantage of this imaging signal is that its impulse response to a brief sensory stimulus is monophasic, with an increase in absorption followed by a monotonic return to baseline, presumably reflecting the stimulus-triggered increase and subsequent decline in local blood volume (Sirotin et

al. 2009; Devor et al. 2003; Sheth et al. 2004; Nemoto et al. 2004). The monophasic stimulus-triggered response makes the imaging signal easy to interpret and to model mathematically (see Supplementary Note).

2.4.1 Spikes poorly predict hemodynamics in periodic task

Our recordings showed, as expected, stimulus-driven spiking and hemodynamic responses with amplitudes monotonically reflecting stimulus contrast trial by trial (Figure 2.1). In addition, many recordings revealed a robust spiking signal locked to trial onset that was common to all of the spike traces and was most evident for blank trials (S_{BLANK}; Figure 2.1b). Additional evidence suggests, however, that this blank-trial spiking, maintained low during fixation and high in between fixations, is also visual (Supplementary Figure 2.8). The time course of this signal matched that of the animal's eye traces (Supplementary Figure 2.8a), and it was extinguished in the dark, even when the animal's eye trace patterns remained unchanged (Supplementary Figure 2.8b). This signal was therefore likely a result of the animal looking around the dimly lit room and then at the gray monitor, periodically, in each trial.

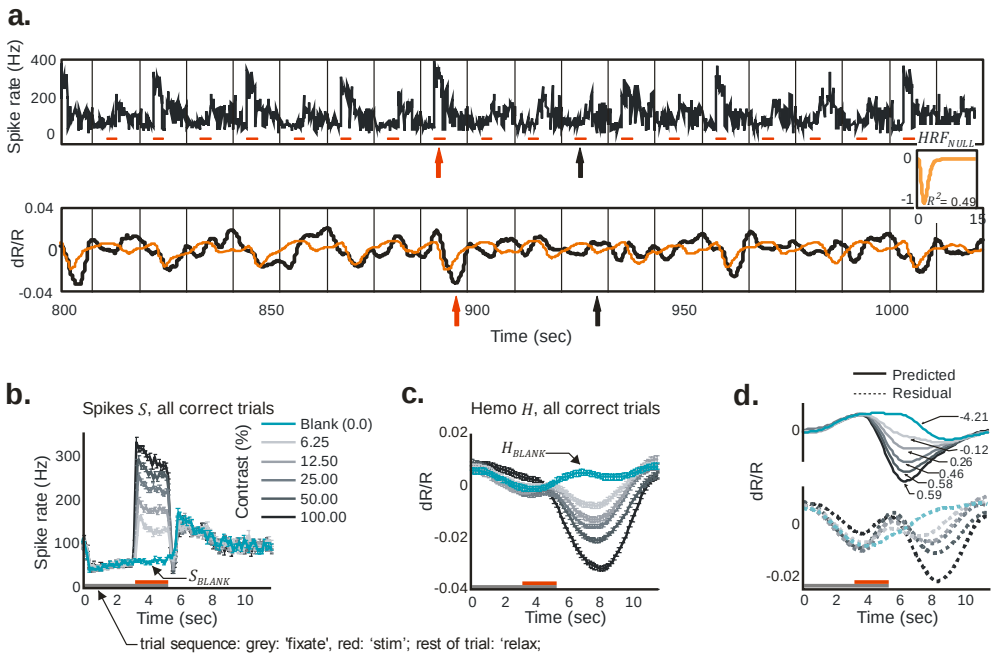

Figure 2.1 – The full hemodynamic signal is poorly predicted by local multi-unit spiking. **(a)** Top, a section of the full recorded spiking signal (S) for a representative experimental session (black trace). Bottom, corresponding measured hemodynamic signal (H, black) and the best prediction obtained from spiking (orange, $H_{NULL}^{PRED} = HRF_{NULL} \otimes S$, $\otimes$ indicates convolution; Supplementary Note, equation (3)). **Inset**, best fitting kernel HRF_{NULL} (amplitude normalized) obtained by fitting *H* to *S*. Mean R^2 = 0.49, as calculated using mean signals averaged across contrasts (*n* = 261 trials total, roughly 43 per contrast). Red line segments indicate stimulus application and vertical dotted lines indicate fixation trial onset. Red and black arrows below traces indicate typical responses to high-contrast (100% contrast) and blank (0% contrast) stimuli, respectively; for hemodynamics, increasing negative amplitudes, that is, increasing absorption of light by cortex, equals increasing blood volume. Note the poor match between the observed and predicted traces leading to a large residual and, consequently, low mean R^2. **(b)** Trial-aligned averages of spiking (*S*) for each contrast. The trial structure is indicated by the color bars (gray, fixate; red, stimulus; no bar, relax). Note the prominent blank-trial spiking signal S_{BLANK}. **(c)** Data presented as in **b** for hemodynamics (H). **(d)** Data are presented as in **b** for corresponding predicted hemodynamics H_{NULL}^{PRED} (solid lines, top) and residuals (H-H_{NULL}^{PRED}, dotted lines, bottom; separated vertically for visibility). Individual R^2, calculated separately per contrast, are shown alongside each prediction. Data were obtained from monkey S. Error bars represent s.e.m.

To set a null model baseline for alert, task-engaged monkeys, we first determined how well the full recorded local spiking could predict the full recorded hemodynamics. We linearly fitted the measured hemodynamics *H* to spiking *S* to generate an optimal linear kernel, HRF_{NULL}, and the corresponding predicted hemodynamic trace (Figure 2.1a and Supplementary Note, equation (1)). Although the prediction appeared to be qualitatively reasonable, quantitatively the match with measured hemodynamics was mediocre, with mean R^2 = 0.49 (the value calculated for the mean signal averaged over all contrasts; R^2 is defined as 1 − (variance of residual error)/(variance of measured signal); Supplementary Note, equation (10)).

The inadequacy of the fit was even clearer when we compared predictions with measured signals, contrast by contrast. We obtained poor R^2 and large residuals that varied with stimulus contrast (Figure 2.1d). Notably, R^2 was poorest for blank trials (0% contrast, R^2 = −4.21, a negative number as the residual was larger than the measured signal) and improved systematically for stimuli of higher contrast. This suggests that, at low spike rates, the hemodynamic signals may be dominated by non-spike-related components, independent of visual input, such as the previously demonstrated trial-related signals (Sirotin & Das 2009). Note that the blank-trial spiking signal that adds uniformly to all the spiking responses (S_{BLANK}; Figure 2.1b) is unlikely to be the cause of this mismatch. Being presumably visual, the blank-trial spiking should have linearly predictable hemodynamic correlates, similar to the hemodynamic correlates of the controlled stimuli.

2.4.2 Modified linear model with two signal components

Given the poor fit of the homogeneously linear null model to signals recorded during a task, and the pattern of residual errors by contrast, we considered a simple alternative modified linear model (MLM; Supplementary Figure 2.9) for such a task context. This model incorporates our earlier finding of a spike- and stimulus-independent anticipatory trial-related hemo-

dynamic signal (Sirotin & Das 2009), a signal that is only present in correct trials Sirotin et al. 2012. To keep the model as simple as possible, we assumed that the trial-related signal adds linearly (Jack et al. 2006; Donner et al. 2008; Fox et al. 2006) to the visually evoked component; this visually evoked hemodynamic component, we still assumed to be uniformly linearly predicted by visually evoked spiking (Boynton et al. 1996; Heeger et al. 2000; Rees et al. 2000), whether driven by controlled stimulation or uncontrolled visual input (as in the blank-trial spiking). We further assumed that the trial-related signal is stereotyped, determined by trial timing alone and is uniformly present in all trials types independent of whether the trial has a visual stimulus or a blank or involves dark-room fixation (Supplementary Note, equation (2)).

This posited structure of the MLM led to two important predictions. First, it predicted that, during visually stimulated tasks, the trial-related hemodynamic signal could be linearly separated from visually evoked responses by subtracting the blank-trial hemodynamic response (H_{BLANK}: Supplementary Figure 2.9 and Supplementary Note, equations (4–6)). Note that this step also uniformly subtracts the hemodynamic correlate of any uncontrolled blank-trial spiking (that is, S_{BLANK}), thereby revealing responses to the controlled visual stimulus alone. We defined this blank-subtracted signal as the stimulus-evoked hemodynamics, H_{STIM}; it should be linearly related to the stimulus-evoked spiking, S_{STIM}, obtained by subtracting blank-trial spiking from the other spike traces. The HRF kernel for the linear part of the MLM could then be estimated by fitting these stimulus-evoked signals against each other (Supplementary Note, equation (7)). Second, it predicted that the trial-related hemodynamic signal seen in visually stimulated tasks should match that seen in dark-room fixation tasks of the same trial timing (Supplementary Note, equations (2, 4–9)). As a corollary, it predicted that the trial-related signal will change to match changes in trial structure, even if the stimulation remained constant.

The MLM led to a marked improvement over the null model. This can be illustrated using the data set described above (Figure 2.1), where blank subtraction led to crisp orderly sequences of S_{STIM} (Figure 2.2a) and H_{STIM} (Figure 2.2b). The optimal kernel HRF_{STIM} (Figure 2.2c and Supplementary Note, equations (7,8)) obtained by fitting these stimulus-evoked signals to each other gave a mean R^2 of 0.99 (versus R^2 = 0.49 for the null model; Figure 2.1a,d). The same kernel also made reliable predictions for each individual contrast, closely matching corresponding measured signals H_{STIM}, with high R^2, and weak and contrast-independent residuals (Figure 2.2c). To assess the statistical significance of these comparisons, we estimated confidence intervals for each value of R^2 with a bootstrap technique using random selections of the given day's trials with replacement (200 runs per experiment, see Online Methods). The estimated 95% confidence limits obtained for all R^2 calculated using the MLM, mean as well as separately by contrast, were comfortably non-overlapping with those of corresponding R^2 from the null model, emphasizing the high significance of the improvement of the MLM over the null model (Supplementary Figure 2.10).

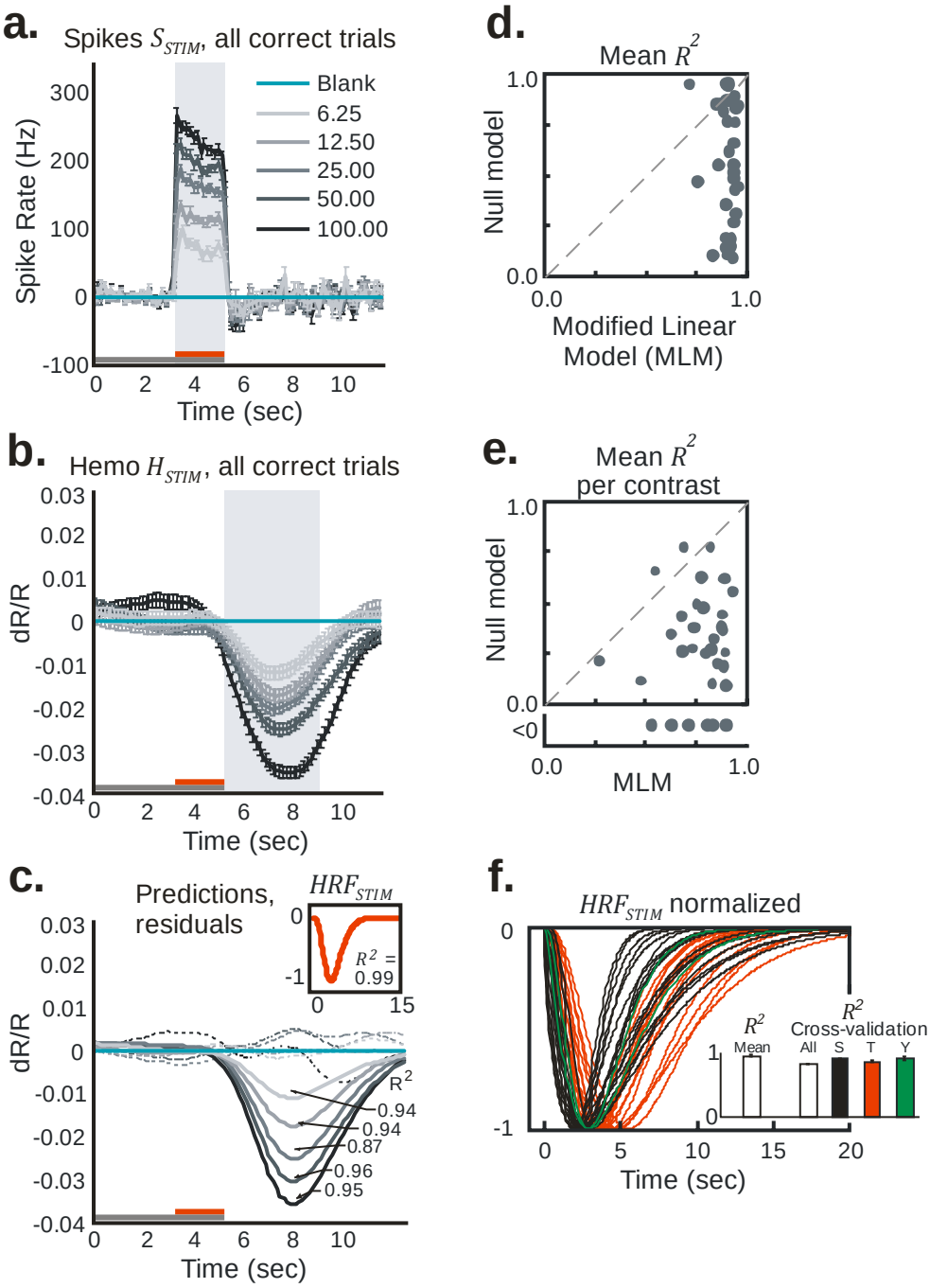

Figure 2.2 – Results using the MLM: stimulus-evoked (blank subtracted) hemodynamic responses (H_{STIM}) are reliably and linearly predicted by stimulus-evoked local spiking (S_{STIM}). **(a,b)** S_{STIM} (**a**) and H_{STIM} (**b**) (shaded regions indicate integration windows for calculating mean response

strength; see Figure 2.3). Data are presented as in Figure 2.1 with error bars indicating s.e.m. The trial structure is indicated by the color bars (gray, fixate; red, stimulus; no bar, relax). **(c)** Predicted stimulus-evoked hemodynamics (H_{STIM}^{PRED} = $HRF_{STIM} \otimes S_{STIM}$; Supplementary Note, equation (8)) and corresponding R^2, contrast by contrast. Dotted traces indicate residuals (H_{STIM} - H_{STIM}^{PRED}). **Inset**, optimal HRF_{STIM} (mean R^2 = 0.99, n = 261 trials). **(d)** Comparing mean R^2 for the null model, that is, without blank subtraction (y axis) against the MLM (x axis). Population average (s.e.m.) of mean R^2 = 0.93 (0.01) for MLM, 0.57 (0.05) for the null model (n = 34 sessions, 3 monkeys). **(e)** Data are presented as in d for R^2 calculated separately by contrast and then averaged (one data point per experiment). Fits for the null model were almost all worse than for the MLM (that is, below the diagonal) and included many negative values (shown below scatter plot; population average R^2 (s.e.m.): MLM, 0.77 (0.03); null model, 0.14 (0.10); n = 34). See Supplementary Figure 2.10 for bootstrap estimates of confidence intervals. **(f)** All HRF_{STIM} kernels (amplitude normalized; color coded by animal; population average latency (s.e.m), 3.1 (0.2) s; population average width (s.e.m.), 3.3 (0.2) s; n = 34). **Inset**, average mean R^2 (s.e.m.) from cross-validation tests using leave-one-out mean kernels, over all animals (0.80 (0.03), n = 34) and separately by animal (monkey S, 0.89 (0.02), n = 17; monkey T, 0.85 (0.03), n = 15; monkey Y, 0.90 (0.01), n = 2). R^2 pop indicates experimental population average (data from d).

Comparable improvements using the MLM were seen over the population. The MLM gave values of mean R^2 clustered close to 1.0, much higher than the corresponding values obtained with the null model in essentially every experiment (Figure 2.2d). The R^2 values calculated separately by contrast showed more scatter than the mean R^2, but even here the null model gave values that were distinctly poorer than those obtained with the MLM, including a number of negative values (Figure 2.2e). Again, confidence limits estimated using bootstrapping were used to quantify the significance of these improvements using the MLM (Supplementary Figure 2.10d,e).

The individual optimal HRF_{STIM} kernels were also highly consistent across experiments. All kernels had similar peak latencies and widths (Figure 2.2f). In a cross-validation test (see Online Methods), the signal in any experiment was well predicted by the leave-one-out mean kernel averaged over all

other experiments, with only a slight improvement in the prediction when conducted separately by animal (Figure 2.2f). This consistency of the HRF kernel across experiments and animals suggests that it represents a neuro-vascular coupling mechanism that is intrinsic to this cortical tissue.

The relationship between stimulus-specific hemodynamics and spiking was robustly linear even though the two signals were individually nonlinear functions of stimulus contrast. This can be seen by comparing the areas under the response curves (Figure 2.2a,b). Both the spiking (Figure 2.3a) and hemodynamic responses (Figure 2.3b) had similar hyperbolic (Albrecht & Hamilton 1982) relationships to contrast while being homogeneously linear when plotted against each other (Figure 2.3c). Note that, unlike in earlier reports (Logothetis et al. 2001), the linear regression line (Figure 2.3c) passes through the origin with essentially no *y* intercept or threshold of hemodynamic signal at low spike rate.

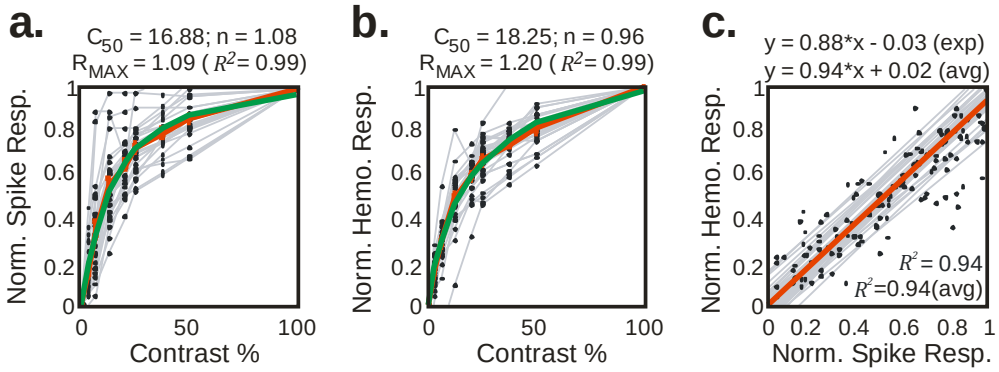

Figure 2.3 – Stimulus-evoked spiking and hemodynamics are hyperbolic functions of stimulus contrast and are linearly related to each other. **(a)** Normalized stimulus-evoked spike responses across contrasts. Each point shows data for a single contrast on a given session, averaged over the integration window as shown in Figure 2.2a. Gray lines link sets of points in individual sessions. The red line (piecewise continuous) indicates the average across sessions. The blue line represents the optimal fitted hyperbolic response function $R(C)$ of contrast C, of the form Albrecht & Hamilton 1982 $R(C) = R_{MAX}\left(\frac{C^n}{C^n+C_{50}^n}\right)$; fitted parameters are shown above. **(b)** Data are presented as in a for stimulus-evoked hemodynamic

responses, averaged over the window as in Figure 2.2b. **(c)** The spiking and hemodynamic responses shown in a and b, plotted against each other. The gray lines are regression lines for each session and the red line is the average of the regression lines. Expressions show regression and R^2, both for the experiments in Figure 2.1 and Figure 2.2a–c (exp) and the population (avg). Population averages were calculated from session values, weighted by number of trials within a session (n = 34 sessions, 3 monkeys).

2.4.3 Trial-related signal consistent in stimulus and dark room

With the stimulus-evoked portion of the signal well characterized by our MLM model, we next estimated the posited spike- and stimulus-independent trial-related signal T (Figure 2.4and Supplementary Note, equation (2,9)). According to the MLM, this is the signal that remains after subtracting away, from the full measured hemodynamics H, all components that can be predicted from spikes. To estimate spike-predicted components, we used our simplifying assumption that the HRF_{STIM} kernel can be applied uniformly to all spiking, whether stimulus evoked or uncontrolled (blank trial). The HRF_{STIM} was obtained, as before (Supplementary Note, equation (7)), by fitting stimulus-evoked spiking (S_{STIM}; Figure 2.4a) to hemodynamics (H_{STIM}; Figure 2.4b). The hemodynamics predicted from full spiking S using this kernel (Figure 2.4c) were clearly different from the full measured hemodynamics (Figure 2.4b). Qualitatively, however, the latter appear to be a sum of the prediction riding on top of a large contrast-independent response.

Indeed, subtracting the predicted from the measured hemodynamics left large remaining signals T that matched each other closely across contrasts. Note, moreover, their substantial strength, which was 1.5-fold greater than that of the maximal H_{STIM} (compare Figure 2.4b with Figure 2.4d). It is important to emphasize that, in our framework, these unpredicted hemodynamic signals are not the results of nonspecific spiking (for example, S_{BLANK}); they comprise the components that, according to the MLM, remain after using HRF_{STIM} to account for the entirety of the spiking-related

hemodynamics, both stimulus evoked and nonspecific (Supplementary Note, equation (9)).

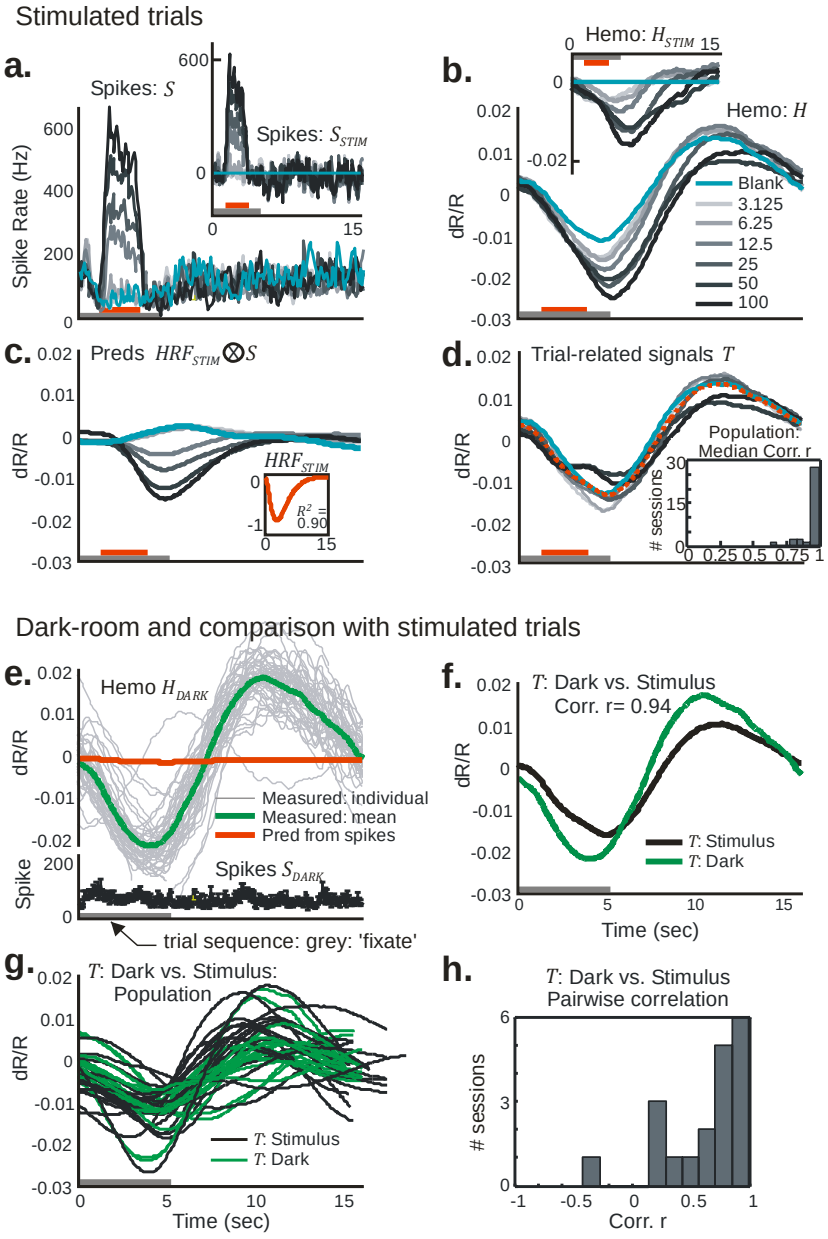

Figure 2.4 – Estimated trial-related signal *T* is consistent across contrasts, across experiments, and between stimulated and dark-room trials. **(a,b)** Spiking (**a**) and hemodynamics (**b**) from another representative session. **Insets**, corresponding S_{STIM} and H_{STIM}. The trial structure is indicated by the

color bars (gray, fixate; red, stimulus; no bar, relax). **(c)** Prediction convolving optimal kernel HRF_{STIM} (**inset**) with full spiking S (that is, $HRF_{STIM} \otimes S$). **(d)** Estimated trial-related signals ($T = \langle H - HRF_{STIM} \otimes S \rangle$; Supplementary Note, equation (9)) shown individually by contrast; red indicates mean across contrasts. Note the high amplitude of mean T (s.d. = 0.0088, compared with 0.0058 for H_{STIM} using 100% contrast; a 1.5-fold difference). Note the marked similarity of signals T across contrasts (correlation (Pearson's r) with leave-one-out means: 0.99, 0.99, 0.99, 0.99, 0.99, 0.99 and 0.96 for contrasts 0–100% in sequence; n = 175 trials, 25 per contrast, 7 contrasts, median r = 0.99). **Inset**, population histogram of median r (mean (s.e.m.) = 0.94 (0.01), n = 34). **(e)** Dark-room trials for the sessions shown in **a**–**d**. Top, hemodynamic traces, H_{DARK}. Gray lines are individual traces, all correct trials (n = 45), the green line is the mean of correct trials, and the red line is the prediction, convolving HRF_{STIM} with dark-room spiking S_{DARK} (bottom trace, black). Trial structure indicated on time axis (periodic fixations in darkness). **(f)** Mean trial-related signals T from stimulus-driven (black) and dark-room trials (green), same session (Pearson's r = 0.94). **(g)** Signals T as in f for full population (n = 19 pairs, monkey T). **(h)** Pairwise correlations between stimulated and corresponding dark-room T over population (mean (s.e.m.), pairwise Pearson's r = 0.61 (0.08), n = 19 pairs).

We quantified the similarity of the trial-related signals T to each other, at different contrasts in an experiment, by correlating the signal T at each contrast (including contrast = 0, blank) with the leave-one-out mean of the signals T calculated at all the other contrasts. All of the resultant correlation (Pearson's r) values were very close to 1.0 (Figure 2.4d). This pattern was repeated over our population of 34 experiments giving, in each case, a median r close to 1.0 (Figure 2.4d).

We wanted to test how well the trial-related signals thus calculated matched each other across experiments and how similar they were to the trial-related signals observed in dark-room fixation tasks (Sirotin & Das 2009). For monkey T, we were successful in getting sets of both dark room and visually stimulated trials in 19 experiments (5 of the current 34, and an additional 14 from a separate project using the same fixation task). Over this population, we found a close match of each residual with the dark-room signal at the

same recording site, as well as a marked similarity of these signals across experiments (Figure 2.4e–h). As in our earlier published data (Sirotin & Das 2009), the dark-room trials evoked high-amplitude stereotyped signals of clockwork-like periodicity despite weak spiking (Figure 2.5e). However, the dark-room trial-related signal *T* (that is, after subtracting the, albeit very small, spike-related prediction obtained by convolving with HRF_{STIM}; Figure 2.4e) closely matched the mean trial-related signal *T* from the visually evoked trials (Figure 2.4f). A similar pattern was seen for each experiment. The sets of all dark-room and visually stimulated trial-related signals were markedly similar (Figure 2.4g) and matched each other well when correlated pairwise for each recording site (Figure 2.4h). This provides compelling evidence for our MLM, that is, that the full hemodynamic signal evoked in an alert task-engaged subject is the linear sum of a spike-related component and a distinct trial-related component that is independent of local spiking or visual stimulation (Supplementary Note, equation (2)).

As an additional test of our premise that the trial-related signal is determined by trial structure independent of stimulus or evoked spiking, we designed a set of experiments in which we varied trial structure while keeping the stimulation parameters unchanged (n = 10 experiments in 2 animals, monkeys S and T; Figure 2.5). Both series consisted of 30-s trials with identical stimulation (gratings, with contrasts: 0% (blank), 12.5% or 100% in block-randomized order, shown once per trial). The trials had different fine structure, however. For one set, the monkey made two fixations at 15-s intervals in each 30-s trial (Figure 2.5a–c), whereas in the other set, the monkey made three fixations at 10-s intervals per 30-s trial (Figure 2.5d–f). The stimulus was presented only during the first fixation, whereas subsequent fixations were on to the blank monitor. Notably, we only considered those trials in which the animal performed sequences of correct fixations extending over the full 30-s trial to be correct trials. Blank trials, correspondingly, consisted of two (Figure 2.5a–c) or three (Figure 2.5d–f) successive correct blank-monitor fixations starting with the blank (0% contrast) stimulus.

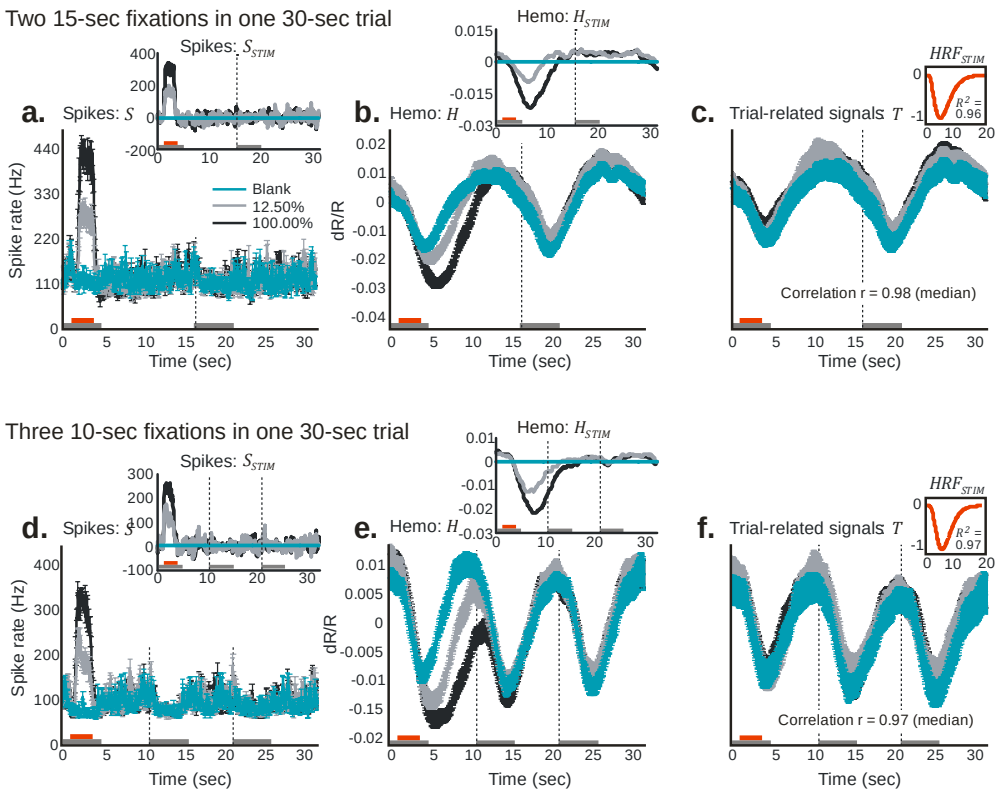

Figure 2.5 – Estimated trial-related signal *T* reflects trial timing independent of stimulus timing or contrast. **(a,b)** Spiking (**a**) and hemodynamics (**b**) for trials consisting of fixation sequences in which the animal fixated with 15-s periodicity, but the stimulus (three contrasts, including 0%, blank) was shown at 30-s intervals, that is, only at the first fixation of each pair. **Insets**, corresponding S_{STIM} and H_{STIM}, calculated by subtracting away blank-trial signals consisting of responses to the pair of fixations on to the blank monitor starting with the blank stimulus (indicated by blue curves). Note monophasic stimulus-evoked H_{STIM} with no evidence of oscillatory rebounds during the blank epoch. The trial structure is indicated by the color bars (gray, fixate; red, stimulus; no bar, relax). **(c)** *T* per contrast. **Inset**, optimal HRF_{STIM} calculated over 30-s trials. Note that the signal *T* is close to exactly periodic at the 15-s fixation periodicity, with identical amplitudes for the first and second fixation periods independent of stimulus strength or evoked spikes in the first fixation (correlation of calculated *T* across stimulus contrasts: 0.98 (median of pairwise correlations between each *T* and the leave-one-out mean of the other two), *n* = 74 trials total, roughly 25 per contrast). **(d–f)** Data are presented as in **a**–**c**, with the same stimuli, presented at the same 30-s intervals, but with the monkey fixating every 10

s. The stimulus was shown only on the first fixation of each triplet (n = 83 trials total, roughly 28 per contrast). All error bars indicate s.e.m.

Even though the recorded spiking S, for both trial structures, was dominated by stimulation at the 30-s trial periodicity (Figure 2.5a,d), the recorded hemodynamics H showed additional powerful modulations, even for the blank trials (Figure 2.5b,e). Notably, this modulation matched the fixation schedule and was thus distinct for the two-fixation versus the three-fixation trials. The signal amplitudes in the second and third intervals were not proportional to the amplitude of the signal in the first fixation interval, as they would have been if they were a result of ringing following the initial stimulation. On subtracting away the relevant blank-trial signals, the stimulus-evoked hemodynamics H_{STIM} in each case showed a monophasic decline to baseline, with comparable time courses (Figure 2.5b,e), as would be expected for a monophasic blood-volume response to the stimulus Sirotin et al. 2009. Finally, the trial-related signals T were, in each case, periodic at the trial fine structure with no apparent modulation by the stimulus (T obtained as above by subtracting away from each measured signal H components predicted from full spiking using the relevant HRF_{STIM}; Figure 2.5c,f).

2.4.4 Spikes poorly predict blank-trial and dark-room signals

As a counterproposal to our MLM, it could be argued that there is no need to invoke any special spike-independent trial-related signal T. Although we have provided evidence that blank subtraction leads to a markedly improved linear fit between the stimulus-evoked portions of the signal, it does not follow that the blank-trial hemodynamics necessarily contain signal components independent of spiking as proposed in the MLM. Instead, it could be that blank-trial hemodynamics are related linearly to the sometimes substantial blank-trial spiking (Figure 2.1b) through a distinct HRF kernel appropriate for low spiking levels that is very different from the kernel linking the stimulus-evoked signals. This, one could argue, is the reason for the mismatch

when trying to predict the full hemodynamics from the full spiking (Figure 2.1). As we show below, however, any such distinct HRF kernels appear arbitrarily variable and unreliable, making this counterproposal highly nonparsimonious and thus implausible.

We first tested whether the blank-trial hemodynamics could be predicted linearly from spiking alone (Figure 2.6a–d and Supplementary Note, equation (11)), as opposed to being modeled by a sum of spike-predicted and trial-related components (that is, MLM; Supplementary Note, equation (4)). Indeed, we could make a reasonable prediction (R^2 = 0.46; Figure 2.6a) by using the optimal blank-fitted kernel HRF_{BLANK} obtained by fitting the blank-trial hemodynamics to blank-trial spiking. This was better than the value of R^2 = −0.19 for the prediction using the same session's HRF_{STIM} (Figure 2.6a). This, however, is not surprising. By definition, the fitting process discovers a kernel that maximally accounts for the variance in the fitted signal. However, the fit here was likely fortuitous. The blank-fitted kernel was fivefold larger in amplitude and opposite in sign to the HRF_{STIM}, giving absurd predictions for the stimulus-evoked signal when convolved with the same session's stimulus-evoked spiking S_{STIM} (Figure 2.6b). Over the population, these blank-fitted kernels were highly variable in amplitude relative to the corresponding HRF_{STIM} (Figure 2.6c) and, moreover, showed a wide scatter in peak latency and width (Figure 2.6c,d). Notably, the presence of both positive and negative amplitudes made it meaningless to even perform a cross-validation test to see how well the kernel from one day can be used to predict the blank signals from other days, in sharp contrast to the reliable predictions obtained through cross-validation for the HRF_{STIM} (Figure 2.2f).

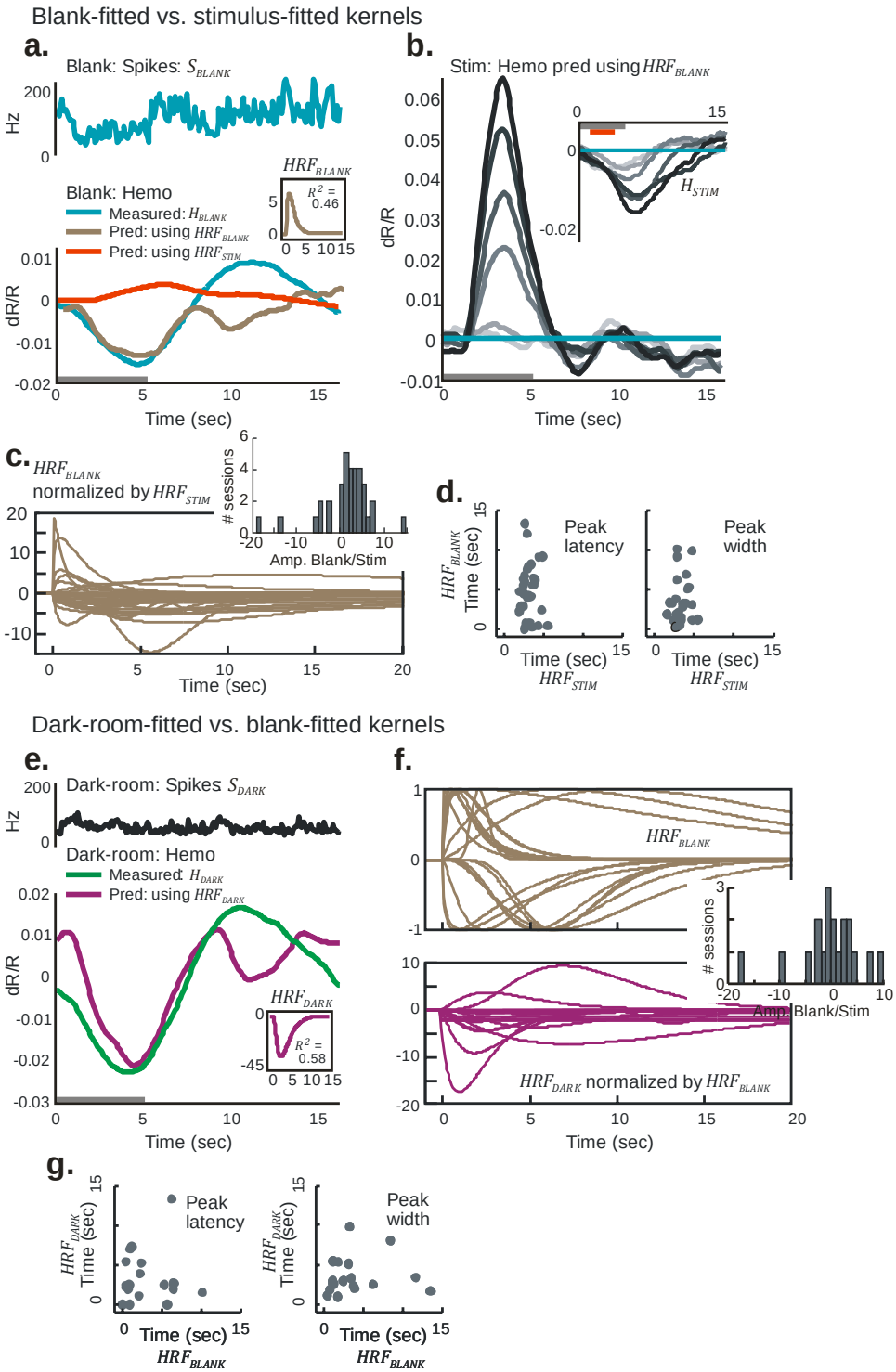

Figure 2.6 – Blank-trial and dark-room hemodynamic responses are poorly fitted to spiking. **(a)** Blank-trial responses (same experiment as shown in

Figure 2.4). Top, S_{BLANK}. Bottom, corresponding H_{BLANK} comparing the measured value (blue) with two alternative predictions: one from S_{BLANK} using session's stimulus-fitted kernel (red, $HRF_{STIM} \otimes S_{BLANK}$, $R^2 = -0.19$, n = 25 trials) and the other using the optimal blank-fitted kernel (brown, $HRF_{BLANK} \otimes S_{BLANK}$, $R^2 = 0.46$). **Inset**, the blank-fitted kernel HRF_{BLANK} (amplitude normalized to HRF_{STIM}). Gray bar indicates fixation. **(b)** Predictions ($HRF_{BLANK} \otimes S_{STIM}$) of stimulus-evoked hemodynamics using blank-fitted kernel. Compare with measured H_{STIM} (**inset**) (mean $R^2 = -11.9$). **(c)** Population of HRF_{BLANK} kernels, each normalized by amplitude of corresponding HRF_{STIM} kernel. **Inset**, histogram of HRF_{BLANK} amplitudes normalized by corresponding HRF_{STIM} (Amp. Blank/Stim., n = 34). **(d)** Peak latencies (left) and widths (right) of HRF_{BLANK} versus HRF_{STIM}. Note the high variability (s.e.m.) in both parameters for the HRF_{BLANK}. Population average latency (s.e.m): blank, 4.6 (0.6) s; stimulus, 3.1 (0.2) s; population average width (s.e.m.): blank, 5.8 (1.0) s; stimulus, 3.3 (0.2) s; n = 33; ignoring one outlier with width = 1.25×10^8 s for the blank). **(e)** Data are presented as in a for the dark-room task (data from Figure 2.4e). Top, S_{DARK}. Bottom, corresponding H_{DARK} comparing measured trace (green) with prediction using the optimal dark-fitted kernel (magenta, $HRF_{DARK} \otimes S_{DARK}$, $R^2 = 0.58$). **Inset**, dark-fitted kernel HRF_{DARK} (amplitude normalized to HRF_{STIM}). **(f) Top**, HRF_{BLANK} kernels normalized by absolute values of their own amplitudes (note variability in time courses). **Bottom**, HRF_{DARK} kernels normalized by corresponding HRF_{BLANK} amplitudes. **Inset**, histogram of HRF_{DARK} amplitudes normalized by HRF_{BLANK} (Amp. Dark/Stim., n = 19 sessions). **(g)** Scatter plots of peak latencies (left, Pearson's r = 0.04) and widths (right, r =0.07) comparing HRF_{DARK} and corresponding HRF_{BLANK} (n = 18; outlier ignored as in **d**).

The presence of both dark-room and visually stimulated trials for 19 recording sites allowed for additional tests of the counterproposal to the MLM. If there exist valid low-spiking-level kernels linearly linking blank-trial spiking to hemodynamics, then such kernels should also be reasonable for linking dark-room spiking to hemodynamics. We tested this possibility by calculating the optimal dark-fitted kernels for each of these sessions (Supplementary Note, equation (12)). These kernels, again provided, by definition, good fits for the given dark-room signals; but they were arbitrarily different from the corresponding blank-fitted kernels. Thus, for the particular

example session, the dark-fitted kernel was opposite in sign and much larger in amplitude (40-fold versus fivefold larger than the amplitude of the session's HRF_{STIM}; Figure 2.6e), reflecting the smaller dark-room spiking amplitude compared with blank-trial spiking. Over the population, we found similarly poor correspondence in amplitude, latency and width between dark- and blank-fitted kernels (Figure 2.6f,g). The apparently arbitrary shapes and sizes of these kernels, when combined with our earlier evidence for lawful and stereotyped trial-related signals when fitting the MLM (Figure 2.4 and Figure 2.5), strongly suggest that dark- and blank-fitted kernels reflect only accidental matches linking weak residual spikes to hemodynamics that are actually dominated by spike-independent trial-related signals.

2.4.5 Blank subtraction required to estimate spikes from imaging

The primary use of neuroimaging is as a proxy for local neural activity. We wanted to quantify the importance of blank subtraction when equating the imaging signal with neural response. To this end, we compared the validity with which we could deduce measured spiking from full versus blank-subtracted hemodynamics by deconvolving (Glover 1999) with the relevant optimal *HRF*. We expected that deconvolving a given blank-subtracted (that is, stimulus evoked) signal H_{STIM} using its optimal kernel HRF_{STIM} would trivially return a valid estimate of the corresponding blank-subtracted (that is, stimulus evoked) spiking S_{STIM}, as these signals were well fitted to each other. What we wanted to assess, for comparison, was the reliability with which the full measured spiking S could be obtained from the full hemodynamics H using a similar deconvolution with its optimal kernel HRF_{NULL}. Given that convolution is equivalent to the product of Fourier transforms in frequency space, we deconvolved by dividing the Fourier transform of the hemodynamic signal by the Fourier transform of the relevant HRF kernel. As HRFs have very little power at high temporal frequencies, reflecting the slow time course of the hemodynamic response Sirotin et al. 2009, we restricted

the effective frequency range of this division with an appropriate filter in frequency space to prevent amplifying high-frequency noise in the hemodynamic signal (Online Methods).

As expected, the estimate of spiking obtained by deconvolving the mean H_{STIM} with HRF_{STIM} closely matched the measured S_{STIM}, albeit without the high-frequency features (mean R^2 = 0.64 for the predicted spike trace; Figure 2.7a,b). The match was even better when comparing the estimated spiking not with S_{STIM}, but with its low pass–filtered version, using the same filter as used for the deconvolution (mean R^2 = 0.82; Figure 2.7b and Online Methods).

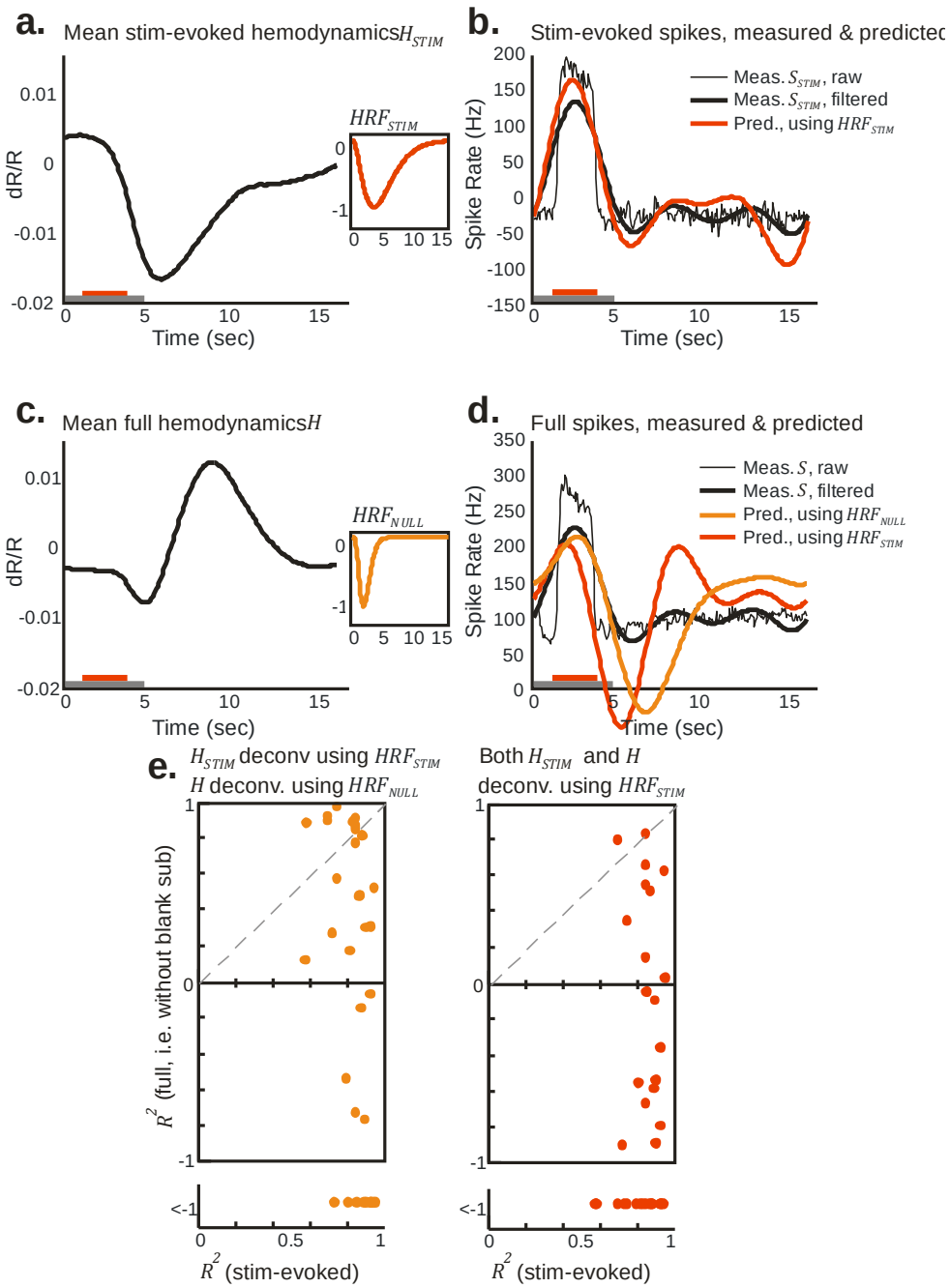

Figure 2.7 – Blank-subtracted, but not full, hemodynamic signal is a good proxy for local spiking responses. **(a)** Mean stimulus-evoked (that is, blank subtracted) hemodynamic response H_{STIM} averaged across contrasts for one experimental session. **Inset**, corresponding HRF_{STIM} (n = 162 trials,

roughly 41 per contrast, mean R^2 = 0.93). The trial structure is indicated by the color bars (gray, fixate; red, stimulus; no bar, relax). **(b)** Mean stimulus-evoked spiking. Thin black line, mean stimulus-evoked (blank subtracted) measured spiking S_{STIM}. Thick black line, low pass–filtered mean stimulus-evoked spiking S_{STIM}. Red, spiking estimated by deconvolving H_{STIM} with HRF_{STIM}. Note the good match with measured S_{STIM} (R^2 = 0.82 with low pass–filtered S_{STIM}, R^2 = 0.64 without low-pass filtering). **(c)** Mean full hemodynamics H: same data as in a, but without blank subtraction. **Inset**, corresponding HRF_{NULL}. Note the poor mean R^2 = 0.37 compared with HRF_{STIM}. **(d)** Mean full spiking without blank subtraction. Thin black line, mean measured spiking S. Thick black line, low pass–filtered mean measured spiking S. Orange, spiking estimated by deconvolving H with HRF_{NULL} (R^2 = −0.53). Red, spiking estimated by deconvolving H with HRF_{STIM} (R^2 = −1.18; session mean spike rate added to deconvolved signals to align with measured spikes on vertical axis). Note the poor match of either estimate with measured full (low pass–filtered) spiking S. **(e)** Comparing R^2 for estimates of spiking from full and stimulus-evoked hemodynamic signals over the population. Orange, H_{STIM} deconvolved with HRF_{STIM} and H deconvolved with HRF_{NULL}. Red, both H_{STIM} and H deconvolved using HRF_{STIM}. Note the uniformly high R^2 for estimating S_{STIM} from H_{STIM} (mean R^2 (s.e.m.) = 0.85 (0.02), n = 34) versus low R^2, including many large negative values for estimating S from full H (using HRF_{STIM}, mean R^2 = −2.5 (0.9); using HRF_{NULL}, mean R^2 = −2.5 (1.0); n = 34).

In contrast, deconvolving the full H using HRF_{NULL} (Figure 2.7c) gave an estimate of neural spiking that poorly matched the mean full S, with large oscillations following the primary peak (mean R^2 = −0.53; Figure 2.7d). As a control, we tried deconvolving not with HRF_{NULL}, but with HRF_{STIM}, as the latter is arguably a better optimal kernel for this data set. This estimate of neural activity was no better (mean R^2 = −1.18; Figure 2.7d). Comparable results were seen over the population (Figure 2.7e), where the measured stimulus-evoked (that is, blank subtracted) spiking was uniformly well estimated from stimulus-evoked hemodynamics. In contrast, the full spiking was very poorly estimated from the corresponding full hemodynamics, whether the deconvolution was performed using HRF_{STIM} or HRF_{NULL}.

2.5 Discussion

We used simultaneous optical imaging and electrode recording to relate cortical neuroimaging signals to local neural spiking in alert subjects performing periodic sensory tasks (from V1 of macaque monkeys performing periodic visual tasks). We demonstrate a parsimonious model of the measured imaging signal, the MLM. In our model, the measured imaging signal is a linear sum of two distinct components: a spike-associated component tightly related to stimulus intensity and local spiking, and a trial-related component that seems to be determined only by the timing and structure of the task, independent of stimulus or local spiking. The trial-related component can be removed linearly, for example, by subtracting the responses to blank trials (Figure 2.2) that have exactly the same timing structure as stimulated trials (Figure 2.5b,e). This blank subtraction leaves a stimulus-evoked signal (Supplementary Note, equation (6)) that is homogenously linear with stimulus-evoked local spiking over the full range of stimulus intensity from baseline to near-maximal (Figure 2.2a–c and Figure 2.3, and Supplementary Note, equation (7)). The HRF kernel relating these two signals is largely invariant in shape across recording sites and animals (five hemispheres, three monkeys; Figure 2.2f), suggesting that it reflects the true neurovascular coupling in this cortical region. By the same token, this stimulus-evoked neuroimaging signal is a faithful proxy for the stimulus-evoked local spiking (Figure 2.7). In contrast with the excellent fit of the stimulus-evoked signals, the second component of our model, the trial-related signal, has a notably poor fit to local spiking (Figure 2.6). It is, however, reliably trial-locked and robust across stimulus conditions, including total darkness (Figure 2.4d–h and Figure 2.5c,f). Given that the amplitude of the trial-related signal can exceed the maximal stimulus-evoked signal (Figure 2.4), failure to account for it properly can lead to marked errors when using the neuroimaging signal to estimate neural spiking (Figure 2.7).

It is instructive to compare our results with the body of recent work relating neural spiking to hemodynamics (Heeger et al. 2000; Rees et al. 2000; Logothetis et al. 2001). First, our results suggest that a simple linear model, with the critical addition of the trial-related, spike-independent signal component, can, in fact, reveal a reliable quantitative relationship between the spike rate of neurons and the hemodynamic response, in contrast with earlier results that have suggested the lack of any such relationship (Logothetis et al. 2001). Note, however, that the good prediction of stimulus-specific hemodynamics from spiking does not imply that spiking causes hemodynamics Lee et al. 2010; the actual signals driving hemodynamics are as yet poorly understood (Logothetis 2008). Next, our observed homogenous linear relationship between stimulus-evoked spiking and hemodynamics (Figure 2.3) differs from the pronounced threshold nonlinearity reported earlier (Logothetis et al. 2001). This difference is unlikely to be a result of trial-related signals, as the previous study was conducted using anesthetized animals. It could be an artifact of anesthesia or it may be a nonlinearity in neurovascular coupling resulting from the long stimulus durations used, up to 24 s, versus the shorter and more natural 2–3 s that we used. Understanding this difference should provide valuable insights into neurovascular coupling.

Although our use of the cortical blood volume signal may have made it easier to validate our model, our findings should be broadly applicable to all hemodynamics-based neuroimaging techniques, including blood oxygen level–dependent (BOLD) fMRI. The monophasic blood-volume impulse response to stimulus-evoked spikes (Sirotin et al. 2009; Devor et al. 2003; Sheth et al. 2004; Nemoto et al. 2004) allowed us to fit the stimulus-evoked signals with high reliability using a single gamma-variate kernel and minimal free parameters. By the same token, it allowed us to unambiguously deconvolve hemodynamics and estimate spiking. This let us easily demonstrate key features of the MLM, including the linear separation of stimulus- and task-related signal components. The more complex BOLD and other blood

oxygenation–related signals with their multiphasic responses and ringing (Ress et al. 2009; Grinvald et al. 1999) could have made fitting hemodynamics to spiking technically more challenging and possibly more ambiguous. However, given our results using the blood volume signal, we expect to see effects in BOLD fMRI that are qualitatively very similar. Although the quantitative relationship between BOLD and blood volume varies across brain regions and even across cortical layers Mandeville et al. 2001, the two signals mostly track each other closely in overall time course in an individual brain region (Mandeville et al. 2001). The strengths of both signals are similarly graded in response to stimulus strength, including similarly non-monotonic and sign-reversed responses (Zhao et al. 2012). Both BOLD fMRI and blood volume signals also share overall broad time courses with concurrent intrinsic-signal optical imaging and can be reliably predicted from the latter (Kennerley et al. 2009). Finally, it should be noted that at least two groups measuring BOLD fMRI signals in humans have, as we have, reported stimulus-independent task-related signals entrained to task timing that need to be subtracted linearly from the overall neuroimaging signal to relate hemodynamics to sensory stimulation (Pestilli et al. 2011; Jack et al. 2006; Donner et al. 2008) (these studies, being in humans, did not include electrodes in the brain to examine the neural underpinnings of the task-related signals).

Our findings have a substantial bearing on the growing field of functional neuroimaging in alert task-engaged subjects. It is now clear that such imaging signals contain robust non-sensory components reflecting, for example, anticipatory attention, task structure and response preparation (Jack et al. 2006; Sylvester et al. 2007; Donner et al. 2008; Kastner et al. 1999; Ress et al. 2000; Serences et al. 2004; Silver et al. 2007). Our trial-related signal likely belongs to the same class. At a practical level, our combination of imaging and electrode recordings quantifies both the effectiveness and critical necessity of task designs that subtract away this task-related non-sensory signal. A number of currently used task designs,

proposed earlier on empirical grounds, already do so effectively; these include designs that linearly subtract either blank (Pestilli et al. 2011; Shtoyerman et al. 2000; Larsson et al. 2006) or nonspecific global from local signals (Donner et al. 2008; Fox et al. 2006), designs that contrast one sensory stimulus against another in a common task structure (Meng et al. 2005; Cheng et al. 2001), and designs that regress the hemodynamic signal against a range of stimulus intensities (Engel et al. 1997; Boynton et al. 1999). Notably, for such subtraction to properly reveal stimulus-related signals, the subtracted trial presumably needs to be identical to stimulated trials in all respects (timing, reward, evoked anticipation, etc.), differing only in not containing the stimulus of interest.

At another level, however, the robust link between stimulus-evoked hemodynamics and spiking throws into sharper relief the lack of such a link for the trial-related signal and suggests that other non-sensory signals may be similarly poorly related to local spiking (Jack et al. 2006; Donner et al. 2008). For example, there is a well-known discrepancy between robust fMRI evidence for attentional modulation in human V1 (ref. Ress et al. 2000) and the lack of such modulation in electrode recordings from macaques (Luck et al. 1997). Our findings raise the possibility that this entire class of non-sensory signals could have neural underpinnings distinct from sensory-driven spiking activity. The trial-related signal described here is also distinct from the coherent ongoing V1 activity imaged in anesthetized animals (Arieli et al. 1995), as the latter was closely correlated with local spiking and LFP (Arieli et al. 1995). The trial-related signal may involve neuromodulatory (Logothetis 2008) input from some brain stem center that tracks behavioral timing or it may reflect feedback from some higher cortical center. Furthermore, it could act preferentially on cells other than pyramidal neurons, such as interneurons or astrocytes. There is also the possibility of direct neuromodulatory control of blood vessels giving rise to the hemodynamic signal (Krimer et al. 1998). Finally, when interpreting recorded hemodynamics as a measure of local neural activity, it remains to be established whether the

strength of the trial-related signal can be equated with that of stimulus-evoked signals on any common measure, such as a metabolic one of energy consumption.

A number of additional questions remain. We have demonstrated the MLM for area V1. It would be important to see how well it generalizes over other brain regions. Furthermore, we controlled spike rate by varying the contrast of large, uniform gratings, which changes activity monotonically over the population of activated neurons. We could get valuable insights by controlling spike rates in a manner that differentially targets different neuronal populations, for example, by having punctate stimuli, thereby possibly getting different rates of spatial drop-off in different signals (LFP, spiking, hemodynamics). We noted that the goodness of fit between sensory hemodynamics and gamma-band LFP was much more variable than with spiking (data not shown), in contrast with earlier reports Logothetis et al. 2001. Finding answers to these questions would be critical for interpreting functional brain imaging.

2.6 Supplementary information

2.6.1 Appendix: Homogeneous Linear ('Null') and Modified Linear Model (MLM) of Spike-predicted Hemodynamics Appendix: Homogeneous Linear ('Null') and Modified Linear Model (MLM) of Spike-predicted Hemodynamics

Let us define the full measured hemodynamic signal as *H(t)* and the net local spiking as *s(t)*. The homogeneous linear model (our 'Null' model) proposes that the two should be related through:

$$H = hrf \otimes s + n \quad (1)$$

where (⊗) denotes convolution, *hrf(t)* is an appropriate hemodynamic response kernel and *n(t)* is noise (the explicit '*(t)*' dependence is dropped in this and subsequent equations to avoid clutter). By contrast, the Modified Linear Model ('MLM') proposes that *H* and *s* are related through:

$$H = hrf \otimes s + T + n \qquad (2)$$

where *T* is the anticipatory trial-related hemodynamic signal Sirotin & Das 2009. is modeled here as a spike-independent signal at trial periodicity, aligned to trial onsets and present in all correctly completed trials Sirotin et al. 2012. We assume that the shape of *T* is determined only by trial timing, independent of whether the trial has a visual stimulus or a blank, or even involves dark-room fixation. Note that these equations are expressions of the functional forms of the respective models; for any data set, the optimal *hrf* satisfying Eq 1 is likely to be different from that satisfying Eq 2.

To test these models against data we assumed that the *hrf* kernels – here, 'impulse functions' quantifying the monophasic spike-triggered increase in local blood volume – can be modeled as standard monophasic gamma-variate functions (Cohen 1997). Optimal kernels were calculated for each model by fitting to data through a standard least-squares routine – specifically, fitting the appropriate mean measured hemodynamic response, aligned to trial onsets and averaged over all contrasts and all correct trials, to the corresponding mean spiking response. (See Methods)

For the 'null' model this process generates the kernel defined as 'HRF_{NULL}' (best fitting the equation $H = HRF_{NULL} \otimes S$) where *S* is the measured spiking. The optimal predicted hemodynamics, using this model, then becomes:

$$H_{NULL}^{PRED} = HRF_{NULL} \otimes S \qquad (3)$$

(A note on nomenclature: upper case '*S*', '*HRF*' etc will be used throughout to distinguish the measured spiking and fitted kernels from their 'idealized' equivalents (in lower case) as in Eq 1,2. This is to formally recognize that while the *H* in Eq 1 can be equated with measured hemodynamics, the measured multi-unit is *S* only a sample of the 'true' net local spiking '*s*'. The sample on any given session depends on the electrode tip, MUA spiking threshold etc. With later control experiments we show that the sampling is reliable across days, with the primary variability being restricted to an

irrelevant scale factor. (see last section of Methods and Supplementary Figure 2.11).)

For fitting the MLM to data it is necessary to first separate the trial-related *T* from spike-predicted hemodynamic components. We do so by subtracting blank-trial responses from other trials, based on our assumption that *T* is stereotyped and present in all correct trials. In blank trials, hemodynamics H_{BLANK} and spiking s_{BLANK} should be related by:

$$H_{BLANK} = hrf \otimes s_{BLANK} + T + n \qquad (4)$$

The s_{BLANK} is the trial-related blank-trial spiking noted earlier (Figure 2.1b), presumably due to uncontrolled visual input associated with the animal's trial-locked eye fixations. Note that the MLM explicitly relates this spiking to its hemodynamic correlate with a common *hrf* like any other visually evoked spiking. On taking means across all correct trials, aligned to trial onsets, (denoted by the symbol ⟨⟩) we get:

$$\langle H_{BLANK} \rangle \approx hrf \otimes \langle s_{BLANK} \rangle + T \qquad (5)$$

which, on subtracting from Eq 2 gives: (Note: blank-trial subtraction has been used empirically earlier in image analysis (Shtoyerman et al. 2000; Larsson et al. 2006)):

$$H - \langle H_{BLANK} \rangle = hrf \otimes (s - \langle s_{BLANK} \rangle) + n \qquad (6)$$

Let us define these blank-subtracted hemodynamics and spiking as the corresponding 'Stimulus-evoked' quantities $H_{STIM} = H - \langle H_{BLANK} \rangle$ and $s_{STIM} = s - \langle s_{BLANK} \rangle$. Eq 6 can then be rewritten:

$$H_{STIM} = hrf \otimes s_{STIM} + n \qquad (7)$$

The *hrf* in this model (identical in Eqs 2 and 4 through 7) can now be estimated by fitting the measured $s_{STIM} = S - \langle S_{BLANK} \rangle$ to the measured $H_{STIM} = H - \langle H_{BLANK} \rangle$ using Eq 7, to give an optimal gamma-variate kernel HRF_{STIM}. The corresponding predicted 'Stimulus evoked' hemodynamics is then:

$$H_{STIM}^{PRED} = HRF_{STIM} \otimes S_{STIM} = HRF_{STIM} \otimes (S - \langle S_{BLANK} \rangle) \qquad (8)$$

This HRF_{STIM} can be used to obtain the presumed trial-related signal *T*. We can define *T* as the mean signal that remains after subtracting, from the full

measured *H*, all signal components predictable from measured spiking whether stimulus evoked or uncontrolled (Eq 2). With our assumption that all visually driven hemodynamics is related to corresponding spiking through a common HRF_{STIM}, we get:

$$T \approx \langle H - HRF_{STIM} \otimes S \rangle \qquad (9)$$

Finally, to evaluate the goodness of fit of each model we compared model predictions with their experimentally obtained correlates. The comparisons were quantified using the measure R^2, defined:

$$R^2 = 1 - \frac{\sigma^2_{RESIDUAL}}{\sigma^2_{MEASURED}} \qquad (10)$$

where $\sigma^2_{MEASURED}$ and $\sigma^2_{RESIDUAL}$ are, respectively, the variance of the measured hemodynamics, and of the residual error. This latter quantity is defined, in general, as the difference between measured and predicted signals. R^2 always has a value <= 1; the closer it is to 1, the smaller the residual relative to the measured signal, and the better the fit. In cases where the prediction is made using the optimal kernel for the given measured signal, R^2 defines the fraction of signal variance explained by the prediction, and it lies, by definition, between 0 and 1. For the null model this is the case, for example, when comparing the mean H^{PRED}_{NULL} averaged across all contrasts, against the corresponding mean measured *H* since these quantities are optimally linked via HRF_{NULL} (see Eq 3. The residual here is defined as $(H - H^{PRED}_{NULL})$). However, R^2 is also a useful measure in other comparisons, e.g. when quantifying how well the optimal kernel for the overall mean signal (averaged across contrasts) predicts the signal for particular contrasts. For the subset of trials at a particular contrast the error can be much larger than the measured signal, leading to large negative R^2 values.

We used the same formalism to test two controls that we contrasted against the MLM (Results, Section 6). As the first control we checked whether the blank-trial hemodynamic signal H_{BLANK} could be predicted linearly from blank-trial spiking alone:

$$H_{BLANK} = hrf \otimes s_{BLANK} + n \qquad (11)$$

This equation can be fitted using the measured S_{BLANK} to formally define an optimal kernel 'HRF_{BLANK}', and corresponding prediction $H_{NULL}^{PRED} = HRF_{BLANK} \otimes S_{BLANK}$. The goodness of this fit could be quantified using a measure R^2 defined as above, with the residual being $(H_{BLANK} - H_{BLANK}^{PRED})$ and the measured signal H_{BLANK}.

The same formalism can be used to test the control model that dark-room hemodynamics can be predicted using dark-room spiking alone:

$$H_{DARK} = hrf \otimes s_{DARK} + n \qquad (12)$$

This equation can be fit similarly using the measured S_{DARK} to define an optimal kernel 'HRF_{DARK}', corresponding prediction $H_{DARK}^{PRED} = HRF_{DARK} \otimes S_{DARK}$, residual $(H_{DARK} - H_{DARK}^{PRED})$ and goodness of fit R^2.

2.6.2 Supplementary Figures

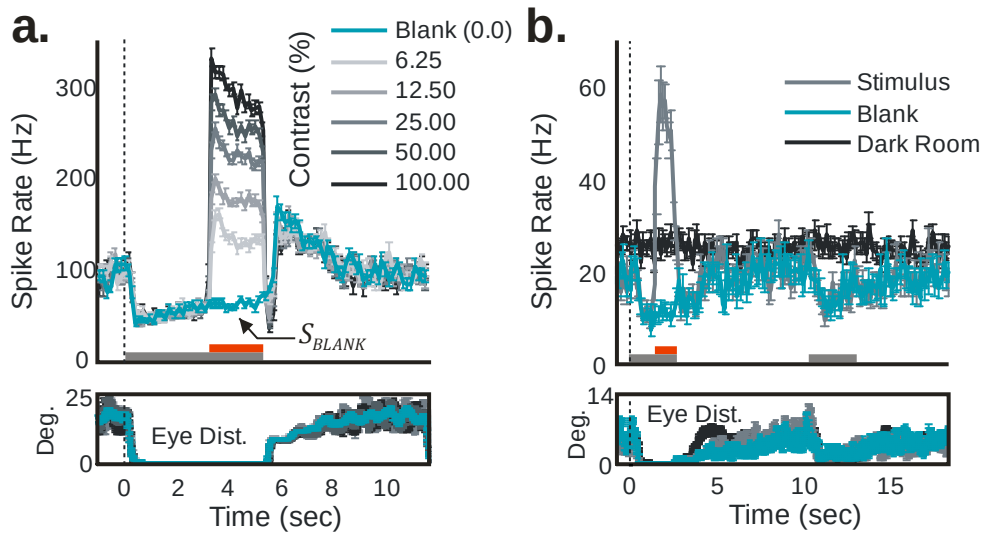

Figure 2.8 – Blank-trial spike trace S_{BLANK} is likely visually driven, entrained to eye fixation schedule. **(a)** Upper panel: Same as Figure 2.1b (full spiking, aligned to trial onsets and averaged by contrast). Lower panel: Corresponding eye tracker records, also averaged by stimulus contrast, showing the monkey's eye position relative to the fixation point. Note the

striking similarity between the eye position traces (for all stimulus contrasts) and the blank-trial spike trace S_{BLANK}: high spiking before the animal fixates (i.e. before t=0 s, trial onset); lower spiking while the animal fixates on the grey monitor (t= 0 to 5.5 s) and high again when the animal looks away at the end of the fixation period. The same spiking pattern forms the common baseline for all spiking responses, independent of stimulus contrast. **(b)** Blank-trial spiking pattern is extinguished in darkness, even though the eye fixation schedule is unchanged. Upper panel: Spiking records from a day with both visually stimulated trials (one 25% contrast stimulus and a blank) and dark-room trials in the same experimental session. (All trials involved a common pattern of two fixations, as in Figure 2.5a-c; 9-s fixations, 18-s trials). Both the 'stimulus' and the 'blank' trials show the same common baseline of reduced spiking as the animal fixates and increased spiking in between fixations. No such fixation-linked fluctuations in spiking can be seen in the dark-room trials. Lower panel: Corresponding eye-position traces, essentially identical regardless of trial type, (stimulated or dark-room). Periods of fixation and stimulation indicated on the time line in color key as in all other figures.

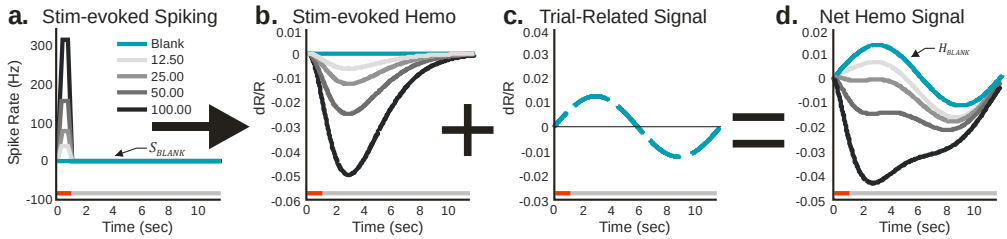

Figure 2.9 – Schematic of Modified Linear Model (MLM). **(a)** Stimulus-evoked spiking, shown as responses to stimuli of different contrasts, linearly predicts corresponding stimulus-evoked hemodynamics **(b)** However, since the animal is engaged in a periodic task, on every (correct) trial there is an additional stereotyped Trial-Related Signal **(c)** that adds on linearly to give the net hemodynamic signal **(d)**. Importantly, because the Trial-Related Signal adds on to every trial, it can also be linearly removed to reveal the 'pure' stimulus-evoked hemodynamics (panel **b**) by subtracting the blank-trial response ('H_{BLANK}', panel **d**) from responses at other contrasts (other traces, panel d). The blank-trial spiking 'S_{BLANK}' is shown here as a flat line in panel **a**. If in addition to the specific stimulus-evoked spiking there had also been a trial-related spiking response – presumably due to the animal moving his eyes periodically away from and back towards the monitor (Figure 2.1b, Supplementary Figure 2.8) – this spiking signal (not shown

here, to avoid clutter) would just have added uniformly to each trace in panel **a**. The corresponding hemodynamic response – predicted, according to the MLM, using the same kernel as the stimulus-evoked hemodynamics – would have added uniformly to each trace in panels b and d including, in particular, H_{BLANK}. On subtracting the net blank-trial response H_{BLANK} these other trial-related signals would also get linearly subtracted away revealing just the stimulus-evoked signals (Figure 2.2a,b). Trial timing is indicated as usual in all panels, with periodic fixation, stimulus presentation and end of trial (i.e. start of next trial). Stimulation period is not indicated in panel **c** to emphasize that the trial-related signal is driven by the task structure alone.

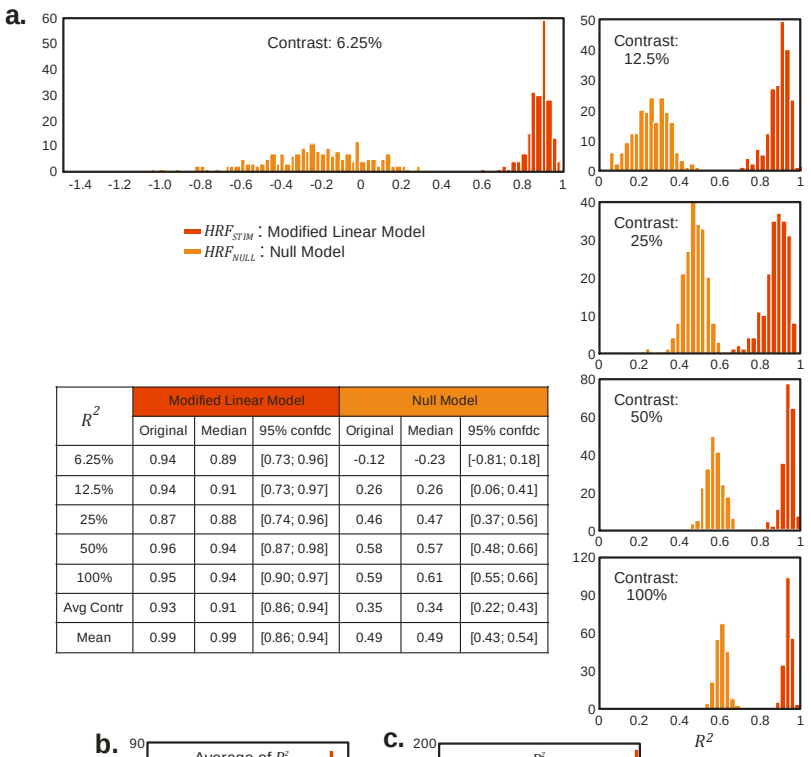

R^2	Modified Linear Model			Null Model		
	Original	Median	95% confdc	Original	Median	95% confdc
6.25%	0.94	0.89	[0.73; 0.96]	-0.12	-0.23	[-0.81; 0.18]
12.5%	0.94	0.91	[0.73; 0.97]	0.26	0.26	[0.06; 0.41]
25%	0.87	0.88	[0.74; 0.96]	0.46	0.47	[0.37; 0.56]
50%	0.96	0.94	[0.87; 0.98]	0.58	0.57	[0.48; 0.66]
100%	0.95	0.94	[0.90; 0.97]	0.59	0.61	[0.55; 0.66]
Avg Contr	0.93	0.91	[0.86; 0.94]	0.35	0.34	[0.22; 0.43]
Mean	0.99	0.99	[0.86; 0.94]	0.49	0.49	[0.43; 0.54]

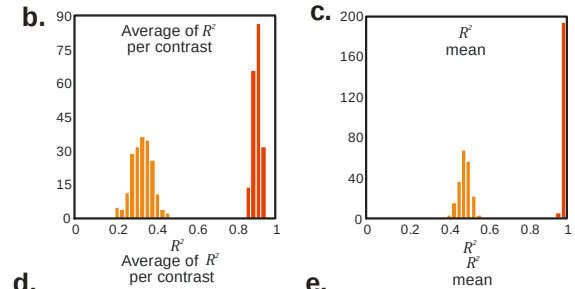

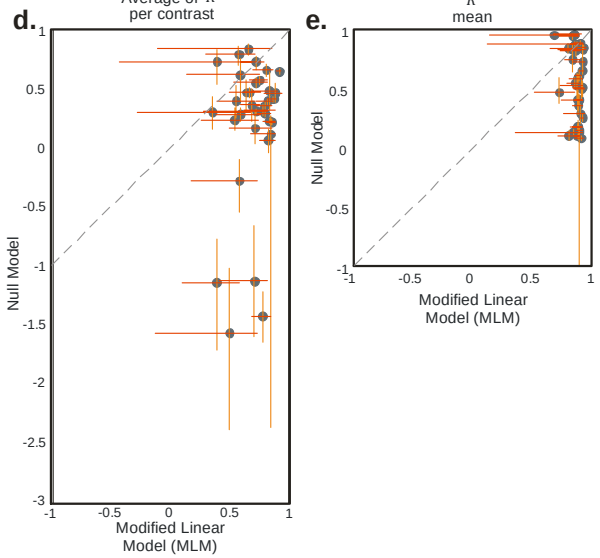

Figure 2.10 – Comparing confidence intervals for the goodness of fit R^2, for the Modified Linear Model (MLM) vs. the Null Model, bootstrap results. (Table and **a**-**c**: for same example data set as in Figure 2.1, Figure 2.2; **d**,**e**: population). **(a)** Superimposed histograms of R^2 distributions, for the Modified Linear Model (MLM), in red, and the Null Model in orange (200 bootstrap runs, using sets of trials chosen randomly with replacement, each set processed using both MLM, i.e. fitting HRF_{STIM}, and Null Model, i.e. fitting HRF_{NULL}, and calculating corresponding R^2. See Methods for details). R^2 calculated separately per contrast, as in the values labeling individual traces in Figure 2.2c. Note that while the histograms for the different contrasts have the same X scale, the 6.25% contrast panel has different X limits because at this contrast the R^2s extend into negative values. N = 261 trials total, roughly 43 per contrast. **Table** summarizing the bootstrapping results for the example data set. Original refers to the R^2 obtained for the full (original) dataset. Median designates the median of the bootstrapping procedure, and '95% confdc' the 95% confidence interval calculated for the bootstrapping. Numbers in left-most column refer to stimulus contrasts; 'Avg Contr' refers to the average across all contrast, i.e. as in panel b, and 'Mean' refers to the mean R^2 i.e. as in panel **c**. **(b)** R^2 values from panel a, averaged across contrasts. Same calculation as in Figure 2.2d. **(c)** Mean R^2 for the same bootstrap trial selections as in panels a,b but calculated after first averaging the trials across contrasts (calculations as in Figure 2.2c inset). **(d)** Comparing bootstrap-derived estimates of R^2 for Null vs. MLM over population of experiments. Calculated separately by contrast and then averaged, as in panel b. We used 80% confidence limits in the population data, to accommodate some data sets with long tails in bootstrap distributions. Data points show the medians of bootstrap estimates while error bars show corresponding 80% confidence limits. Same data as shown in Figure 2.2e. Note, however, that the data points in Figure 2.2e indicate R^2 for the experimentally obtained set of trials and are thus consistently slightly higher than the medians of the corresponding bootstrap estimates here. **(e)** Same, but for 'Mean R^2' calculated as in panel c. Same data as shown in Figure 2.2d (again, data points slightly different from Figure 2.2d since Figure 2.2d shows R^2 for actual trial set).

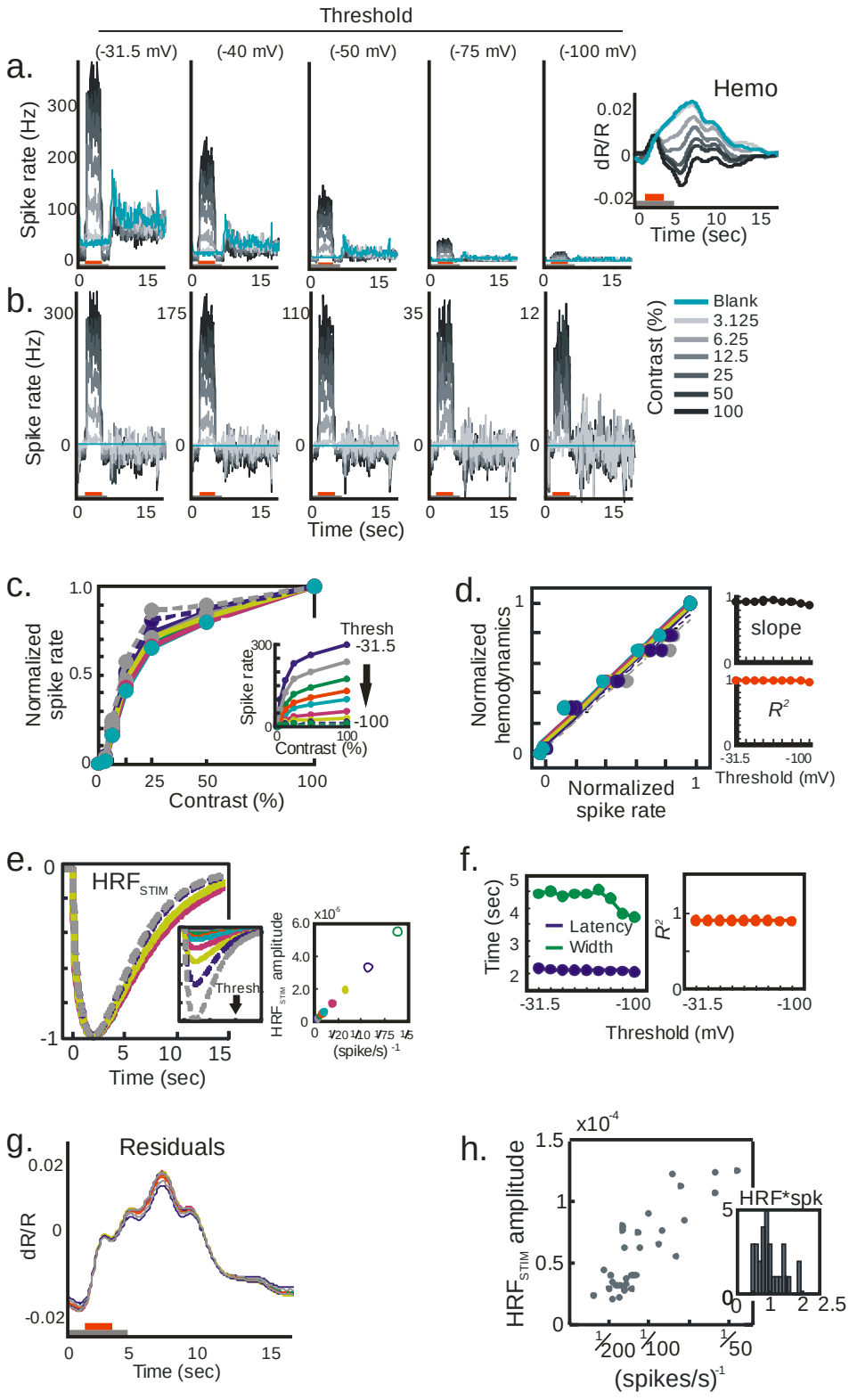
Threshold
a.
(-31.5 mV)
(-40 mV)
(-50 mV)
(-75 mV)
(-100 mV)
Spike rate (Hz)
Hemo
dR/R
Time (sec)
b.
Contrast (%)
Blank
3.125
6.25
12.5
25
50
100
Time (sec)
c.
Normalized spike rate
Contrast (%)
Thresh
-31.5
-100
d.
Normalized hemodynamics
Normalized spike rate
slope
R^2
Threshold (mV)
e.
HRF_{STIM}
Thresh
Time (sec)
HRF_{STIM} amplitude
(spike/s)$^{-1}$
f.
Time (sec)
Latency
Width
Threshold (mV)
g.
Residuals
dR/R
Time (sec)
h.
HRF_{STIM} amplitude
HRF*spk
(spikes/s)$^{-1}$

Figure 2.11 – Primary findings of this study are stable against variations in electrode recording conditions, which result in no more than an irrelevant scale factor in the *HRF* kernel amplitude. Panels **a**-**g**: Simulating the effect of varying spike rates by changing spike thresholds for a fixed imaging signal. Panel **h**: Testing linearity of fitted *HRF* amplitude against the inverse of measured spike rate, over the full population of experiments. **(a)** Measured sets of full spiking responses *S* obtained using different spike thresholds, for one dataset that was re-thresholded offline (thresholds levels are indicated above each panel for the first downward-going voltage excursion). **Inset**: the corresponding full measured hemodynamic signal *H*. N = 248 trials (between 35 and 36 per contrast). **(b)** Similar to corresponding panels in a, but blank subtracted (i.e. S_{STIM}) and scaled, in each case, to approximate peak spike rate at given threshold level. Note different spiking rate scale limits. **(c)** Normalized stimulus-evoked spiking across contrasts for the different threshold levels (as in Figure 2.3a; integration window for mean spike rate: coextensive with stimulus duration, as in Figure 2.2a). **Inset**: Same data, without normalizing spike rates. **(d)** Main panel. Linear relationship between spike and hemodynamic responses (similar to Figure 2.3c) for various threshold levels. Note that only the spiking (but not the hemodynamic) responses change for the various thresholds. Side panel insets: **Top**: the distribution of slopes (from the linear regression between normalized spike rates and normalized hemodynamic responses as in Figure 2.3c). **Bottom**: the corresponding R^2 for the different thresholds. **(e)** Main panel: Population of the optimal fitted HRF_{STIM} kernels for the different thresholds, normalized for peak amplitude. Side panels: **Inset left**: Same kernels, non-normalized. **Inset right**: HRF_{STIM} amplitude plotted against the inverse of the spiking rate. Note the linear relationship. **(f)** Left: distribution of the parameters: latency (blue) and width (green) of the different HRF_{STIM} kernels for the different thresholds. Right: corresponding goodness of the fits, R^2 (red). **(g)** Estimated trial-related signals $T = \langle H - HRF_{STIM} \otimes S \rangle$ calculated using the different *S* and corresponding HRF_{STIM} for the different thresholds. Note: they essentially overlay each other precisely. **(h)** Distribution of amplitudes of the optimal HRF_{STIM} versus the inverse of the spike rate amplitude S_{STIM} for the full population of experimentally measured values; each data point corresponds to one experimental session. Linear regression: correlation (Pearson's r) = 0.91, N=34. Note robustness of the linear regression despite measured values of S_{STIM} ranging from 329 spikes/s down to 32 spikes/s across our data sets. **Inset**: distribution of the product of amplitudes, (HRF_{STIM} x S_{STIM}). Values are shown normalized by the median of this product, to highlight clustering around 1.0. Note that

measured hemodynamic amplitudes were roughly similar across experiments since we used similar ranges of stimulus intensities. This allowed for a simple scaling of HRF_{STIM} with inverse S_{STIM} over the population. Note, further, that through the course of the chapter we have already shown that the major features of the MLM model are constant across experiments (*HRF* shape, goodness of fit, trial-related signal *T* for an animal, etc.). This demonstrates that the primary effect of variation in electrode recording conditions appears to be restricted to an irrelevant scale factor in the kernel amplitude.

2.7 Acknowledgements

We would like to thank J. Krakauer, F. Pestili, T. Teichert, L. Paninski, G. Patel and S. Small for critical comments. The work was supported by US National Institutes of Health grants R01 EY019500 and R01 NS063226 to A.D., a National Research Service Award to Y.B.S., and grants from the Columbia Research Initiatives in Science and Engineering, the Gatsby Initiative in Brain Circuitry, and The Dana Foundation Program in Brain and Immuno Imaging to A.D. M.M.B.C. was supported by Fundação para a Ciência e a Tecnologia scholarship SFRH/ BD/33276/2007.

3 The hemodynamic task-related signal in primary visual cortex of alert non-human primates performing simple tasks

3.1 Introduction

Up until here we have discussed the hemodynamic response to an external visual stimulus, and how this response can be related to underlying neural activity, in the context of an ongoing task. We described a simple model to separate task-related components and stimulus related components of the hemodynamic response (Cardoso et al. 2012). However there remain open questions about the task-related hemodynamic response. Whether there is a behavioral role for this signal? What is the underlying pattern of neural activity associated with this hemodynamic signal if any? Can this signal be modulated? And if so, how? We know that the hemodynamic task-related signal does not elicit local concurrent changes in the firing rate in multi-unit activity recordings (Sirotin & Das 2009).

It is worth mentioning that this task-related hemodynamic response has been observed in human fMRI BOLD experiments (Jack et al. 2006; Griffis et al. 2015), confirming the observations made in non-human primates. However, in those experiments, other than BOLD fMRI no other neuronal measure was made.

Here we aimed at understanding the relevant events in a trial that might trigger the hemodynamic task-related response. To test this we used four manipulations of the original task where the hemodynamic task-related response was described (Sirotin & Das 2009). First, we manipulated the trial duration. The aim was to understand how the temporal pattern of the task-response changed for different trial durations. Second, following the previous line, we looked at the effect of fixation. In particular, we looked at the effect of the duration of time the animal was requested to hold fixation, by varying fixation duration. The aim was to understand if fixation even in

the absence of direct visual stimulation in the recording area could influence the hemodynamic task-related response. Third, we changed the reward the animal received after completing trials. We achieved this by changing the reward amount. Here the goal was to look for the influence of motivation on the resulting task-related response. Fourth, we looked at a task using a different sensory modality, until here all experiments were based on visual fixation, while recording in the same region of visual cortex. We used an auditory/motor task described below that aimed at emulating the visual fixation task (using mostly sound as cues). With these experimental manipulations of how the subjects perform the task, we expected to shed some light on the richness and complexity of the hemodynamic response. The message we aim to convey with these manipulations is that the hemodynamic response is rather complex. Even in an early sensory area, there are responses that seem to be influenced by modulatory systems.

Previously in the laboratory we tapped into the idea that the hemodynamic response does not purely reflect a combination of local neural activity (as spiking and different bands of local field potentials) and physiological heart rate changes (Sirotin & Das 2010a). In this preliminary work (Sirotin & Das 2010a) the aim was to estimate the full hemodynamic signal as a linear combination of different regressors (MUA, LFP gamma-band, 66-120Hz, LFP nMod-band, 20-56Hz, LPF alpha-band, 8-16Hz, LFP theta-band, 4-8Hz, LFP delta-band, 2-4Hz and heart rate). The results indicate that only about half of the variance was explained with this approach. There was also significant variability on the resulting kernels shapes for each regressor (kernels, the resulting transfer functions that relate each regressor to the hemodynamic response). Hence, this hints at the complexity of the hemodynamic response. It is worth noting that in the experiments mentioned, the multi-linear regression model aimed at explaining the hemodynamic response in a rest condition; no task. We have preliminary analysis in the context of the fixation task with similar results (results not included in this thesis).

The data presented here concurs with the view that the hemodynamic response integrates activity from a variety of sources. Considering local neural activity as the sole predictor of hemodynamic activity does not give an accurate picture of the resulting response.

3.2 Methods

Methods used here were the same as described in Sirotin & Das 2009. Simultaneous intrinsic signal optical imaging and electrophysiology were acquired from alert macaques engaged in different tasks. All experiments presented here were performed in darkness or quasi-total darkness. All experimental procedures were performed in accordance with the US National Institutes of Health Guide for the Care and Use of Laboratory Animals and were approved by the Institutional Animal Care and Use Committees of Columbia University and the New York State Psychiatric Institute.

Detailed methods description of the experimental methodology used in the lab can be found elsewhere (e. g. Sirotin & Das 2009, Cardoso et al. 2012, Lima et al. 2014). Here are only referenced the methods that are particularly relevant for the data presented below. The data included in this chapter reflects a combination of different experiments, hence specific experimental details or analysis are included when appropriate throughout the text.

Imaging data was acquired at either 7.5 or 15 Hz, at this rate pulsation is observable in the imaging response. Cortical pulsations were removed by low-pass filtering, using the Chronux MATLAB Toolbox function runline.m (typical heart rates were ~2–3 Hz, much faster than the typical hemodynamic response frequencies of ~<0.5 Hz). Heart rate was estimated from the pulsation. Each pulsation event has a peak and trough; the distance between peaks and troughs was used to identify lawful pulsation events. Heart rate was estimated as the frequency of the pulsation events. Slow temporal drifts (>30 s) were removed with high-pass filtering (using the

Chronux MATLAB Toolbox function runline.m), except: when calculating the power spectrum of the hemodynamic response on the variable inter-trial-interval manipulation and when looking at the slow changes on the hemodynamic response as the animals progress into blocks of high or low reward, in the experiments of manipulation of reward amount. In these exceptions, a linear trend (regression on the full time series) was subtracted from the response. Exceptions described in the text.

In the section where we manipulated fixation duration, one of the fixation duration schedules that we presented obeyed the rule of a 'memoryless' process. By memoryless process it is meant that the probability of an event happening in the future given it has not yet happened is independent of the time that has passed since the beginning of that process. More formally: $p(x > t_a + t_b \mid x > t_a) = p(x > t_b)$. Using the rules of conditional probabilities: $p(x > t_a + t_b \mid x > t_a) = p(x > t_a + t_b \cap x > t_a) / p(x > t_a)$, and as time is continuous: $p(x > t_a + t_b \cap x > t_a) = p(x > t_a + t_b)$, therefore it comes that $p(x > t_a + t_b \mid x > t_a) = p(x > t_b) = p(x > t_a + t_b)/ p(x > t_a)$, thus $p(x > t_a + t_b) = p(x > t_a) * p(x > t_b)$. Not demonstrated here, but mathematically this universally will be valid if the $p(x > t_i)$ will be given by an exponential function: $p(x>t_i) = e^{-t_i/\tau}$ (the probability will be between 0-1, we will use a random number between 0-1 to generate samples for t, fixation duration). We sampled fixation durations within fixed time intervals (there was a minimum fixation time, t_{min} and a maximum one, t_{max}) $t = t_{min} - \tau * \log(rand[0;1])$ and $t \leq t_{max}$ (if $t > t_{max}$, then a new t is calculated, until $t \leq t_{max}$).

3.3 Variable Trial Durations

Aiming at characterizing different aspects of the task-related response, we present data collected similarly to data in Sirotin & Das 2009, with small variations mentioned below. Subjects performed a fixation task in quasi total darkness with the monitor having only a small fixation point exposed

(otherwise all light from monitor was blocked, as in the original study by Sirotin & Das 2009). In this manipulation of the task, the subject was asked to perform the fixation task in two different schedules. Either the schedule was of short trials, with a shorter inter-trial interval, ITI, (from 6 to10 s, only one short ITI used in each session), or long trials, with a longer ITI (12 to 20 s, only one long ITI used in each session). The task the animal performed was a fixation task. The color of the fixation point cues the subject of when to aim for fixation. Once the animal achieves fixation the color of the fixation point changes and once the fixation period ends the fixation point turns off and the animal receives a liquid reward for holding fixation. Finally, there is a time delay (ITI) between trials. Trials in which the animal did not hold fixation for the requested period were not rewarded.

Trials were presented in different schedules, where ITI was changed. The different schedules were presented in blocks. In general, we requested the subjects to perform 20 complete trials until the schedule changed (starting a new block). The animal was not cued for the change in ITI schedule. Sessions could start with a short or long ITI (the order of the first ITI, if long or short, did not affect the results). Once again, the subject's task was to hold fixation for the period the fixation point had a particular color (the subject was requested to hold fixation for 2-4 s, varying between sessions).

We recorded the hemodynamic response using intrinsic signal optical imaging, already described, and simultaneous electrical recordings in the imaging region. Furthermore, from the imaging response we extracted the heart rate response (see methods).

Based on what we know about the task-related response from prior work done in our laboratory (Sirotin & Das 2009), we hypothesized that, within the total trial lengths that we have used here, the task-related response should, on average, entrain to the trial duration. Still several aspects of this entrainment are not understood. One of the questions we had about the task-related response was: what are the events that trigger the entrainment of the hemodynamic response?

With this systematic alternation of blocks of short and long trials, we wanted to evaluate if there were systematic changes in the time course of the responses. In particular we wanted to know if there are changes early in a short vs. a long trial, up until the duration of the shorter ITI. Behaviorally, trials should be similar (until the duration of the shorter ITI) as the task the animal has to do is the same: fixation. Up until when the duration of the ITI does not exceed that on a short ITI trial, all the trials (short or long ITI) are indistinguishable. The aim was to understand what aspects of trials (e.g., effort of fixation, reward) could influence the hemodynamic entrainment, i.e., what behavioral events could be involved in eliciting or triggering the hemodynamic task-related response.

Simultaneous to the recording of the hemodynamic response, we recorded MUA activity of one or two electrodes in the same region where we recorded the neuroimaging data. We also recoded the heart rate response; reconstructed from the brain pulsation observed in the neuroimaging response. We looked for concomitant changes in either of these additional metrics with the hemodynamic response.

Figure 3.1 shows a typical session (11 sessions were recorded for one subject, monkey T). In Figure 3.1a is the mean hemodynamic response to short (top) or long (middle) trials. It can be noticed that the responses to short or long trials are different, but the profiles up until the duration of the short trial are similar (Figure 3.1a bottom panel). For the session shown, the mean trial duration for a short trial was 15.92 $\pm$ 0.02 s and for a long trial was 23.95 $\pm$ 0.03 s (changes in trial durations reflect small changes in the time the animal takes to achieve fixation on each trial).

Looking at the spectral profile of the hemodynamic signal (Figure 3.1d) it can be noticed that there are peaks in this spectrum that closely match the two schedules of completed trials (15.2 and 21.4 s, for short and long trials, respectively). There are other peaks in the spectrum not directly related to the schedule of completed trials, though. It should be mentioned that incomplete trials had shorter durations because the subject did not hold

fixation during all the requested period and no reward is administered, These time windows were not discounted from the duration of the inter-trial interval. Incomplete trials have less stereotypical durations as the animals interrupt trials at different moments. For all sessions there were more complete than incomplete trials. Still, the presence of peaks at higher frequencies than either short or long trial frequencies could be related to incomplete trials.

The profile for the heart rate response in Figure 3.1b was also similar for the two trial schedules, and different from the hemodynamic response. It is worth noting that the heart rate spectrum for this session did not show clear peaks at the different trial schedule frequencies (Figure 3.1e). Finally, the spiking rates of a multi-unit electrode located the same region as the imaging did not show a significant pattern associated with this task (Figure 3.1c), as expected from Sirotin & Das 2009. For this session, the MUA spectrum had multiple peaks, but not tightly matching the trial schedules (Figure 3.1f).

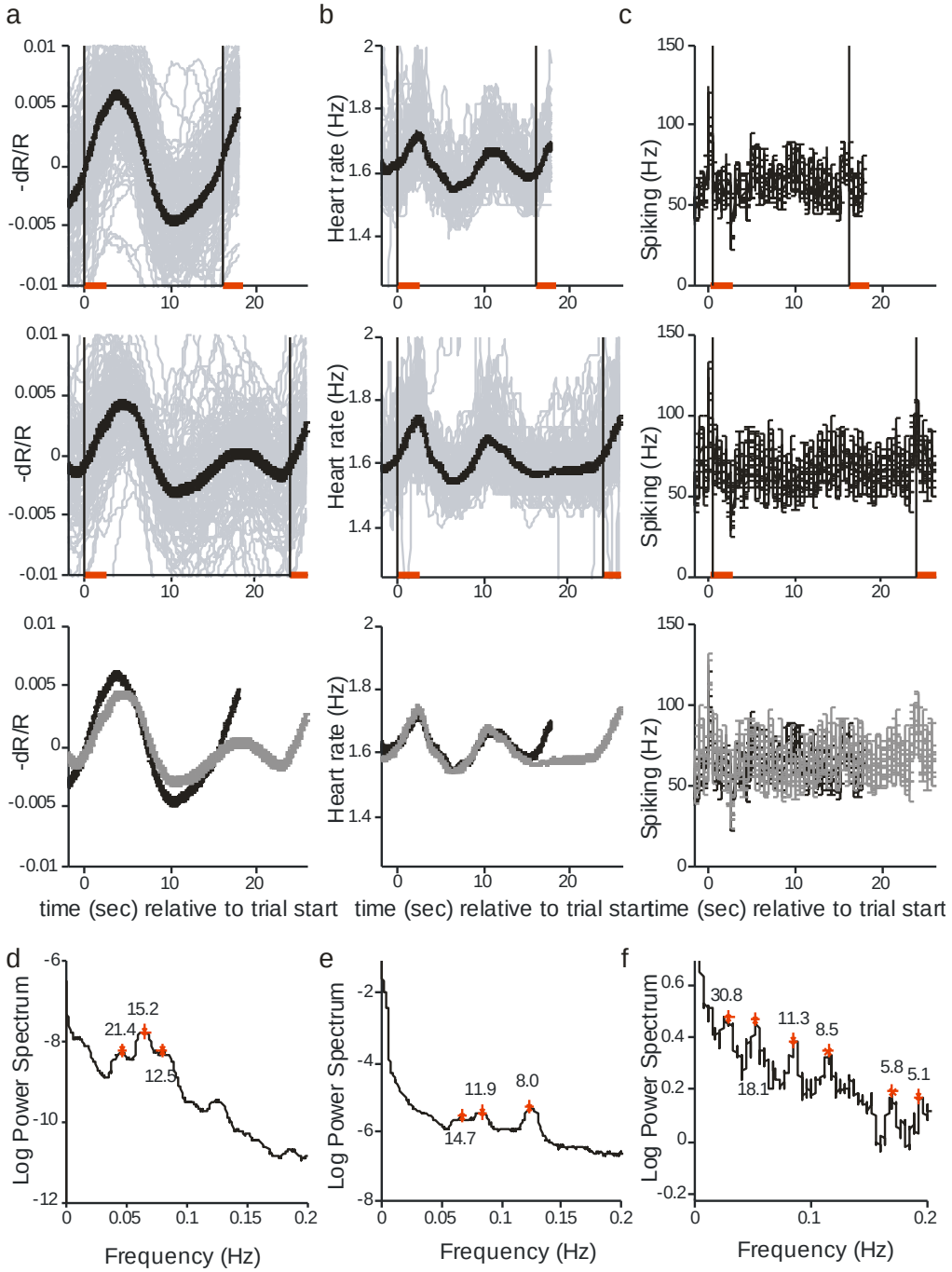

Figure 3.1 – Single session showing that different trial schedules have associated different hemodynamic, heart rate and MUA responses. **(a)** Hemodynamic responses to short trials (**top**), long trials (**middle**) and overlay of average short trials (black) and long trials (gray) (**bottom**). Error

bars calculated as s.e.m.. The red horizontal lines indicate the period the animal was requested to hold fixation. **(b)** Similar to **a**, but for the heart rate response. **(c)** Similar to **a**, but for the multi-unit spiking activity. **(d)** Log-power spectrum of the hemodynamic response. (Power spectra were calculated on the data without discounting of slow drifts that might occur throughout the imaging session, that were in general always used, unless otherwise stated, as here.) The red crosses indicate peaks around the trials' periodicities; the numbers indicate the corresponding period. **(e)** Log-power spectrum of the heart rate; similar to **d**. **(f)** Log-power spectrum of the MUA activity, similar do **d**.

From observing the single case presented in Figure 3.1 it is noticeable the apparent similarity of the hemodynamic response during some initial period in which short and long trials are indistinguishable. We therefore went on to quantify the similarity in the shape of the hemodynamic profile within the first seconds of completed short or long trials. We looked at the initial 10 s of all completed trials, either for trials coming from blocks of short or long trials (n = 11 sessions). We selected this interval because it was smaller than the length of a short trial (for all considered sessions). For this quantification we first computed the Pearson's correlation coefficient for the initial 10 s of all pairs of short trials; and the Pearson's correlation coefficient for the initial 10 s of all pairs of long trials. We established the distribution of correlation coefficient profiles for short-short and long-long trials. We then calculated the Pearson's correlation coefficient for the initial 10 s of all the pairs of short and long trials. We used the previous correlation coefficients for the pairs of short-short and long-long trials to have a comparison baseline for the correlation coefficients of short-long trials. Our null hypothesis was that the distribution of correlation coefficients for short-long trials is indistinguishable from the distribution for short-short (or long-long) trials. In Figure 3.2a, it can be noticed that the distribution of Pearson's correlation coefficients for short-short trials or long-long trials are similar. In this session the hemodynamic task-related response is fairly stereotypical: the correlation profile is skewed towards 1. More importantly this distribution was also similar for compari-

sons between short-long trials (lighter gray, Figure 3.2a). Independently of the particular shapes of the task-related response on each session, or how stereotypical this response was within a session, we observed that the distribution of our similarity measure (the Pearson's correlation) was preserved (within a session). The similarity between short and long trials was independent of the variability of the task-related response within each session. For each session we tested how similar the distributions were for short-short trials versus long-long trials (Figure 3.2b); no session reached significance. Then we used a non-parametric Wilcoxon signed-rank test to compare the distribution profiles of correlation coefficients short-short vs. long-long vs. short-long trials. Once again the comparison of the shapes of the distribution of correlation coefficients for short-long trials against either short-short or long-long trials did not reach significance for any session (Figure 3.2c). This indicates that the three distributions were not statistically different. It supports the hypothesis that for the initial duration of short or long trials the hemodynamic responses are indistinguishable (within the trial schedules that we have tested).

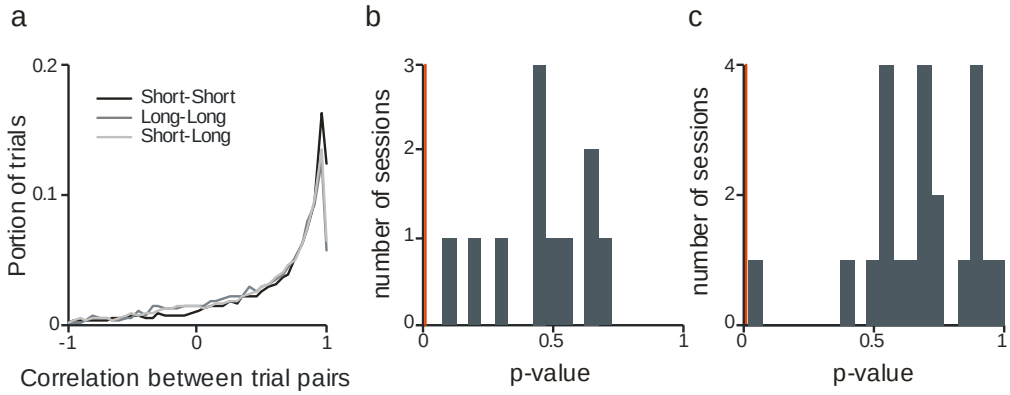

Figure 3.2 – The initial few seconds (10 s) are indistinguishable for short or long trials. **(a)** For the same session as in Figure 3.1, the computed correlation between the initial 10 s of all completed trials, either long or short. In black is the correlation profile between the initial seconds of short trials (trials share a significant similarity, therefore correlation tends to be high: close to 1). In dark gray is the correlation profile between the initial seconds

between long trials. In light gray is the correlation profile between the first few seconds of long and short trials. Each correlation profile was normalized by the total number of pairs compared. **(b)** Population data summary for 11 sessions. p-value of the comparison between the correlation shapes for short or long trials. Note: red line markes significance level (significance value, α, corrected for multiple comparisons; correlation profiles were binned in 21 intervals: Bonferroni correction, resulting $\alpha = 0.05/21$); no session is below the significance level. **(c)** Similar to **b**, but for the combination between the correlation shapes of short-long trials relative to either short of long trial only correlation distribution (total of p-values: 22, two for each of the 11 sessions). Note: no session reaches significance (same significance level as in **b**).

We observed that the hemodynamic response tended to entrain to the trial schedule, but the initial response to short or long trials (which contains the initial increase in blood volume) was indistinguishable for the two conditions. We cannot disregard that for different trial schedules (much shorter, much longer or larger difference between short and long trials) the hemodynamic response to short and long trials could be dissimilar.

Lastly, for these set of experiments we wanted to understand if some of the observed peaks in the power spectrum could be related to the periodicity of short and long trials. Furthermore, we wanted to know if either of the activity measures (hemodynamic, heart rate or MUA) had spectral peaks that better matched the trial schedule, than the other metrics. In this attempt we generously looked for 20 peaks in the power spectrum, below 0.5 Hz. The number of peaks found per metric (hemodynamic, heart rate or MUA) per session was variable. Some sessions did not present clear peaks below 0.5 Hz (this is the reason for the different number of data points in Figure 3.3b-d). Next, for each session, we computed the minimal distance between the spectral peaks and the frequencies corresponding to short and long trials (Figure 3.3a, in seconds). In this sample of sessions there was no clear superiority of the hemodynamic response in having peaks that matched the short and long ITIs. This metric is rather crude; the spectra did not always

have clear peaks. It suggests that spectra might be noisy or the entrainment of the different measures with trial periodicity, even though weak, happens to all measures (for these trial durations).

In Figure 3.3b-d we plotted the peak positions against the period of the trials (short or long). The peak positions were chosen to be the closest to the actual trials durations (short or long). The different panels (In Figure 3.3b-d) reflect the different metrics, hemodynamics, heart rate and MUA. If the spectral peaks would fully reflect the trial duration, then the distance between the closest spectral peak and the trial period should be zero; there is however large dispersion. The peaks' positions tend somewhat to follow one another on the different metrics. Heart rate had the lowest number of detectable peaks (below 0.5 Hz) and its relationship with the other metrics was the least uniform. Heart rate seems to entrain less with trial duration, when compared with the hemodynamic response or multi-unit activity.

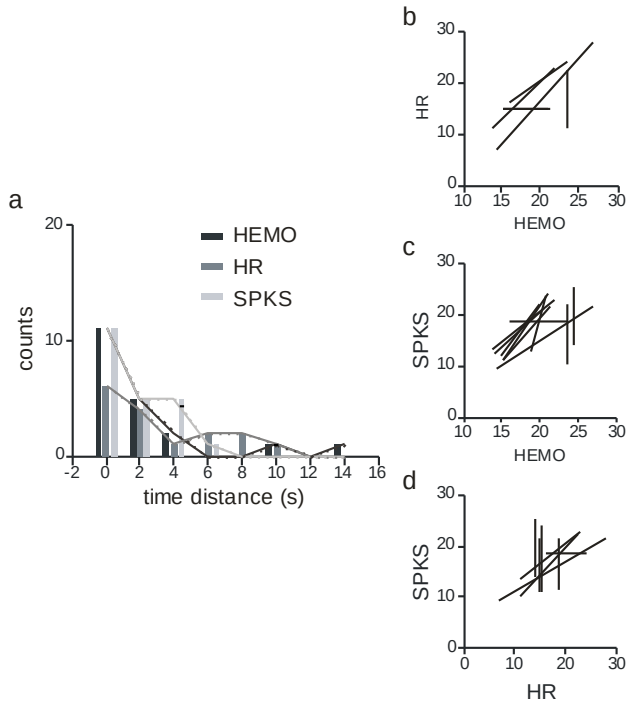

Figure 3.3 – Power spectrum peaks only partially reflect the difference in trial lengths. **(a)** Histogram of distance (in seconds) between the lengths for

short and long trials and the closest spectral peak for hemodynamics, heart rate and MUA (for each session, if there were 2 recording electrodes, the one with peaks closest to the trial short-long durations was the one used). Dotted lines added for visual guidance of the decay of the counts with time distance to trials periodicity, for each neural measure. **(b)** Scatter of spectral peak positions (in seconds) to hemodynamics versus heart rate (lines connect the peaks for the short and long trial ITIs for the same session). **(c)** Similar to **b**, but for hemodynamic spectral peak positions versus MUA ones. **(d)** Similar to **b**, but for heart rate spectral peak positions versus MUA.

This manipulation of the trial length using a block structure produced results that suggest that within the initial portion of short or long trials the task--related hemodynamic response is similar, independently of the total ITI. This suggests that some component of the initial part of the trial, potentially effort of fixation, anticipation of reward, might play a role in triggering this hemodynamic task-related response and therefore also its overall shape.

3.4 Variable Fixation Durations

We observed that the shape of the hemodynamic response did not seem to significantly change for trials with different inter-trial-intervals even though the task-related response entrained to different trial durations. As a follow up on this observation we looked at what happens when we manipulate the duration of the fixation period. We present data from 13 experimental sessions in 3 animals (monkey S, monkey T and monkey E).

The fixation duration was manipulated in three different ways. In 6 sessions (for monkeys T and E) it was changed pseudo-randomly between trials, the fixation time was selected randomly from a uniform distribution (fixation limits: 1-5 s, in this manipulation the ITI was fixed). In 3 other sessions (for monkey T) fixation duration was changed pseudo-randomly between trials, in this case the fixation duration in each trial was picked from a *memoryless* process (fixation times selected using a hazard function, with failure rate, τ, of 1.5 or 2 s within fixation limits of 1-5 s). The use of a hazard function was

to make the fixation duration more unpredictable; the fixation time elapsed did not help predict when fixation would end. This is not a completely memoryless process as we have lower and upper limits on fixation duration. In this manipulation the ITI was kept fixed. Finally, in 4 other sessions (for monkey S) the fixation duration was changed in blocks (of trials). The ITI was adjusted, in each block, so that the total trial length (of complete trials) was kept constant independently of the fixation duration.

In Figure 3.4 we present one example of each type of manipulation. The average eye position for trials with shorter or longer fixations clearly shows that the subjects held fixation for different amounts of time (Figure 3.4a-c: top panels). From looking at the average hemodynamic responses to briefer or longer fixations (Figure 3.4a-c: middle panels) one can notice that longer fixations tend to be associated with more delayed and higher amplitude peak responses.

The heart rate responses (Figure 3.4a-b: last to bottom panels) showed a fairly different trend: with a tendency to exhibit more peaks: the first preceding the peak in hemodynamic response, but the second one tending to lie after the hemodynamic peak. The heart rate response to the session in Figure 3.4c shows a different picture; on average no clear peak after the start of long fixation duration trials. For all the sessions presented here, it suggests that if the first observed peak in the heart rate could have some influence on the hemodynamic response, it is less probable that the second peak would have a causal influence on the hemodynamic peak response. Interestingly, and once more, in this anecdotal evidence, the changes in the first peak to briefer or longer fixations do not seem significantly different.

Finally, for the presented session on which we had electrophysiological recordings (Figure 3.4a: bottom panel), it did not show significant changes with the duration of fixation, other than a brief spiking peak upon fixation. We observed different spiking effects with fixation in these tasks, performed in quasi total darkness. Fixation could increase or decrease slightly average MUA rates, and this change could be more sustained during the fixation

period or more transient with the onset or offset of fixation. We have not found lawful relationships relating this MUA rate changes with the hemodynamic response changes.

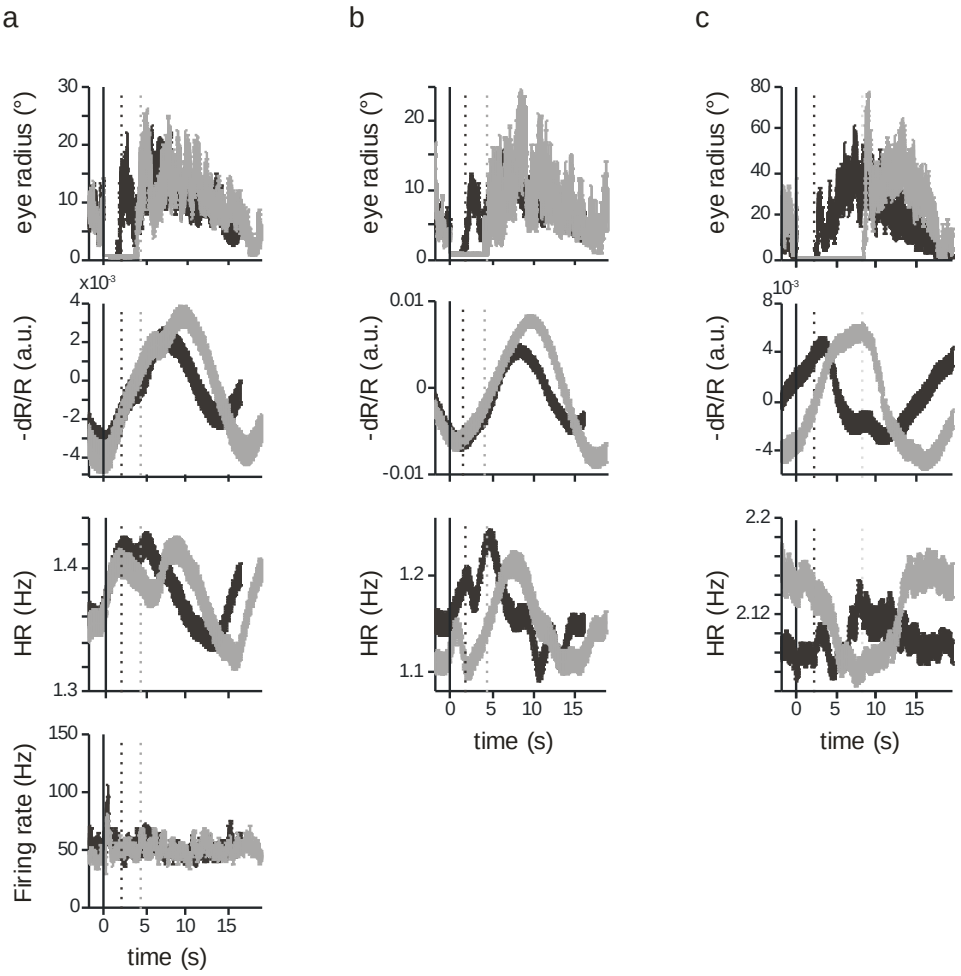

Figure 3.4 – The effect of duration of fixation: single cases. **(a)** Mean trial responses to: eye distance relative to the fixation point (in degrees of visual angle), hemodynamic response, heart rate and firing rate response profiles of a session with fixation durations uniformly distributed between 1-5 s. In dark gray is the average response of 177 trials with fixation durations between 1 and 2.5 s. In light gray are the average responses to 163 trials with fixation durations between 3.5 and 5 s. The vertical solid line indicates the beginning of the fixation period; the dashed lines indicate the average fixation durations for briefer and longer fixations, in dark and light gray, respectively (Monkey E). **(b)** Similar to **a**, on top the average eye positions,

in the middle hemodynamic response, in the bottom is the average heart rate response (no electrode recordings were made in this session). In this session fixation durations between 1 and 5 s, distribution following an exponential decay distribution with hazard period, λ = 2 s. In dark gray are the average response to trials with fixation durations between 1 and 1.5 s (n = 167 trials). In light gray are the average responses to trials with fixation durations between 3 and 5 s (Monkey T, n = 132 trials). **(c)** Traces similar to **a** and **b**, for a session with fixation durations changed between blocks, fixation duration of either 2 and 8 s (dark gray, n = 70 trials and light gray, n = 70 trials, respectively, for Monkey S).

We wanted to know if, within our population of sessions, the changes in average peak positions for hemodynamic and heart rate responses presented consistent trends. The hemodynamic responses are intrinsically small and noisy. We therefore looked at changes in the peaks for the average responses to each fixation duration schedule, in each session. (It was too noisy to look at the same behavior on a trial by trial basis.) Within each session we found the peak hemodynamic (and heart rate) responses for the average trial for short and long fixations. In Figure 3.5a,b we present the results for the position of the peaks and their amplitudes, as a function of the actual fixation duration. For most of the data, the position of the hemodynamic response peaks for longer fixation durations was more delayed than for shorter fixations (Figure 3.5a) and the amplitudes for the peaks corresponding to longer fixations also tended to be higher (Figure 3.5b). This suggests that the hemodynamic response can reflect the duration of fixation.

In these sessions we often lacked accompanying electrophysiological data. However, we had available extensive number of sessions with electrophysiological data in which the animal performed a fixation task in quasi total darkness and where we can confidently say that this task-related hemodynamic response does not reflect visually driven local spiking changes. Additionally, in the laboratory, the spatial profile of the hemodynamic response in the imaging chamber was also analyzed, finding that it is spatially uniform, and does not present increasing gradients as one

approached the location of the fovea (Sirotin et al. 2012). As the animals were performing a fixation task with a very small fixation point, in quasi total darkness, the fovea is where visual responses should be present. As a note, we did not have coverage of the retinotopic location of the fovea with our imaging chambers.

We should acknowledge that the data presented here is a panoply of slightly different manipulations, a more consistent set of repetitions of these experiments would be necessary to clearly answer if there is a direct influence of fixation duration in the hemodynamic response. Nevertheless, this preliminary evidence suggests that there might be vestibular or extra-retinal mechanisms, associated with the oculomotor command, influencing the hemodynamic response in primary visual cortex, in the absence of concurrent local spiking changes. Alternatively the hemodynamic response could also be strongly influenced by the administration of reward. In these experiments reward was given at the end of the fixation period, we cannot disregard that the rise in hemodynamic response could be anticipating the upcoming reward.

Apart from looking at the hemodynamic responses, we also looked at the peak positions and amplitudes for the average heart rate responses. For the positions of the peaks we observed a similar trend as for the hemodynamic response. Longer delays for peaks were associated with longer fixations, Figure 3.5c. The amplitude changes did not show a clear trend (similar portion of blue and red segments in Figure 3.5d). Finally, we wanted to understand if there were any consistent relationships between the peak positions and amplitudes across these two metrics (hemodynamics and heart rate). The peak positions tended to be positively correlated traces mostly situated on the first quadrant (Figure 3.5e). The amplitudes did not show a consistent relationship (Figure 3.5f).

Here we did not look at the peak positions for the electrophysiological response because we had very few sessions with electrophysiological recordings (n = 4). Moreover, the MUA responses did not show sustained

changes beyond the fixation period, and even those were not present in every session. Once more, we observed both increases and decreases in the baseline MUA rates, varying with session and electrode locations.

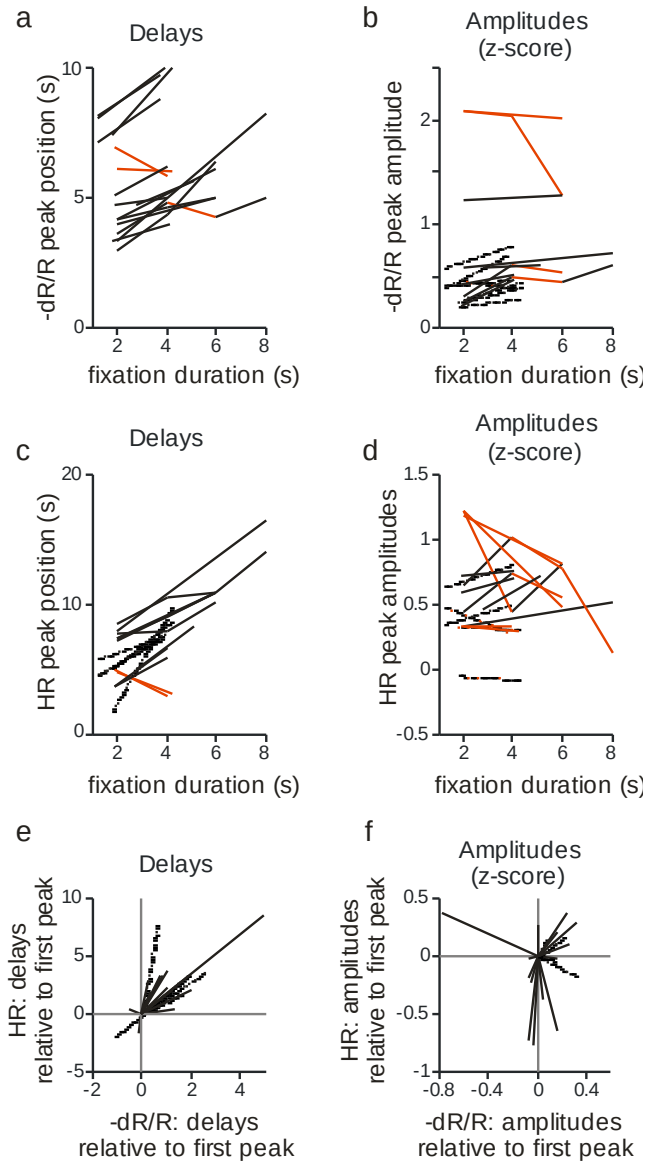

Figure 3.5 – Hemodynamic and heart rate trial locked peak responses change with fixation duration. **(a)** The distribution of peaks for the trial average hemodynamic response, relative to the duration of fixation. Each segment line connects consecutively increasing fixation duration intervals for each session (in the block structure, we sometimes used more than two fixation

intervals, that explains why there are more segments than experimental sessions). In black are the segments that had a longer peak for longer fixations, in red the sessions where the hemodynamic response for the longer fixation peaked before the one for the shorter fixation. Note that most lines are blue. Dotted segments were used for monkey T, solid ones for monkey S and dotted-interrupted ones for monkey E. **(b)** The distribution of the amplitudes associated with the peaks in **a**. The peak amplitudes were z-scored so they could be represented on the same plot. Same color code and line style as in **a**. **(c)** Similar to **a**, but for the heart rate peak response (here we considered the maximum peak, independently of how many peaks the average response exhibited). **(d)** Similar to **b**, but for the heart rate peak amplitude. **(e)** Scatter plot of the peak positions of the hemodynamic versus heart rate responses showing, for each experimental session, the value for the longer fixation relative to that for the shorter (set to zero). Lines join short-long pairs for each session. Note: responses tend to be predominantly in the first quadrant. Dashed, solid and dotted-interrupted segments used for monkeys T, S and E, respectively. **(f)** Similarly to what was done to the peak positions in **e**, here for the peak amplitudes.

The data presented comes from several variations on the fixation task, with only a small number of sessions for each manipulation. Nevertheless it opens interesting questions pertaining the task-related response: could the effort of fixation or anticipation of reward, for example, play a role in triggering this hemodynamic task-related response?

3.5 Variable Reward Amount

Previously we manipulated aspects of the timing of the trials; but wanted to further explore behavioral correlates of the mean hemodynamic task-response. We set up a slightly different task with the goal of altering the reward level that the animals experienced, and thus explore potential hemodynamic task-related response changes. We manipulated the reward amount that the subject received in each trial, in a block wise manner (no additional cues). Otherwise the animals performed the same fixation task.

As in the previous manipulations, the fixation task was presented in quasi-total darkness. Reward was manipulated in blocks; blocks of either of low or high reward. There was at least a twofold difference between the reward levels. The block structure we imposed required the animal to complete 10 trials before the reward level changed.

Behaviorally, the animals tended to be sensitive to the level of reward; breaking fixation or engaging in trials less frequently when the reward was lower, as shown in Figure 3.6. In Figure 3.6, the probability of completing trials of low reward, in red, was in general lower than for high reward trials, in blue. It should be mentioned that the ideal behavior is to complete trials independent of reward level. Incomplete trials were not rewarded and incurred in a 'punishing' inter-trial-interval until the start of a new trial (no active punishments or additional time details were included). In 3 of the 35 sessions the performance in blocks of low reward trials was higher than for high reward ones.

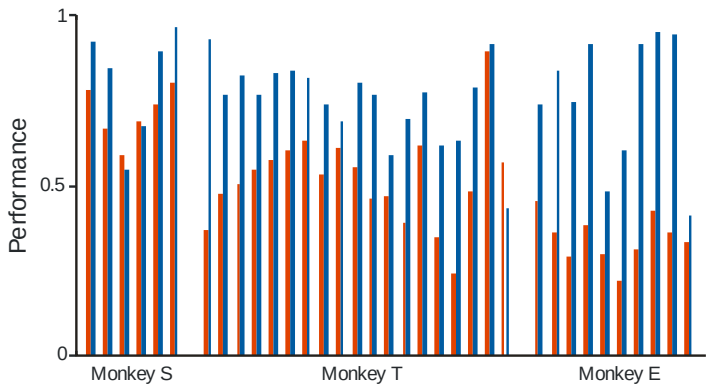

Figure 3.6 – Behavior of the fixation task in blocks of high and low reward. In red is the fraction of completed low reward trials and in blue the fraction of completed high reward trials. Each pair of lines (red-blue) is for one session. (3 monkeys: S: 6 sessions, T: 19 sessions and E: 10 sessions.)

Once more we looked at trial average hemodynamic task-related response. In Figure 3.7a-d are illustrated responses to a single session (for monkey T). In Figure 3.7a-c are the average trial triggered hemodynamic responses for

low and high reward trials. It could be noticed that for this session the magnitude of the hemodynamic response for high reward trials was higher than for low reward ones. This was not accompanied by concurrent spiking changes (Figure 3.7d). We wanted to know if the same trend was observed for the population; we tested the magnitude of high and low reward trials. To test for significance, we used a Wilcoxon signed-rank test (p-value=6.7×10^{-6}) indicating the magnitude difference between high and low reward to be directional (Figure 3.7e). Magnitude of low reward trials was on average smaller than for high reward ones.

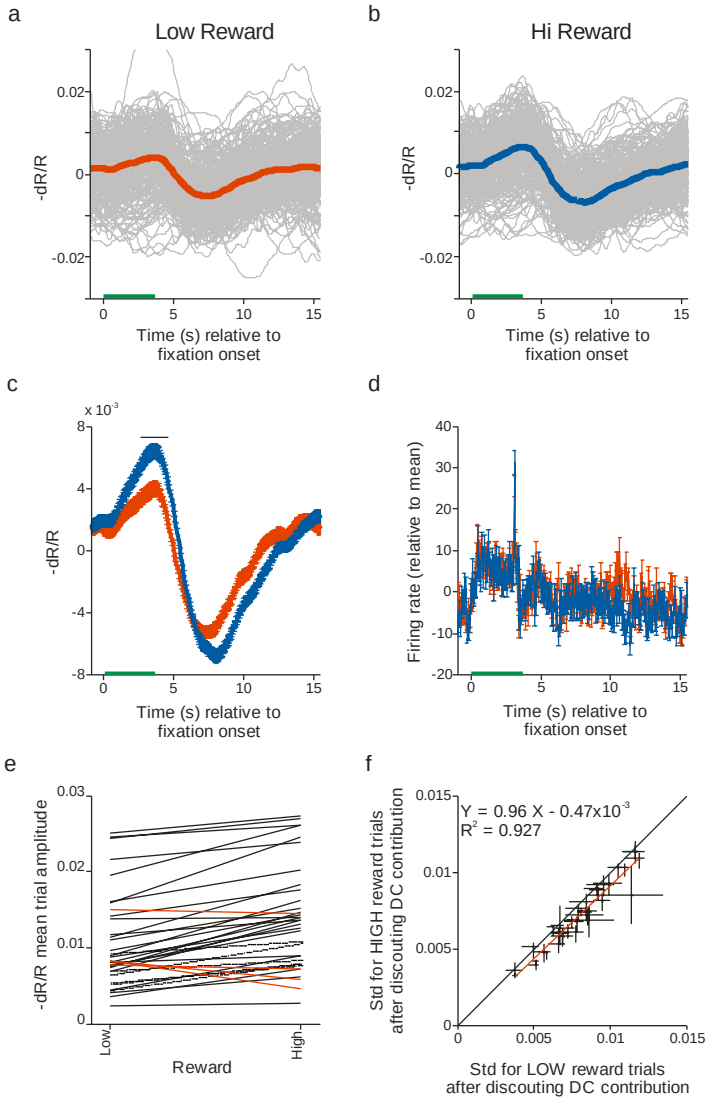

Figure 3.7 – Magnitude of the hemodynamic task-related response changes with reward amount. **(a)** Hemodynamic task-related response for an individual session. In gray the individual response on each completed trial of low reward; in red is the average response. **(b)** Similar to **a**, but considering all complete trials of high reward in the same session; in blue is the average response. **(c)** Overlay of the average responses in **a** and **b**. Error bars represent standard error of the mean. **(d)** Similar to **c**, but for the electrophysiological data. Note that the difference between the two distributions of spiking responses is only significantly different at one time point, in this session, which probably coincides with reward delivery (not consistently observed for other sessions). **(e)** Hemodynamic amplitude (peak to trough) of low and high reward trials. Each line represents one session, where the peak to trough amplitude of the average low reward trial is on the left and the corresponding peak to trough for high reward is on the right, for the same session. In red are the sessions where the reported amplitude for low reward trials was higher than for high reward ones. Significance test: Wilcoxon signed rank task, p-value: 6.7×10^{-6}. **(f)** Noise variability measure between low and high reward trials. Scatter plot of the mean standard deviation (in time) for low versus high reward completed trials (before estimating the standard deviation of each trial, for subsequent average, to each trial the mean response on the trial was subtracted, as in panels **a**-**c**). The 90% confidence intervals were estimated from bootstrapping (100 repetitions). Red line represents a regression line through the data (parameters indicated on the plot's **inset**). Note that this regression is below the equality line.

We looked at the time dynamics of the task-related signal in low and high reward trials. We noticed that the trials in lower reward blocks had higher variability in time, than in higher reward blocks, (Figure 3.7f, a regression line through the data is below the equality line). Taken together, we observed changes in the hemodynamic response with reward level. Both the response magnitude and its variability in time changed with reward level: higher response magnitude and lower time variability for high reward trials and lower response magnitude and higher time variability for low reward trials.

Finally, we noticed that between blocks of low and high reward trials, there were slower fluctuations in the hemodynamic signal. To quantify this observation we took the initial hemodynamic signal change and removed only a linear trend from this signal and no other low frequency changes. For each trial we calculated the mean hemodynamic response to each trial (across the duration of each trial). As exemplified for the single session in Figure 3.8a,c. it shows a segment of a session; one could notice that mean hemodynamic response fluctuates with reward amount as one moves along a block of low or high reward. In this dataset, as one goes along a low reward block the mean hemodynamic level tended to increase (increased blood volume level changes), and as one moved along a high reward block, the mean hemodynamic level tended to decrease (decrease in blood volume changes). Looking in more detail at what was happening at the block level, as we illustrate in Figure 3.8c, where we looked at the same segment of data as in Figure 3.8a, but where only the mean trial response to completed trials is represented. We noticed that along a block the mean trial hemodynamic response to each trial seemed to evolve in a monotonic way. To evaluate if mean trial responses changed systematically with progression along a reward block, a regression line was fit to the mean trial response of the first 10 completed trials in each block (reward blocks with fewer completed trials were not included, and for the ones with higher number of completed trials, only the first 10 completed trials were considered). The regression lines are illustrated by the black lines on the plot Figure 3.8c. To test if there were systematic differences between regression lines of each of the reward levels (low or high), the slopes of the regression lines of all sessions were combined, segregated by reward level on each block, and we tested if the two distributions (slopes for low reward blocks and slopes for high reward blocks) were the same, using a Wilcoxon rank-sum test. In Figure 3.8d, it can be noted that the distributions are different, indicating that along a block of lower reward the hemodynamic mean trial response tended to increase and conversely for high reward blocks.

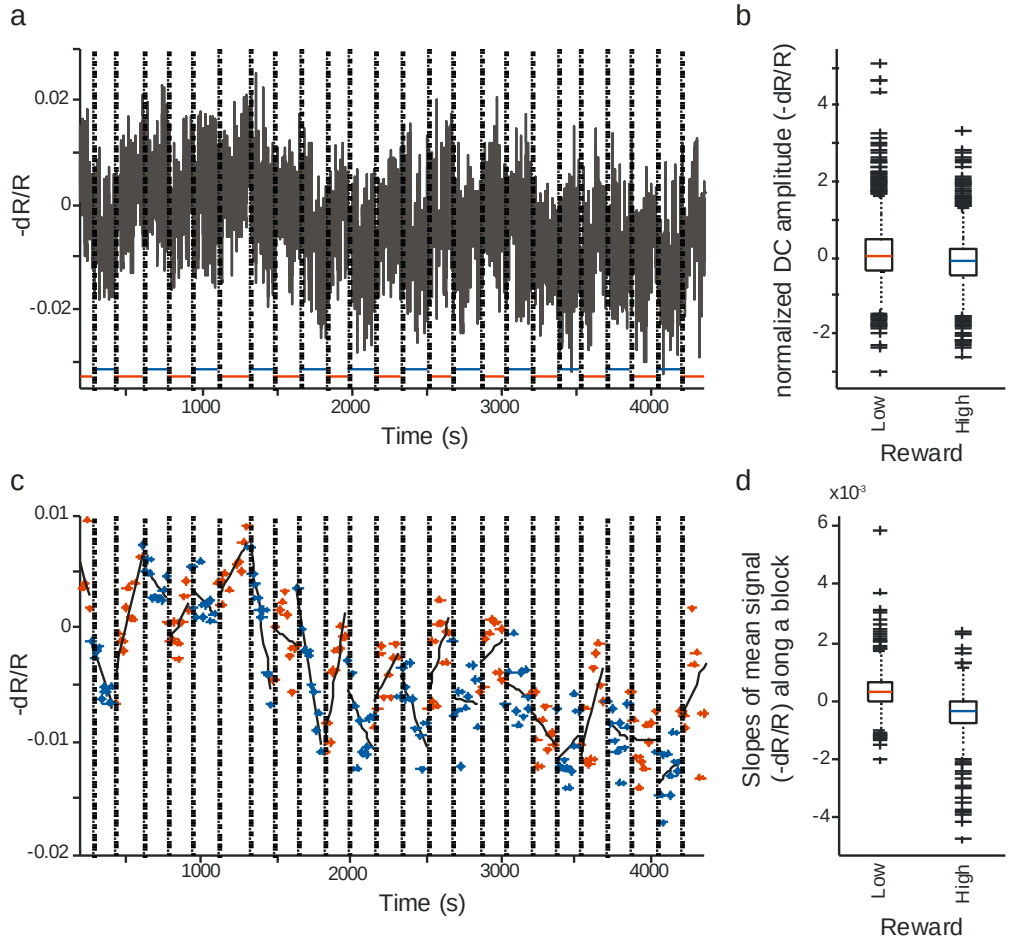

Figure 3.8 – Reward modulates not only the average hemodynamic response as well as the mean hemodynamic level. **(a)** Hemodynamic response on a segment of a session (same session at in Figure 3.7a-d). The dotted lines represent the separations between blocks of low and high reward, reward level on each block is indicated by the horizontal colored lines on the bottom; red for low reward blocks, and blue for high reward ones. **(b)** Distribution of the amplitude of the mean hemodynamic response for each complete trial (normalized by the standard deviation of the hemodynamic response change for the same session as in a), separated by reward amount (n = 7462 and 7315, low and high reward trials) (Additionally, in 29 of the 35 session the blood volume was lower on the average of trials for high reward trials than for low reward ones.) Wilcoxon rank-sum test on the two distributions: p-value = $4 \times 10^{-89} < 0.05/(7462 \times 7315)$, using the conservative correction of dividing the rate significance value by of the total possible combination of comparisons. **(c)** Same segment as in **a**, here only complete

trials are considered; the hemodynamic response to each trial is represented by the mean response on that trial (in red low reward trials, in blue to high reward ones). Dotted vertical lines (as in **a**) show transitions between reward blocks. Solid black lines represent individual regression lines that were fitted to each individual reward block (only blocks with 10 or more complete trials were included). Note: predominantly positive slopes in blocks of low reward trials, versus the predominantly negative ones for high reward blocks. **(d)** Distribution of the slopes for all the considered blocks from all sessions segregated by reward level on the block (n = 35 sessions, 487 blocks for low reward and 565 blocks for high reward). The distributions tested with Wilcoxon rank-sum test: in p-value = $5x10^{-63}$ < 0.05/(487x565), using the conservative correction of dividing the rate significance value by total possible combinations of comparisons.

This manipulation of reward amount clearly showed that the hemodynamic response in visual cortex changes with reward level. The hemodynamic task-related response had higher magnitude and lower variability for high reward trials than low reward ones. These effects rode on top of the slower changes observed on the hemodynamic response, specifically, the mean hemodynamic signal tended to fluctuate slowly (we measured it at the trial period) and decreased as the subject progressed into a high reward block, and then increased as the subject progressed into low reward blocks.

There is extensive research on the effects of reward in the brain. It has been shown in BOLD fMRI experiments with human subjects that increased reward probability is associated with increased stimulus BOLD fMRI activity (Serences 2008). Contrasting with these and our results, there is work using contrast-agent-enhanced fMRI techniques as well as D1-selective dopamine antagonist in alert non-human primates performing a range of visual tasks (Arsenault et al. 2013). This work was focused on changes in visual areas as the animals performed visual tasks. Their observations contradict somewhat we present here; they observed a selective decrease in fMRI activity when comparing rewarded to un-rewarded conditions, and they were able to relate these changes to D1 dopamine receptor activity (using a D1-selective antagonist they got smaller effects). There is a significant experimental

difference between Arsenault et al. 2013 experiments and Serences 2008 (and ours), they both used conditions with uncued rewards and not 100% contingency between cues and reward. The approach Arsenault et al. 2013 took is interesting, as they aimed at a looking at the effects of reward in visual areas independently of potentially other effects as attention. If a particular task, time or stimulus predicts an upcoming reward then a subject will naturally tend to attend to the predictive cue.

In a different BOLD fMRI study, using a complex visual detection task, the effects of 'incentive' in the visually evoked responses, showed enhancement of those in several areas including visual cortex (Engelmann et al. 2009). Incentive was manipulated by the amount of future reward (money) for correct trials; arguably not the same as our reward manipulation. Moreover, we also did not have a stimulus, which we use look for changes in visually evoked responses. Still it is conceivable that the changes we observed in trial responses might be of the same class as the ones mentioned in Engelmann et al. 2009.

The effects of attention in BOLD fMRI are well known, with associated increases of BOLD response with attention (Jack et al. 2006, Sylvester et al. 2007, Donner et al. 2008, Pestilli et al. 2011). In humans a similar reduction in BOLD fMRI responses in visual cortex for visual tasks with the presence of reward has been observed (Knapen et al. 2012). Here similarly, reward was not predicted by any specific stimuli. In the primate, Arsenault et al. 2013, observed as well that a decrease in fMRI response with reward was related to the reward amount (higher rewards caused larger decreases in the fMRI response). Using a paradigm where different stimuli in the visual field were associated (or not) with reward in human fMRI BOLD experiments, it was observed that the responses associated with reward stimuli had enhanced responses relative to unrewarded presentations of the same stimuli (Knapen and Donner, personal communication). Our experiments were performed in quasi total darkness and even though we did not image in the cortical representation of the fovea and reward had 100% probability if

subjects held fixation, we would not expect to find the difference in results arising from the fact we were not recording the fovea representation.

These ambiguous results of the influence of reward in cortical visual areas as the subjects perform visual tasks, suggest that reward might be enhancing rewarded stimuli representation as well as reducing the signal-to--noise ratio by means of reducing the mean signal. Further research is needed to better understand this question.

3.6 Task-related Hemodynamic Response in Visual Cortex to an Auditory-Motor Task

Finally, we wanted to further explore the specificity of the task-related hemodynamic response to visual tasks. On the initial assessment of this problem in the laboratory an auditory/motor task was used, while recording in primary visual cortex. At that point results were inconclusive (it was not the focus of that study, but see supplementary material of Sirotin & Das 2009). We repeated and expanded those initial experiments. Here, we present data (15 sessions for monkey T and 1 session for monkey S) for the same task as initially used in Sirotin & Das 2009. In this task the animal initiated trials by pulling a lever, after a fixed delay (in the range of 10-15 s, in different sessions) a tone started, lasting for a fixed duration (2-4 s, in different sessions) after which, the tone changes pitch, cueing the animal that it could release the lever, the animal had a grace period (up to 2.5 s) to release the lever, if it did release it within that grace period, then a reward was delivered and the trial ends. All this was done in darkness, the monitor is off. Animals tended to entrain to this task and initiate a trial soon after the end of the previous one. It resulted that these trials had comparable durations to one another. The fixed time interval was selected so that the duration of a completed trial of this motor-auditory task was similar to the timing of the fixation task previously used.

We present also data from 7 sessions (for monkey E) of a modification of this task. Monkey E was initially trained on this same auditory/motor task that the other 2 animals performed, but with very poor performance. We modified the task making it closer to the fixation task, and the animal's performance improved. The data presented here for monkey E is for this modified auditory/motor task. In this modified task, trials started with the presentation of a tone, cueing the animal to pull a lever. The animal was given a grace period to pull the lever (up to 2.5 s), failure to do so, meant an aborted trial. If the animal pulled the lever within the grace period, then the tone changed pitch and the animal was expected to hold to lever until the tone was turned off (2-4 s, in different sessions), cueing the animal that it could release the lever. Once more the animal was given a grace period (up to 3 s) to release the lever, and if it did release it within that grace period, then the animal was given reward and a fixed inter-trial interval (10-12 s, in different sessions) started until the beginning of the following trial.

The data presented here (for either version of the auditory/motor task) was from recording days where at least one other session was also recorded. This other experiment was a fixation task done in quasi-total darkness. We aimed at recording trials in both sessions (fixation task or auditory/motor task) with similar durations. The recordings are always from primary visual cortex (for a subset of sessions, 12, electrophysiological data was also recorded, data not included here).

We compared the trial average hemodynamic response for each session to each task type: fixation or auditory-motor task. The similarity between the task-related responses' shapes to both task types in V1 is striking. In Figure 3.9, are two recording examples Figure 3.9a-f is for monkey T on the original auditory/motor task (compared with the fixation task) and Figure 3.9g-l is data for monkey E on the modified auditory/motor task. Both examples were compared against the fixation task. The hemodynamic task-related responses were similar between either of the auditory/motor tasks, when compared to the fixation task performed on the same day.

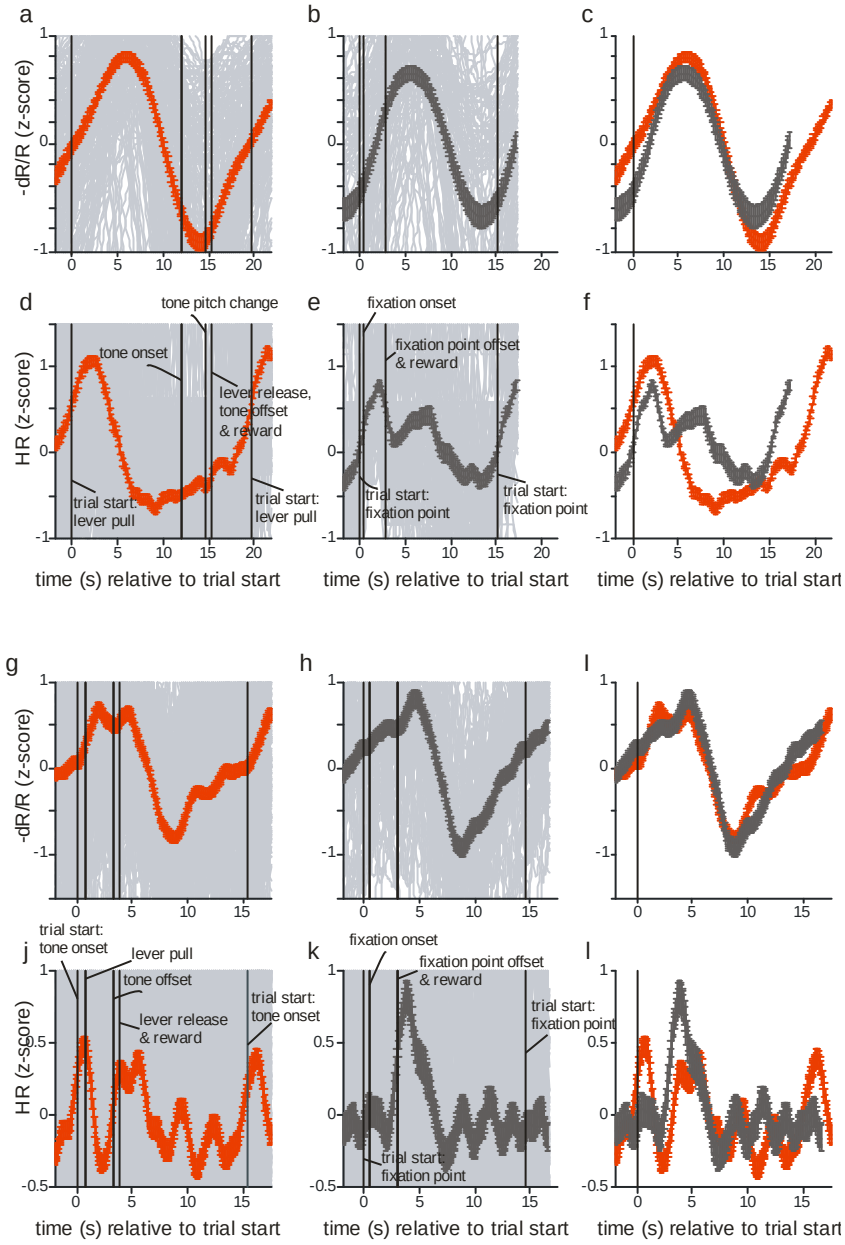

Figure 3.9 – There is a hemodynamic response in visual cortex for an auditory/motor task. **(a)** Z-scored hemodynamic trial-locked response to the auditory/motor task (n = 118 trials), for a single session (monkey T). Single trials in gray, average trial response in red. (Response to the self paced auditory task.) In **d** is the sequence of trial events in time. **(b)** Z-scored hemodynamic trial locked response to the fixation task (n = 227 trials), for a single session (monkey T) collected in the same day as A. Single trials in

light gray, average trial response in dark gray. In **e** is the sequence of trial events in time, for the fixation task. **(c)** Overlay of the average responses in **a** and **b**. Note: in either circumstance the average trial traces were aligned to the trial start. **(d)** Similar to **a**, but here is the trial-locked average z-scored heart rate response to the auditory/motor task. Mean auditory/motor task event sequence is overlaid with heart rate response. **(e)** Similar to **d** for the heart rate response to the fixation task. **(f)** Overlay of the average responses in **d** and **e**. **(g-l)** Similar to **a**-**f** for monkey E (n = 214 and n = 101, for auditory/motor and fixation task, respectively). The auditory/motor task here is the one where trials are automatically initiated.

We next aimed at quantifying how similar were the shapes of the hemodynamic responses in the two task conditions (visual versus auditory/motor). We started by comparing the magnitudes (defined as peak to trough amplitude) of the average task-related responses to either task type (Figure 3.10a). The hemodynamic response to either task type had similar magnitude (magnitudes were compared as percent signal change and not on z-scores). Even though we were in primary visual cortex, the magnitude of the hemodynamic task-related response was not consistently larger for the fixation task than for the auditory/motor task.

Moreover, we compared the shapes of the task-related responses for the two task types and found significant correlations between their shapes ('visual' and 'auditory/motor' tasks), Figure 3.10c. Shapes were compared by the correlation coefficient on the z-scored responses (we were interested on the shape similarity, independent of magnitude). Firstly, we calculated the correlation coefficient between the average task-related hemodynamic responses for the visual or the auditory/motor task (Figure 3.10c, open circles). There is significant variability on the task-related hemodynamic response for individual trials, still we aimed at quantifying the correlation between pairs of individual trials (with one trial for a fixation task and another for a auditory/motor task); this is indicated with green makers on Figure 3.10c. Finally we wanted to confirm that this correlation between individual trials was significant; with this aim, we compared the distribution

of correlation coefficients to pairs of trials where the time structure of the trial was destroyed and sampled randomly. This was repeated 1000 times, the results are indicated in black, with 95% confidence intervals (resulting from the bootstrapping approach). There is no overlap between the points in green and the confidence intervals; therefore we do not expect the correlations to be spurious.

Given the variability of the hemodynamic response on a trial by trial basis, we also compared the resulting average correlation between pairs of individual trials of visual and auditory/motor task, against the average correlation between pairs of trials of each task individually. We compared the correlation visual/auditory-motor (green), with visual-visual (grey) and auditory/motor-auditory/motor (red), Figure 3.10e. It could be noticed that the visual-auditory/motor average correlation was often, but not always, lower than either visual-visual or auditory/motor-auditory/motor, but in similar range. Suggesting that the shape similarity we observed between trials of different experiments is maintained within experiments.

Not only the mean shape of the task-related response to both task types was similar, the magnitude of this response was also of the same scale. In Figure 3.10a, it can be noticed that even though there is no clear relationship between the magnitudes, their values fell in the same dynamic range.

It is worth mentioning that in particular for the first type of auditory/motor task the timing of the behavioral events was significantly different when compared to the fixation task. Both trial types were compared based on the trial beginning, but for the fixation task a succession of events leading to reward was in the initial part of the trial The same was not true for the other task type; trials started with the motor action of pulling the level, then there was a wait period, only over midway into the trial did the auditory stimulus came on, then changed pitch, and eventually reward would be delivery.

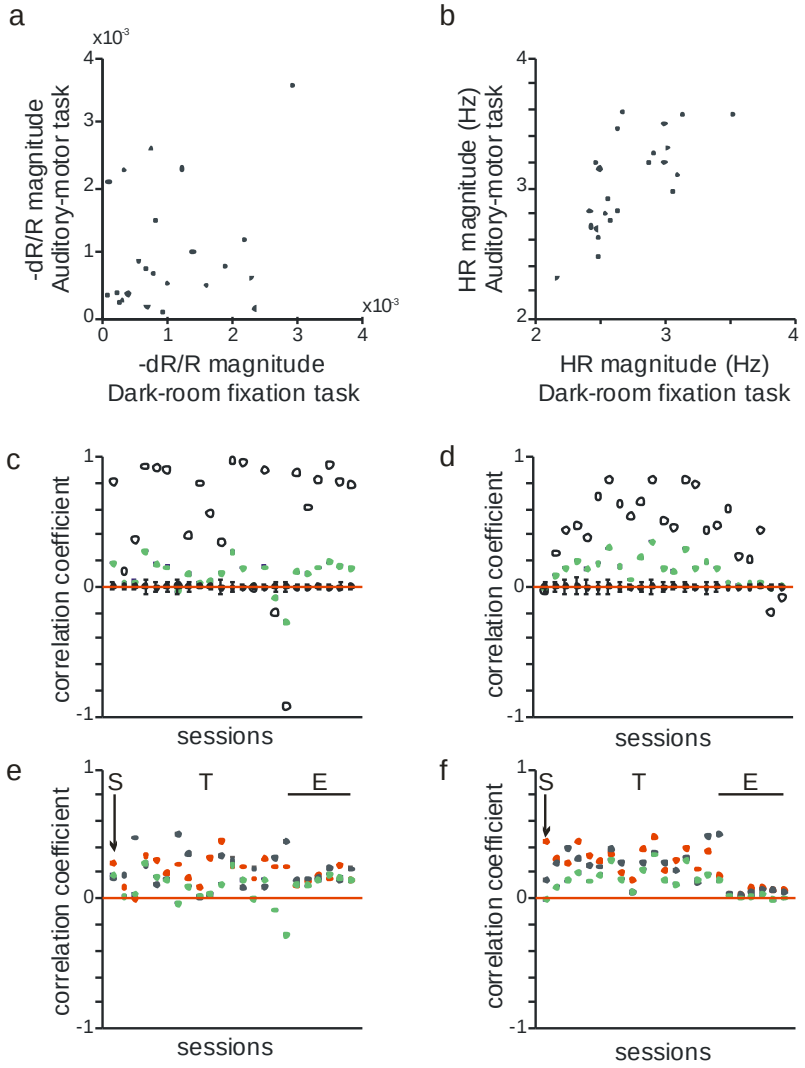

Figure 3.10 – The amplitude and shape of the response to the auditory task are similar to the response to the fixation task. **(a)** Magnitude of the average trial response to the fixation task versus the magnitude to the auditory task (linear fit: $y = 0.73x10^{-4} + 0.28x$, $r^2 = 0.06$). **(b)** Same as **a**, but for the heart rate response (linear fit: $y = 0.80 + 0.83x$, $r^2 = 0.51$). **(c)** The average response to the auditory task is correlated to the response to the fixation task (open circles), for most of 23 pairs of sessions. In green is the average correlation coefficient for each pair of trials belonging to either task. In black is the bootstrapped version of the green traces, where time was randomized (95% confidence interval). **(d)** Same as **c**, but for the heart rate response. **(e)** In green is the same mean correlation value as in **c**. In red is the mean correlation between all pairs of trials of the auditory/motor task. In gray is a

similar correlation as in red, but for the fixation task. The letters indicate the animal associated with the different data points (the order was maintained for the other panels). **(f)** Similar to **e**, but for heart rate.

The heart rate data was subject to similar analysis as the hemodynamic data (Figure 3.9d-f and j-l, and Figure 3.10b,d,f). The heart rate responses had their own time courses, on average displayed a peak prior to the peak in the hemodynamic response (Figure 3.9a vs. d, b vs. e, g vs. j h vs. k). Once more the average heart rate response displayed a more complex pattern than the average hemodynamic response, with more apparent peaks. When looking at the magnitude changes (Figure 3.10b), heart rate in the visual or auditory/motor task did seem to have a positive correlation; we expect heart rate to be characteristic of each animal, and potentially be more correlated in individual experimental days depending on the physiological tonus of the animal; our data followed this interpretation. Comparison of the z-scored amplitudes still exhibited a positive correlation, although weaker ($y = 0.83 + 0.25x$, $r^2 = 0.11$, data not displayed here). Note that this was different from our observation in the hemodynamic response where we did not find such a clear trend. Finally, when we compared the similarity in shape between the heart rate responses to the two classes of tasks, the results (Figure 3.10d,f) were somewhat similar to the observed in the hemodynamic response.

It is worth noting that in Figure 3.10f, when comparing how the average similarity between individual trials of visual vs. auditory/motor tasks against the average similarity between trials within the same task category, it was noticeable that in all instances the average correlation between tasks was lower than the one within task. No such clear trend was observed in the hemodynamic responses. This observation suggests that there are intrinsic differences between the tasks; and those that are better grasped by the heart rate response than the hemodynamic response – for the hemodynamic response the different task types had rather similar profiles. This

suggested that the hemodynamic response (for these tasks) is less dependent on the specific sequence of events and might reflect more the fact the that subjects were engaged in the task.

3.7 Discussion

Looking at the task-related hemodynamic response, we found trends on average behaviors. At a trial by trial level and even on a session by session there could be too much variability, making more assertive statements on the behavior of the hemodynamic response hard. Even the shape of the task--related response could change for different animals, or within different sessions for the same animal. Nevertheless we have more evidence on the importance of characterizing the hemodynamic task-related response, its behavioral correlates and its neuronal underpinnings.

We presented data for a few experimental manipulations mostly on fixation tasks. Our goal was to further explore potential correlates to the hemodynamic task-related signal, in primary visual cortex. Unfortunately these experiments opened more questions than convey answers. Many lines of further experiments could be explored to follow on observations presented above.

On the one hand the task-related response entrained to different trial durations (spectral peaks, Figure 3.1 and Figure 3.3) but the temporal dynamics of those did not seem dependent on trial duration, in particular, in periods common to both short and long trials, Figure 3.2, with the caveat that we only tested a small range of trial durations.

On the other hand, when we looked at the role fixation duration plays in the position and amplitude of the peak of the hemodynamic response. We observed a dependence of peak position and amplitude on fixation duration (Figure 3.5). This evidence could suggest that either the effort of fixation or the delivery of reward could be marking events which elicit this task-related hemodynamic response.

To explore the role that reward is playing in the hemodynamic signal, we designed another variation of the fixation task where we manipulated reward amount. If on the one hand this reward-related task does not disambiguate the aforesaid question, it unequivocally suggested that the task-related response is influenced by reward. Not only was the amplitude of the task-related response modulated by reward amount, but also a change in a slow, trial length, hemodynamic response reflected reward level.

Finally, in the last experiment presented, where a fixation task was compared to an auditory/motor task, lead us to conclude that the hemodynamic task-related response can be a global response. At least a task that did not engage visual cortex, as the one used, still elicited a hemodynamic task-related response in primary visual cortex. Equally importantly, it was the striking finding that independent of the differences in the timing of the two tasks, in V1, the hemodynamic task-related response had on average a similar profile. Once more, this opens further questions. It points to some role of the decision of engaging on a trial, or some effort in doing or attending to trials, independent of the specific details of the task.

There is something intrinsically related to the decision of taking up a trial that might be influencing the existence of the hemodynamic task-related response.

On a different analysis of the same fixation task previously published in the laboratory, we observed that in trials that the animal fails to initiate did not on average present a task-related response (Sirotin et al. 2012, Figure 6). These non-initiated trials were significantly different from initiated ones, independently of the subject receiving or not a reward. In non-initiated trials the subject did not make an active effort of engaging with task on that trial. In trials the animal did not complete, but initiated, the difference to completed ones, rewarded, and the ones the animal initiated but does not complete was not as compelling as the difference between completed trials and non-initiated ones.

We looked back at the analysis and data included in Sirotin et al. 2012, Figure 6. We calculated a Pearson's correlation coefficient between each trial in a session and the average completed trial for that session. For each session we have an average correlation for each trial category (non-initiated, initiated and rewarded, or completed, and initiated and not rewarded, or aborted). Figure 3.11 shows a scatter plot of the average correlation between completed trials and non-initiated or aborted ones, for each session previously used for Figure 6 in Sirotin et al. 2012. This suggested that independently of completing a trial there was a significant difference between engaging or not in a trial.

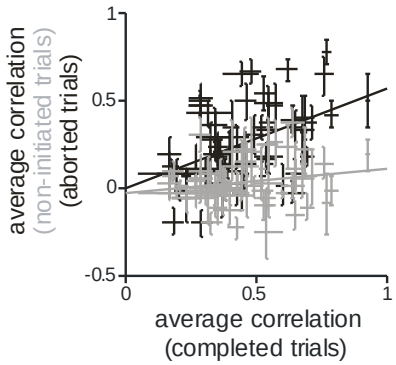

Figure 3.11 – Lower correlation between non-initiated trials and completed ones, than between aborted trials and completed ones. Scatter plot of the session by session correlation between completed trials with the average completed trial (for each session) and the correlation between either aborted (black) or non-initiated trials (grey) (n = 68 sessions, 2 animals, monkey S and T). Error bars reflect s.e.m. Regression lines: grey (scatter plot aborted vs. completed trials), $y = 0.19x10^{-3} + 0.57x$, $r^2 = 0.21$, black (scatter plot non-initiated vs. completed trials), $y = -0.28x10^{-1} + 0.14x$, $r^2 = 0.04$.

The task-related hemodynamic activity in V1 probably reflects different aspects of behavior other that just visual properties of the scene. Even though some of the experiments presented here were testing the influence of fixation on the hemodynamic task-related response, it can be argued that the effects observed there were small and as observed in Figure 3.5A

(distribution along the vertical axis) for each fixation duration presented there was a wide range of hemodynamic response delays. This suggested that fixation duration should not be triggering the hemodynamic response (at least as could be described by a simple hemodynamic response function).

The hemodynamic response, probably reflects many aspects of behavior and physiology, we cannot exclude the possibility that there is a role for fixation in this response, but it should not be the sole driver specifically to the task-related hemodynamic response.

The combined anecdotal evidence of a few experimental variations allows speculation on what mechanisms might be (or might not be) underlying this hemodynamic task-related response. Bearing in mind that we expect this response to be global (present in visual cortex in response to an auditory/ motor task, independent of the different timing of sequence of events for the auditory/motor task relative to the fixation task) and that there is a more pronounced difference between non-initiated trials to completed ones than between aborted trials and completed ones. It seems like a mechanism as attention could be very relevant when considering this signal. Potentially not attention in the sense of spatial attention, when one would expect at least some cortical dedication to the tasks performed, but a more global attention or anticipation of upcoming events.

There is evidence from research in humans of global attention-like (e.g. Ress et al. 2000, Silver et al. 2007, Sylvester et al. 2007, Donner et al. 2008, Pestilli et al. 2011) and task-related changes in BOLD fMRI (Jack et al. 2006, Elkhetali et al. 2015, Griffis et al. 2015). We would be eager to see fMRI experiments that would look at other brain areas (cortical and sub-cortical) that could shed some light into potential neuromodulatory mechanisms. One can also entertain the idea that there is some potential for a global response related to arousal/engagement to have a role in this signal. Recent publications on the physiology of the locus ceruleus in the context of behavior, explore the role of phasic locus ceruleus firing with the decision of execute actions that are task relevant (Kalwani et al. 2014 and

Joshi et al. 2016). For the simple tasks that we used, it might be foreseeable that the most relevant decision that requires execution pertains engaging in the task. Without further experiments this remains in the realm of speculation.

Hence, our empirical observations suggest that there is the potential that the hemodynamic response is reflecting the influence of different neuromodulatory systems. Finally, we have failed to find neural measures that reliably parallel the hemodynamic response; the closest related metric, in these observations was heart rate, but even heart rate did not fully track the observed nuances of the hemodynamic response. This reflects prior work in the laboratory where multi-linear regression models combining a set of neural regressors (MUA, various LFP bands) were used to predict the hemodynamic response (Sirotin & Das 2010a). Such models were only able to account for less than half the variance in the hemodynamic response.

4 Slow drifts in brain blood volume are associated with behavioral changes in primate V1

4.1 Abstract

Neuroimaging signals (e.g. BOLD fMRI signals) are complex and reflect both exogenous and endogenous responses. There is extensive knowledge pertaining hemodynamic exogenous responses, while endogenous responses remain largely elusive. In the past, most studies of neuroimaging have typically focused on short-term stimulus-related hemodynamic changes on timescales of a few seconds. Here, we focus on the less investigated long-term fluctuations in local brain blood volume, and its correlation to behavioral engagement. We assessed behavioral changes through spontaneous fluctuations in the performance of monkeys engaged in a periodic fixation task. We simultaneously acquired hemodynamic signals (through intrinsic signal optical imaging), multiunit neuronal activity and local field potentials - LFP - (through intracortical microelectrode recordings), heart rate (derived from the optical imaging signal) and behavioral metrics related to quiescence. Notably, we observed robust increases in local brain blood volume during epochs in which the monkey was less engaged in the fixation task, as compared to lower blood volumes when the monkey was actively engaged or more motivated to perform the task. Accordingly, epochs of lower engagement were associated with increased power in lower LFP frequency bands, lower firing rates and lower heart rate. Therefore, epochs of low brain blood perfusion were associated with higher heart rate. Finally, we compared the state-dependent slow drift in brain blood volume with the hemodynamic task-related signal. The interplay between changes in blood volume and heart rate is complex; if on the one hand the slow drift in blood volume is negatively correlated with heart rate, the trial-related changes are positively correlated.

4.2 Introduction

There is extensive use of neuroimaging signals for inferring neural activity. Techniques like blood-oxygen-level dependent (BOLD) functional magnetic resonance imaging (fMRI) that are minimally invasive and can measure signals from the full brain represent an advantage when compared to electrophysiology.

When talking about neuroimaging signals one tends to focus on signals driven by external events. However there is significant evidence showing the presence of endogenous responses (like attentional or task-related) in neuroimaging signals (Corbetta et al. 1990, Tootell et al. 1998, Kastner et al. 1999, Ress et al. 2000, Serences et al. 2004, Jack et al. 2006, Sylvester et al. 2007, Donner et al. 2008) that are not correlated with local electrophysiology (Sirotin & Das 2009). The neuroimaging response is then the result of endogenous and exogenous contributions. Exogenous contributions reflect responses to external stimuli (like visual stimuli in visual cortex) and have a linear relationship with local neural activity (Cardoso et al. 2012, Lima et al. 2014) and endogenous neuroimaging signals do not trivially reflect underlying changes in local neural activity (Sirotin & Das 2009). Finally, in the visual system, there is ample evidence of the presence of both stimulus-related and endogenous contributions to the hemodynamic response, in human and non-human primates (Jack et al. 2006, Donner et al. 2008, Pestilli et al. 2011, Sirotin & Das 2009).

There are different activity patterns that reflect endogenous contributions to the BOLD signal; in particular work in humans shows the presence of BOLD modulation with spatial attention and task structure (Jack et al. 2006). In Jack and colleague's study, subjects were asked to perform a near threshold visual detection task and report their decision immediately or after a fixed delay. They observed that the BOLD signal had two clearly separable components: an increase in BOLD associated with spatial attention to the near threshold stimulus, and another BOLD signal increase associated with

the structure of the task, and independent of the presented stimulus. The second, the task-related signal, has also been observed in our lab in non-human primates (Sirotin & Das 2009). An endogenous signal that has been widely reported in BOLD fMRI studies is associated with attention, there are several examples of attention in visual cortex (Kastner et al. 1999 Somers et al. 1999, Gandhi et al. 1999, Ress et al. 2000, Ress & Heeger 2003, Shulman et al. 2003, Serences et al. 2004).

Previous work from our laboratory (Sirotin & Das 2009) in non-human primates performing a periodic visual fixation task compared task-related and stimulus-related hemodynamic signals with electrode recordings, in primary visual cortex. Sirotin and Das showed a task-related signal entrained to trial timing, in the absence of visual stimuli. This signal was comparable in magnitude to some stimulus related responses and could not be predicted from local multi-unit activity (MUA) or local field potentials (LFP), unlike the stimulus component. There are BOLD fMRI studies (Elkhetali et al. 2015; Griffis et al. 2015) as well that show evidence of a task-like activity in human subjects that is dependent of performance. In this study, subjects were asked to detect a change in a stimulus's temporal frequency, in the context of visual, auditory stimulation, or bimodal auditory-visual stimulation (subjects were requested to report changes in one of the sensory modalities). In this task, there was evidence of a 'task-initiation activity' reflected in an increase in BOLD response in visual cortex with starting a block of trials when the subjects were asked to detect a visual stimulus, relative to performing the auditory detection task. The authors observed as well sustained changes in BOLD responses. They reported an increase in baseline activity within a block of visual detection trials relative to a block of auditory detection trials – 'task-maintenance activity'. This last signal had higher magnitude in visual cortex for subjects performing better on the visual detection task; hence performance influenced the BOLD fMRI response.

In the present study, we aimed at exploring the potential correlation between different states of engagement and the hemodynamic response. We explo-

red the behavioral correlates of the hemodynamic response in the alert animal preparation, using the laboratory's established technique of simultaneous functional neuroimaging (intrinsic-signal optical imaging) and electrode recordings from primary visual cortex of non-human primates performing periodic visual fixation tasks.

There is extensive literature relating changes in mental state to physiological changes. There are reported changes in heart rate and skin conductance concomitant with indices of arousal. Malmstrom and colleagues have shown changes in these metrics while subjects were watching a benign film (Malmstrom et al. 1965). Even earlier work by Angelo Mosso in cortical pulsation showed changes in pulsation rates and profiles with different mental states, for example sleep (translation of original publication: Raichle & Shepherd 2014).

There are also known changes in LFP wavebands with arousal/attention, in particular the early work of Hans Berger and the development of electroencephalography. Hans Berger showed that alpha-band activity increased when subjects laid with their eyes closed relative to when they had their eyes open (for review see Millett 2001). Given the extensive evidence for different markers of endogenous activity in the brain we aimed at measuring neural and physiological signals with the goal of shedding light into the functional role of endogenous hemodynamic responses. Specifically, we recorded: MUA, pair-wise MUA correlation, LFP and heart rate.

As mentioned, there are physiological and neural metrics that characterize different aspects of behavioral state. In this study we propose that there is a signature of task engagement that is reflected on the hemodynamic signal. To support our claims, we also report other behavioral markers. In the task we have used, we looked at periods in which the subjects were engaged in the fixation task, but we also looked at periods in which they were disengaged, not completing trials. This work parallels work done in a more established behavior change: arousal. We compared our observations with those known to occur with changes in arousal and alertness.

A common physiological marker of arousal is pupil diameter (for a review see Aston-Jones & Cohen 2005). Recent work (Reimer et al. 2014, Vinck et al. 2015) looked at different states of arousal in rodents (probing locomotion versus quiescence) observing distinctive patterns in visual cortex: increased gain of visual responses with increased arousal, decreased spiking noise-correlations, and even recruitment of different cell classes. In terms of neuronal activity, they presented evidence for changes in spiking patterns with attention and arousal. Arousal was associated with improvement of signal to noise ratio in cortical areas with changes in 'noise-correlations' across electrodes, even though increased arousal was associated with lower firing rates (Livingstone & Hubel 1981). Changes in similar metrics are associated with attention; comparing correlations in the firing patterns of individual cells on a trial by trial basis ('noise-correlations') it has been shown that attention is associated with increases in firing rate (Moran & Desimone 1985, Luck et al. 1997), while attentional improvement was associated with decreases in interneuronal correlations (Cohen & Maunsell 2009, Cohen & Kohn 2011). We have used interneuronal correlations slightly differently in this study, computing those in time as opposed to across trial conditions, which was more appropriate for this study (visual cortex is sensitive to variations driven by eye movements, and for periods the subjects do not fixate it becomes meaningless such comparisons across engaged and disengaged trials, as the patterns of eye movements can be distinct).

Finally, there is recent evidence of changes in hemodynamic signal that match changes in arousal, as measured by pupil dilation (Pisauro et al. 2016). In this study they looked at the hemodynamic response in the visual cortex of mice while viewing visual stimuli. They reported that hemodynamic response had two components; one related to the visual stimuli the other, more global and correlated with pupil diameter. The study we present here parallels Pisauro's study and aims at further exploring the task-related component of the hemodynamic response to global changes in hemodyna-

mic signal, in different states of engagement in the task. In our study we did not use visual stimulation, so we could reduce influence of visual stimuli in the recording region. Moreover we include here electrophysiological data not included in Pisauro's study.

We trained subjects to perform a periodic fixation task in quasi total darkness, as reported before (Sirotin & Das 2009). Animals performing this task naturally exhibit periods of more and less engagement in the task. Our performance metric uses the segregation of initiated versus not initiated trials to estimate engagement in the task. We compared how the different measured signals relate to periods in which the subject was engaged in the fixation task versus periods in which it was not. Our data suggests that endogenous changes on the hemodynamic signal have a significant correlation with behavior; we observed increases in blood volume change with disengagement in the task. The changes in engagement were accompanied by changes in heart-rate; increased heart rate was associated with periods of higher engagement. We have observed a tendency towards an increase in lower frequency LFP power and decrease in higher frequencies in more disengaged periods. There was a slight decrease in firing rates a more robust increase in firing 'noise correlations, across electrodes, in more disengaged periods relative to more engaged ones. This study brings attention into the importance of accounting for endogenous signals' contribution to neuroimaging when using such techniques.

4.3 Methods

4.3.1 Summary

In this chapter we used some data previously used in other publications (Sirotin & Das 2009; Sirotin et al. 2012) reanalyzed it for the questions addressed in this publication and collected a significant number of additional experiments.

Results were obtained using intrinsic-signal optical imaging (Bonhoeffer & Grinvald 1996, Sirotin & Das 2009) in three monkeys performing visual fixation tasks: 68 sessions were analyzed (14 sessions from monkey S, 40 sessions from monkey T and 14 sessions from monkey E). In a subset of these experiments, multi-unit electrophysiological data was collected, and in some of the experiments there were 2 electrodes (3 sessions for monkey S, 3 recording sites; 25 for monkey T, 44 recording sites, and 6 for monkey E, 10 recording sites). For the electrode pair-wise correlations the numbers are: 19 sessions for monkey T and 4 sessions for monkey E. All recordings were acquired continuously. Data analyses were performed offline using custom software in MATLAB (MathWorks). All experimental procedures were performed in accordance with the US National Institutes of Health Guide for the Care and Use of Laboratory Animals and were approved by the Institutional Animal Care and Use Committees of Columbia University and the New York State Psychiatric Institute.

4.3.2 Surgery, recording chambers and artificial dura

After the monkeys were trained on visual fixation tasks, craniotomies were performed over the animals' V1 and glass-windowed stainless steel recording chambers were implanted, under surgical anesthesia, using standard sterile procedures, to image a ~ 79mm^2 area of V1 covering visual eccentricities from ~1 to 5° visual angle. The exposed dura was resected and replaced with a soft, clear silicone artificial dura. After the animals had recovered from surgery, their V1 was optically imaged, routinely, while they engaged in the fixation task. Recording chambers and artificial dura were fabricated in our laboratory using published methods (Arieli et al. 2002).

4.3.3 Behavior

Animals had to perform a fixation task in a dark-room environment (as the dark-room fixation task in Sirotin and Das, 2009). The monitor was covered,

except for a small fixation point (<0.3° visual angle). The animals were cued to fixate on the small fixation point by changing its color from grey to red. Once they achieved fixation, the fixation point switched to green, and by the end of the fixation period the fixation point turned back to gray. Successful trials were the ones where the animals kept fixating while the fixation point was on (green); by the end of successful fixation the animals received a liquid reward (juice). On each trial there were three possible outcomes based on the animal's eye position. The animal could either fixate during the whole fixation period, and receive a reward by the end of it (completed trials); the animals could start by achieving fixation but failing to hold fixation until the end of the fixation period, not receiving any reward (aborted trials: in this type of trial the animal had to wait for a fixed inter-trial interval until the start of a new trial); or the animals could not even attempt to fixate during the initial fixation time and not receive a reward either (not-attempted trials). Trials were segregated into one of two categories: attempted (clustering completed and aborted trials) or not-attempted trials. Eye fixation and pupil diameter were recorded using an infrared eye tracker (Matsuda et al. 2000), and sampling frequency was 60 Hz.

4.3.4 Imaging

Images were acquired on a Dalsa 1M30P (binned to 256 × 256 pixels, 7.5 or 15Hz); frame grabber, Optical PCI Bus Digital (Coreco Imaging). Software was developed in our laboratory based on a previously described system (Kalatsky & Stryker 2003). Illumination, high-intensity LEDs (Agilent Technologies, Purdy Technologies) with emission wavelength centered at 530 nm (green, equally absorbed by oxy- and deoxyhemoglobin, and therefore proportional to local cortical tissue hemoglobin, i.e. blood volume). Lens: macroscope of back-to-back camera lenses focused on the cortical surface.

Prior to analysis, acquired images were (if necessary) motion corrected by aligning each frame to the first frame by shifting and rotating the images using the blood vessels as a reference (Lucas & Kanade 1981). Breathing and cortical pulsations (typical heart rates were ~2–4 Hz, much faster than the typical hemodynamic response frequencies of ~<0.5 Hz) were removed by subtracting a high-pass filtered version of the hemodynamic response using the Chronux MATLAB Toolbox function 'runline.m'. The hemodynamic responses were recorded from the CCD camera, after the corrections mentioned were converted into fractional change (dividing by the mean hemodynamic response on the session). In this chapter they come presented as negative fractional reflectance as that measure is proportional to blood volume changes. A linear trend on the hemodynamic response was discounted on each individual session, but performing a linear regression through the entire session and subtracting this regression. Heart rate was estimated from the observed cortical pulsation (corresponding to the high-pass filtered version of the recorded light reflected data).

Two different aspects of the hemodynamic response (similar procedure was done for all the other physiological measures) were analyzed in this chapter: the mean task-related signal on each trial, and the time course of this signal. Figure 4.1, Figure 4.2d refer to analysis on the mean task-related signal (averaged in time), and the remaining ones refer to the time course of the task-related signal.

4.3.5 Electrophysiology

Electrode recordings were acquired simultaneously with the optical imaging. Recording electrodes (FHC, AlphaOmega; typical impedances ~600–1,000 kΩ) were advanced into the recording chamber through a silicone-covered hole in the external glass window, using a custom-made microdrive. Recording sites were mostly, but not exclusively, confined to upper cortical layers. Signals were recorded and amplified using a Plexon recording system. The

electrode signal was split into spiking (100Hz to 8kHz band pass) and LFP (0.7–170Hz). No attempt was made at isolating single units and all measured spiking was multiunit activity (MUA) defined as each negative-going crossing of a threshold that was about 4 times the r.m.s..

Chauvenet's criterion was used to remove potential outliers in the LFP signal (using 20 standard deviations at threshold criteria). The continuous time-varying LFP power spectrum for a full recording session was estimated for frequency bins 4-170Hz using the multitaper method (Thomson 1982) implemented in the Chronux MATLAB Toolbox (http://www.chronux.org/, Mitra & Bokil 2008). Different sets of parameters were used for frequency decompositions 4-30Hz and 20-170Hz. For the lower frequencies we used 1000 ms windows displaced at 250-ms steps, a single taper and a spectral concentration of -/+ 1.0Hz. For frequencies 20-170Hz we used 250ms windows displaced at 62.5-ms steps, three tapers and a spectral concentration of -/+ 8Hz. Two band-limited power LPF measurements were specifically included in the analysis (*alpha*: 7-12Hz and *gamma*: 30-90Hz), obtained by averaging the time-varying induced LFP spectral power over the defined frequency bands. They were down sampled to the imaging frame rate (7.5 or 15Hz) and aligned in time with the imaging trials.

4.3.6 Arousal Related Index (ARI)

An arousal related index was defined as the ratio between the normalized power envelop at alpha-band LFP and the normalized power envelop at gamma band LFP. The power envelops were calculated as the norm of the Hilbert transform of each LFP band. The Hilbert transform was computed on the 1kHz data, the reported ARI for each trial is the median of the 1kHz index for the duration of each trial. The ARI calculated here is based on Moore et al. 2014.

4.3.7 Alertness metrics: brain movement and eyes open/closed

For sessions with vascular patterns prominent and well focused, motion correction algorithm were used (Lucas & Kanade 1981), as mentioned on the imaging section. This algorithm looks for the best alignment of each frame relative to a reference frame. The imaging correction gives an estimate of movement in x and y (in number of pixels). For each trial we calculated a movement index which is the sum of the variability (measured as standard deviation) of movement in x direction and of the variability in the y direction.
From the eye movement traces, it was possible to classify each imaging frame into either of three classes: eyes open; blinks; eyes closed. Categories were found by thresholding, by visual inspection of a scatter plot with xy distribution of positions for each session. Periods of eyes open and looking in the general direction of the monitor were trivially well characterized (value 0). Periods with eyes out of range for the duration of the whole frame were considered probably closed (value 1). Periods with blinks tended to be distinct from the other two classes (value 0.5). The metric reported below reflects an average of these categories for each trial; overall a proxy of the probability of eyes closed.

4.3.8 Interneuronal correlations: electrode pair-wise correlations

The correlation between the activity of pairs of electrodes recordings (MUA) was measured using a sliding window of 1400ms. For each time point the correlation value reflects the Pearson's correlation coefficient between the activity in the 2 electrodes, in a 1400ms window centered on each sample.

4.3.9 Correlations between performance and different responses

Performance was measured as the probability of starting a trial. This performance was smoothed on a moving window considering a neighborhood of 10 trials (MatLab function 'smooth'). For individual sessions, a Spearman's correlation coefficient was computed to estimate the similarity between

hemodynamic, heart rate, spiking, different LFP waveband responses or pair-wise electrode correlations with performance. When comparing the correlation of the different physiological measures with performance, it was considered the mean task-related signal on each trial (as each trial was associated with a single outcome). For each considered session was presented a correlation coefficient between performance and either of the neural measures. For the comparisons between physiological measures a similar approach was taken; comparing the mean response on each trial for each measure with performance.

4.3.10 Correlations between heart rate and hemodynamics

Cross-correlation between heart rate and hemodynamics were performed for each session individually. The reported cross-correlation level refers to the peak (maximum magnitude, can be either positive or a negative number) of correlation between the two signals. Only positive lags of the hemodynamic response relative to heart rate were considered. The cross correlation was calculated within a maximum lag of 10 seconds between the hemodynamic and heart rate signals. Two conditions were compared: either cross correlation was calculated between the full traces or the average response on each individual trial was subtracted to the corresponding segment in the trace (and then the cross correlation was calculated).

4.3.11 Cross-validation (k-fold cross-validation)

Each session was divided in 5 parts (each containing contiguous 20% of the data). The response to the trials in each segment were segregated into 'initiated' versus 'non-initiated' (based on the animal's performance), resulting in 5 parts comprised of 4 segments for the training data (of initiated trials) and 1 value for the validation data (of initiated trials). The same was done for non-initiated trials. Each session had an average training and validation value for each class (initiated and non-initiated trials). The scatter of these

values for each session is exemplified in Figure 4.1b. For comparisons across sessions, data was z-scored, and the average training and validation numbers were averaged, with each session contributing equally (Figure 4.1d). To further test the relationship between the values for initiated and non-initiated trials, for each pair (corresponding to the mean response on each 20% of the data for the two classes) an angle was also calculated (having initiated trials as the reference). By plotting the distribution of these angles one can observe how consistent or not is the relationship of initiated and non-initiated trials (Figure 4.1c).

4.4 Results

4.4.1 Hemodynamic mean trial response correlates inversely with engagement

We wanted to understand if slow changes in the hemodynamic response were influenced by behavioral signals, similarly to previously reported (Pisauro et al. 2016) , in our setup, in primary visual cortex (V1),. We set up to record responses from non-human primates performing a fixation, in quasi total darkness, where only a fixation point was present. We simultaneously recorded intrinsic signal optical imaging, extracellular MUA and LFPs.
The fixation task the subjects performed was rather simple, and with a limited number of possible outcomes. Animals could hold fixation for a required amount of time and receive reward; we call these trials completed or rewarded. Animals could initiate the fixation task, but interrupt fixation before the end of the required fixation time, not receiving reward: aborted trials. Or animals could not even initiate the fixation task: non-initiated trials. The behaviors exhibited were rather simple, but adequate to exploring correlates of task engagement in the hemodynamic signal. Therefore we focused our analysis on initiated vs. non-initiated trials. We defined a performance metric as the smoothed probability of initiating a trial (see methods).

The fundamental relationship between the animal's performance in a task, hemodynamics, and different neural and physiological measurements is illustrated for a representative session in Figure 4.1.

Blood volume changes increase when the subjects were less engaged in the fixation task. This can be observed in Figure 4.1 during periods of low engagement (shaded gray periods; performance below 50%) the trial mean hemodynamic signal tends to be higher. To quantify the relationship between hemodynamic signal and performance, we calculated the Spearman's rank correlation between the mean trial hemodynamics and performance (ρ = -0.531, p-value < 0.01, in this session). In this session there was a negative relationship between the animal's engagement and changes in blood volume; lower engagement was associated to higher volume.

To understand if the observed changes were reliable for this session, or represented an average tendency but were not observed in shorter time periods, within each session; we used a 5-fold cross validation method. We split each session in 5 contiguous segments; one segment was kept as validation, the other 4 comprised the training set. We compared the mean hemodynamic signal to initiated versus non-initiated trials within the test and validation sets (Figure 4.1b). For this session we could segregate initiated from non-initiated trials. In particular when looking within each of the 5 individual segments (see the gray lines, which connect the average response to initiated and non-initiated trials in each segment) one could observe that in all instances the non-initiated trials (in red) had a higher hemodynamic signal than initiated ones (in blue). We quantified this directionality of initiated trials within each segment of 20% of the data having on average a smaller hemodynamic signal change than non-initiated trials. This quantification measured the angle between initiated to non-initiated trials. The measure of this angle is cartooned for one of the k-fold segments on Figure 4.1b. Angles within the first quadrant indicate higher mean blood volume changes for non-initiated than initiated trials (the reference were the initiated trials, and the same for all the other measures).

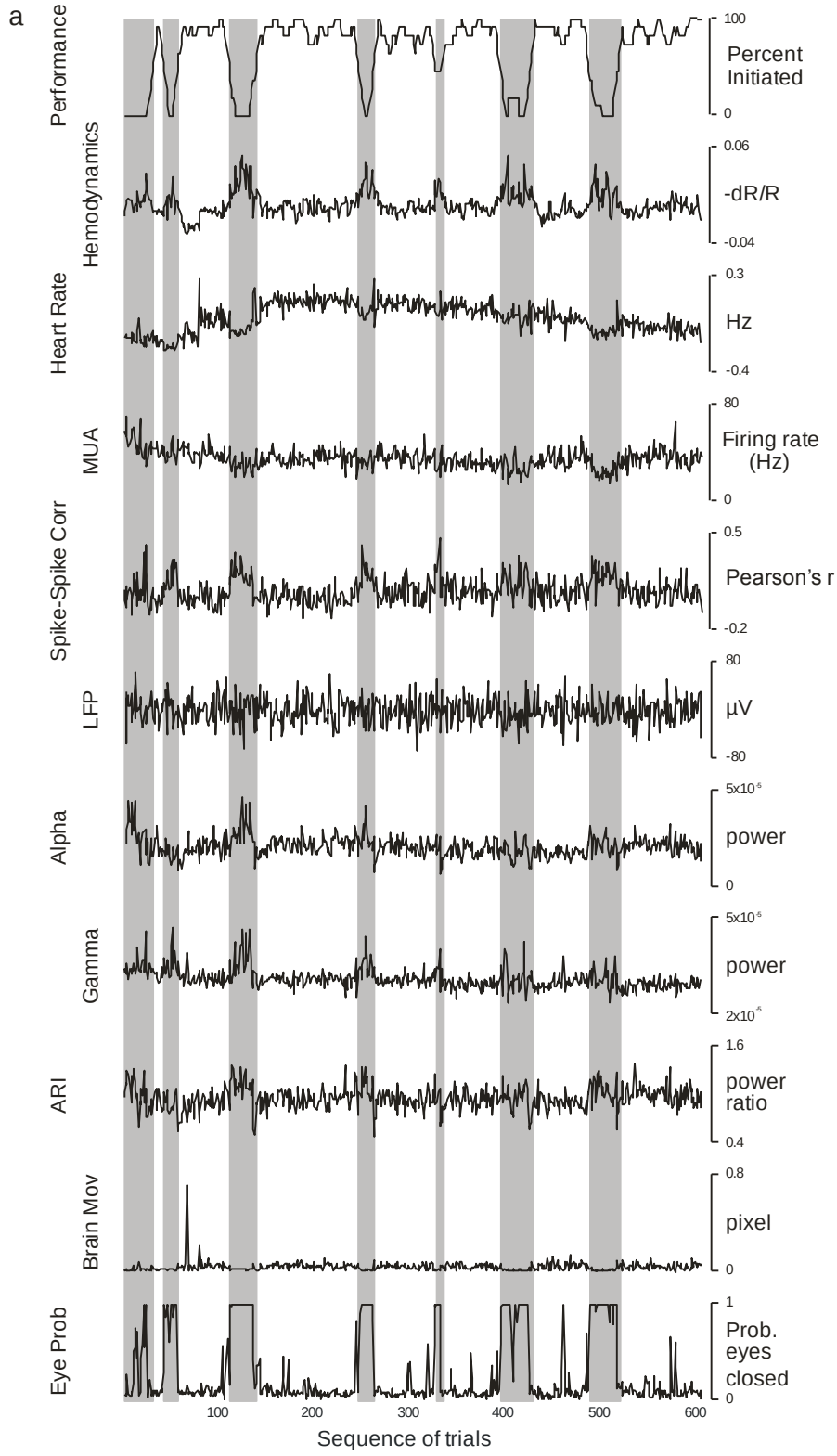
a
Performance
100
Percent
Initiated
0
Hemodynamics
0.06
-dR/R
-0.04
Heart Rate
0.3
Hz
-0.4
MUA
80
Firing rate
(Hz)
0
Spike-Spike Corr
0.5
Pearson's r
-0.2
LFP
80
μV
-80
Alpha
5x10⁻⁵
power
0
Gamma
5x10⁻⁵
power
2x10⁻⁵
ARI
1.6
power
ratio
0.4
Brain Mov
0.8
pixel
0
Eye Prob
1
Prob.
eyes
closed
0
100
200
300
400
500
600
Sequence of trials

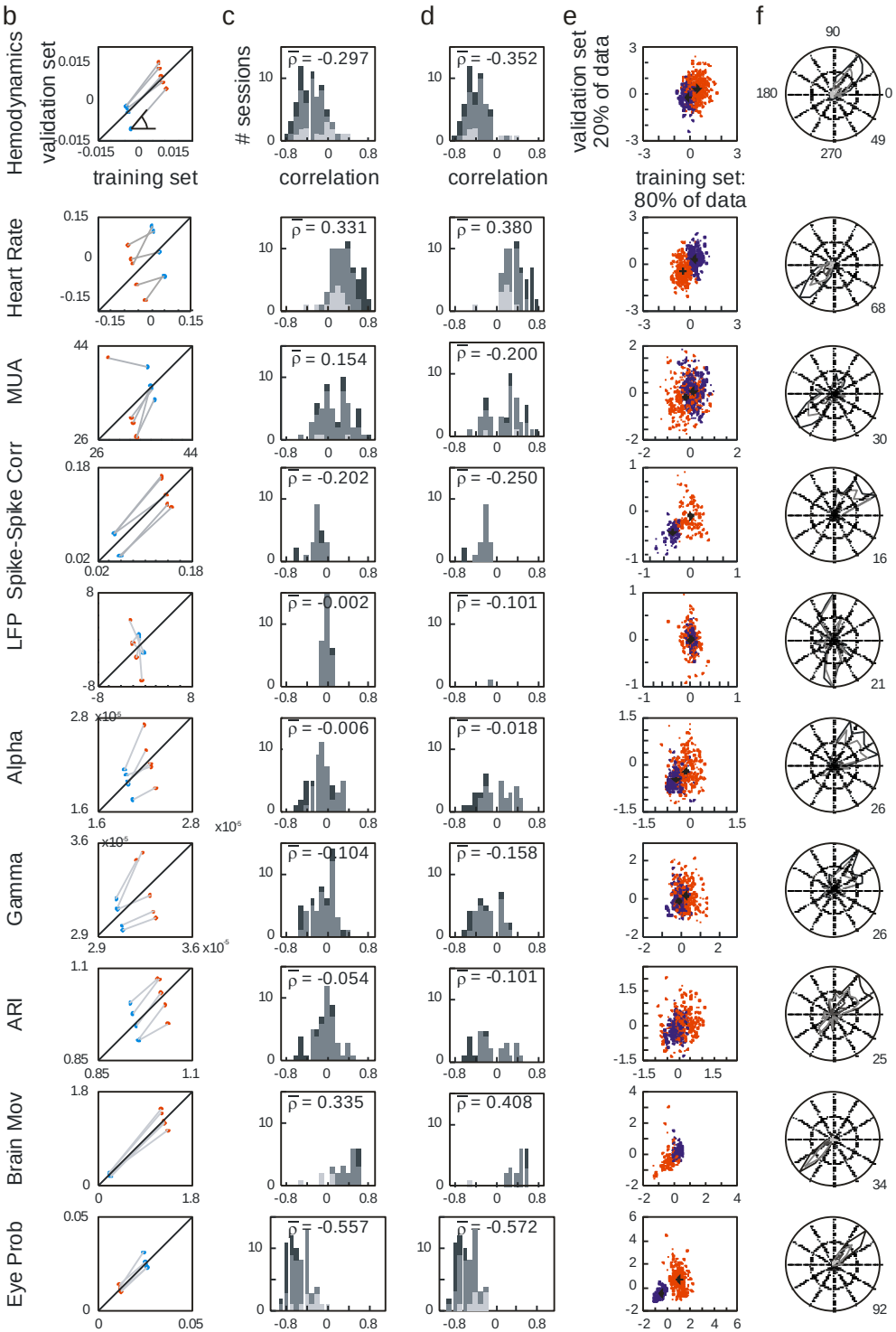

Figure 4.1 – How hemodynamic, heart rate and different neural and physiological measures track changes of performance in fixation task. **(a)**

Data from a single experimental session (for monkey T). **Top**: Animal's performance (see methods) along a session as the probability of initiating a trial. Shaded grey periods reflect periods in which the animal's performance was below 50%. Different traces: Mean hemodynamic response on each trial, for the same session as in **a**. Note the increases on the hemodynamic response during periods of lower performance (shaded gray areas). Similar analysis to the hemodynamic response for: heart rate, multi-unit activity electrode ('MUA'), spiking correlations between electrodes ('spike-spike corr'), local field potential ('LFP'), power of alpha-band LPF (8-12Hz), arousal related index ('ARI'), "brain movement", and eye status. **(b)** Within session cross-validation for the hemodynamic response, for the same session as in **a**. Vertical axis: average response to 20% of the data (in successive segments) in initiated trials (blue) versus non-attempted trials (red); on the horizontal axis is the average response to the remaining 80% of the data (once more segregated by initiated and non-initiated trials, respectively). The lines connect initiated versus non-attempted trials in each 20% segment. Note, within each color category, there is less dispersion on the horizontal than vertical axis (as otherwise expected, that responses to 20% of the data are more variable between one another, than responses to 80% of the data). The angle measurement will be used in later analysis (**e**); the metric used considers the slope of the line that connects initiated to non-attempted trials. **(c)** Stacked histogram of the Spearman's correlation between hemodynamic responses and performance for each session. Different shaded regions indicate the contribution of each of the three monkey (lighter grey: S, intermediate grey: T, darker grey: E). **(d)** Similar to **c** but for the subset of sessions that had p-value associated with Spearman's correlations < 0.05, note that most tendencies get more evidenced. **(e)** Similar to panel **b**, for the population of data (not single session), data presented as z-score. Different animals are coded with different symbols (S: circle, T: diamond, E: square). The colored crosses indicate the mean for each condition (for clarity sake it is not included the means for each animal, but they are on average consistent with the global mean). **(f)** Population measure of the angular distributions of the slopes between the neural responses from initiated to non-attempted (individual angles as in panel **b**). Different color codes for the different animals as in panel **c**.

The session presented is representative of the population, as noted when looking at the summary of the population data, Figure 4.1c-f. The distribution of Spearman's rank correlation for the different sessions was on average

negative for all 3 animals. It indicates a clear tendency of increased blood volume during lower performance periods (Figure 4.1c, even more for the subset of sessions that had reached a significant Spearman's correlation, Figure 4.1d); these results are reinforced by looking at the population of z-scored 5-fold cross validation for all session, Figure 4.1e, and the angular directionality resulting from the same analysis, Figure 4.1f.

4.4.2 Complex interplay between hemodynamics and heart rate

When looking at neuroimaging signals, one other relevant metric is heart rate. In healthy subjects, the rate at which new fresh blood arrives will be intimately linked to cardiac output. In the context of behavior there are several known heart rate modulatory effects: resting is also associated with decreased heart rate, cardiac deceleration in anticipation of behavioral events; startle responses associated with increased heart rates, bradycardia associated with attention, to name a few (for a summary for early results see e.g., Lacey & Lacey 1970, Lacey & Lacey 1978).

We therefore looked at heart rate in periods of higher and lower engagement, similarly to the analysis presented for the hemodynamic response. On Figure 4.1a it can be noticed that periods of lower engagement in the fixation task were associated with decreases in heart rate (ρ = 0.384, p-value < 0.01, for this single session, and it had the same trend for the population, as can be noticed in Figure 4.1c-f). This suggested a counter intuitive anti-correlated relationship between the mean trial hemodynamic signal and mean trial heart rate. One other aspect of the relationship between hemodynamics and heart rate was that the correlations tended to be more negative for sessions with lower overall engagement of the animal, as noted in Figure 4.2a.

The changes in mean trial heart rate with disengagement match our expectation. Similar trends can be observed in arousal; increases in arousal are associated with increases in heart rate, conversely decreases in arousal

come associated with decreased heart rate. In what concerns slow changes in blood volume the observed results were more unexpected. Earlier observations from the lab (Sirotin & Das 2009) of heart rate changes during a trial showed concomitant changes with the hemodynamic response – no anti-correlations were found in that study. To confirm that the relationship between *short term* changes in heart rate and hemodynamics were positively correlated even when looking at different states of engagement, we looked at the average dynamic responses of both signals in a sub second scale (we looked at the signals at the imaging frequency).

We looked at the average responses to initiated and non-initiated trials. Note that non-initiated trials are a construct from the way we present trials to the subject. In our paradigm, trials were presented periodically, independently of the animal engaging on them or not. Therefore, we recognize that this comparison can disproportionately average out contributions within non-initiated trials, as there is no event time structure. We observed that the average hemodynamic response to initiated trials had a peak a few seconds into the trial (Figure 4.2b). This response was overall lower for initiated than for non-initiated trials. Similarly, the average heart rate responses for initiated trials had also a peak (earlier than the peak in the hemodynamic response, Figure 4.2c). It should be noted that the average hemodynamic response change to completed trials (a subset of initiated trials; the ones that were rewarded) corresponds to the previously described *task-related hemodynamic response* (Sirotin & Das 2009). Moreover, these observations are consistent with our earlier observations (Sirotin & Das 2009). It is worth noting that the mean heart rate for non-initiated trials was lower than to initiated ones (as already seen in Figure 4.1). This suggests a positive correlation between changes within a trial in heart rate and hemodynamics, on top of anti-correlated changes in slower time scales, slower than the scale of individual trials, between the same metrics.

To establish if the correlation between the hemodynamic and heart rate signals was in the full time series dominated by the faster time scales

(positive correlation) or by the slower time scales (negative correlation) we computed the cross-correlation for each session in two conditions. In the first, we simply calculated the Pearson's correlation coefficient between the full time series for changes in hemodynamic and heart rate. This resulted in a preferentially negative correlation (Figure 4.2d). On the other hand, in the second approach we discounted the slow changes in the two metrics, by subtracting to the time course of each trial the mean response to that trial. In this case the correlation was preferentially positive (Figure 4.2e).

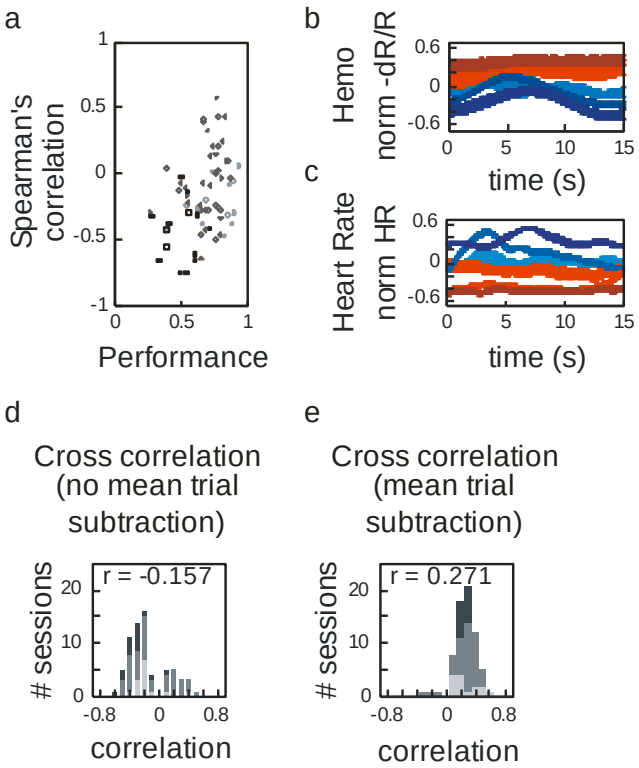

Figure 4.2 – Relationship between the hemodynamic response and heart rate. **(a)** Session by session, Spearman's correlation between the mean trial hemodynamic response and the mean trial heart rate response as a function of average performance on the session (open circles: monkey S, open diamonds or rhombus: monkey T, open squares: monkey E). **(b)** Trial triggered average of the magnitude normalized hemodynamic response. In blue, the average response to initiated trials, in red, the response to non-initiated trials (the different tones indicated different animals, lighter blue and lighter

red indicate animal S, intermediate tones, monkey T, and darker tones, monkey E). **(c)** Similar to **b** but for heart rate changes. **(d)** Peak cross correlation coefficient for the full hemodynamic trace and full heart rate trace (only positive lags considered). **(e)** Similar to **d**, but where to the hemodynamic and heart rate traces the mean trial (for each trial) were subtracted.

The relationship between hemodynamic signals and heart rate changes is of complex nature, and not linear. On a *fast time scale* (sub-trial time duration), they are correlated; the events happening with in a trial might trigger changes in heart rate that will have a reflection in the same direction in the hemodynamic response. On a slower time scale, the two metrics tended to be anti-correlated. Predicting the hemodynamic response based on heart rate is therefore not trivial: mathematically the two metrics have a non-linearity relationship.

4.4.3 Different neural metrics and their correlation to engagement

To understand the neural correlates of the hemodynamic changes we simultaneously recorded MUAs and LFPs with the imaging response (in the same cranial window). Firing rates tended to decrease in the periods the animal was less engaged in the fixation task: there was a weaker and positive correlation between firing rates and performance (Figure 4.1a,b, ρ = 0.171, p-value < 0.01, for MUA). We speculate that in periods the animal was less engaged in the task, the subject could take more breaks and close its eyes more often and for longer periods reducing even further the faint effects of having visual stimulation from fixation (virtually, the only source of light in the room). On the other hand, we observed the reverse pattern for the correlated activity across electrodes (see methods for our definition of the correlated activity between electrodes). In most of the sessions that we had electrophysiological recordings, we had two electrodes in visual cortex a few millimeters apart. This spike-spike correlation was on average higher for periods when the animal was less engaged in the task (Figure 4.1a,b 'spk-spk-corr': ρ = -0.366, p-value < 0.01). It should be noted that this relationship is inverse of what happens with spiking, and so the increases in

spike-spike correlation are not the result of overall increases in firing rates. The relationship between interneural correlations and performance could have been expected from what is known of arousal and 'noise correlations' (Livingstone & Hubel 1981, Cohen & Maunsell 2009, Cohen & Kohn 2011).

Local field potentials (the extracellular potential in the vicinity of the electrodes) had no consistent relationship with performance on the task (Figure 4.1a,b, LPF: $\rho = 0.013$, p-value = 0.7) and the same lack of relationship held true for the population (Figure 4.1c-f). We looked at different wave-bands of the LPF signal, alpha is reported here, given its relevance in the arousal literature. Alpha power (7-12 Hz) had a negative correlation with performance (alpha: $\rho = -0.083$, p-value = 0.04, for the session in Figure 4.1a,b). Our observation that alpha power increased in periods that animal performs poorly is consistent with prevailing ideas of vigilance/attention literature (e. g. Davies & Krkovic 1965). In our experiment, presumably in less engaged periods the animal was also less attentive. Similar to the observations in alpha, gamma band power (30-90Hz) had a similar profile (gamma: $\rho = -0.340$, p-value < 0.01, for the session in Figure 4.1a,b). This was unexpected, alpha and gamma tend to be anti-correlated. Concerning trial anticipation there is evidence of gamma increases relative to conditions of low expectation (Lima et al. 2011). We therefore looked at one other metric, 'arousal related index' (named and described elsewhere: Moore et al. 2014, see methods for details). Summarily, this index tracks the tendency that in sleep one observes increases in low frequency power and decreases in the high frequency power. Our results indicate that this index does not fully track performance (ARI: $\rho = -0.166$, p-value < 0.01, for the session in Figure 4.1a,b). It is worth mentioning that occipital coverage as the one we had for V1 imaging experiments is not the appropriate location to identify sleep episodes. Nevertheless, we do not expect these results to reflect mostly sleep, as the population data in Figure 4.1c-f shows a significant

range of possible correlations values (overall the average did not diverge much from zero).

With our experimental design, we could not confirm if the animal had periods of sleep and when did those occur. We wanted to confirm that periods of poor performance were associated with more often eyes closed and a certain level of quiescence. To do so we included two other metrics, one related to how much the imaging responses co-register, or if they required significant re-alignment, with the aim of having an estimate of brain movement. We were interested in periods with little image correction versus periods with higher one (as measured by the number of pixels necessary to displace the image for alignment). We defined a metric looks at the variability for each trial on the pixel drift (see methods). We observed that periods with lower performance were associated with less movement correction ('brain mov': $\rho = 0.489$, p-value < 0.01, for the session in Figure 4.1a,b, and such a positive trend could be observed for the population in Figure 4.1c-f). Finally, we also classified the subjects' eyes to be open, closed or blinking, for each imaging frame (see methods). Robustly, periods of poor performance were associated with eyes probably not open ('eye prob': $\rho = -0.579$, p-value < 0.01, for the session in Figure 4.1a,b, same trend could be observed for the population in Figure 4.1c-f). We could not fully disambiguate this question, but we expect periods of low performance to be periods of low arousal. Still, from the recently published work by Pisauro and colleagues we expect the measured hemodynamic changes to be at least in part related to arousal (Pisauro et al. 2016). Contrary to their study we did not focus on pupil diameter, as the animals often closed their eyes.

Finally, to further understand the relationship between the different neural measures, we also looked into the temporal dynamics of the different measures long initiated and not initiated trials. Here we include information for one representative single session (the same as in Figure 4.1a,b). In initiated trials relative to not initiated ones, there was both a decrease in low frequency powers (Figure 4.3a,d) and an increase in firing rates (Figure

4.3b). This probably reflected the fact the animal had to perform the fixation task; some residual visual drive might increase firing rates, on the one hand. On the other hand the fixation attentional effort might reduce alpha power. It is worth noting that on average not initiated trials had a higher correlation on the interneural rates than for initiated trials, this effect was sustained beyond the fixation period. This pointed to potential multiple relevant time scales that could have influence to the resulting hemodynamic response.

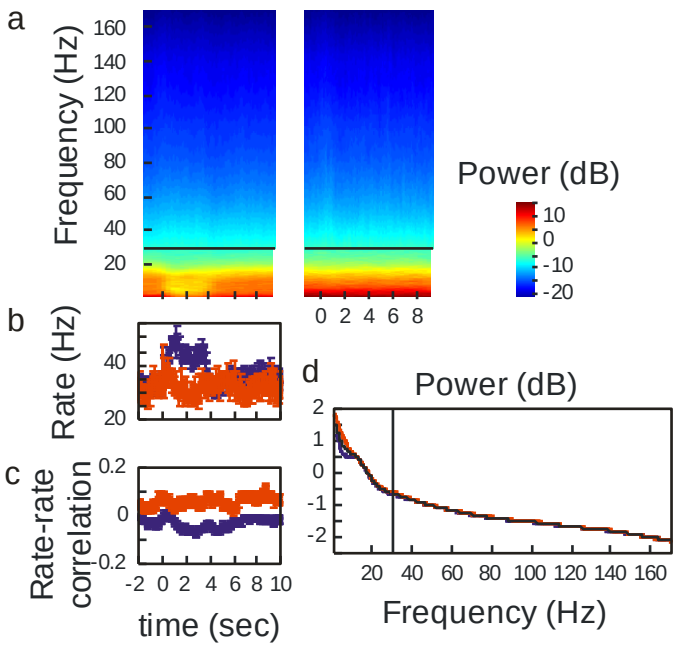

Figure 4.3 – Neural signatures of engaged versus not engaged in fixation task, for a relevant session. **(a)** Average LFP spectrogram for initiated (left) and not initiated trials (right), relative to time on trial. Note: the black line indicates that the tapering used below and above 30Hz was different. **(b)** Average firing rates for the same unit as in **a**, average response to initiated trials in blue and to not initiated trials in red. **(c)** Similar to **b**, but for the correlated activity across the two recording units (for this session). **(d)** Similar to **a**, but collapsed in time. Average power for initiated trials in red, for not initiated trials in blue, and in black is for both trial types averaged together.

4.5 Discussion

In this study we looked at how endogenous contributions to the hemodynamic response could be reflected in the imaging signal. Furthermore, we were interested in how such endogenous changes unveil in different neural and physiologic metrics. Specifically we looked at the influence of engagement in the mentioned metrics.

Non-human primates performing a fixation task, like the one presented here, will naturally have periods of good performance and periods of disengagement of the fixation task. It should be noted that even though animals were water deprived and receive a liquid reward for completing trials, they could still have periods of disengagement early in a recording session, as well as periods of good performance towards the end of the session. We therefore harvested their natural behavior, and we looked at periods of higher and lower engagement.

Summarizing, we observed decreased blood volume changes with increased engagement in the fixation task, accompanied by increase in heart rate, decrease in correlated activity across electrodes. However we do not expect these to exclusively reflect disengaged states associated with sleep.

In our experiments it remains open if the signal reported here mostly reflected arousal or not (differently than Pisauro et al. 2016). We have framed it in the context of task engagement, as this was the metric we aimed characterizing. Typical arousal experiments involve sleep, neither this was aimed in our paradigm, nor we had in place appropriate measures for it (e.g. surface EEG electrodes), or metrics as pupil diameter (periods with closed eyes make pupilometry measures inapplicable).

Engagement is a less characterized metric. In rodents, engagement is known to reduce stimulus-specific responses in barrel cortex (Crochet & Petersen 2006) and auditory cortex (Otazu et al. 2009), of alert rodents. In the barrel cortex experiments, it was observed that when comparing a quiet state with a period the animals were more engaged with the environment,

whisking, the amplitude of membrane potential sensory responses was larger in quiet than whisking states (Otazu et al. 2009). In the experiments in auditory cortex were reported stimulus specific reductions in spiking rates of neurons in auditory cortex. Moreover this reduction in auditory stimuli representation was independent of the modality in which the animal was engaged performing a task; a set of animals was trained to perform an auditory task with simultaneous presentations of odors, or an olfactory task with presentation of sounds. They observed that when animals were engaged in the olfactory task there was still suppression of the representation of auditory stimuli, suggesting a more global change. It is worth noting that their study included periods of data where the animals were for more prolong periods of time 'immobile', probably in a more sleep-like state, which makes this signal somewhat different from general arousal. Here the behavior they presented contrasts with the one we observed. In their experiments they observed only stimuli related changes and no changes in spontaneous activity. Similarly to the observations in rodents, it was observed in non-human primates performing a pitch change detection, or passively listening to the same auditory stimuli that on the engaged condition MUA and LFP activity was depressed relative to the passive condition (O'Connell et al. 2015). The prevailing interpretation is that this stimuli related suppression in the engaged condition promotes sharpening or refinement of stimuli representation to be encoded.

Our main metric is the hemodynamic signal, rather different from electrophysiology, and in our MUA activity we did not observe large changes with periods of more or less engagement in the task. This goes in line with the absence of changes in spontaneous activity in the rodent auditory experiments (Otazu et al. 2009). More importantly we did not look at stimulus representation. We looked at a very different endogenous signature: slow changes, on the time scale of trial duration; or 'spontaneous' activity. It cannot be disregarded that the signals we were looking at did not reflect the same form of engagement described in the mentioned engagement work.

To test for stimulus related changes with engagement, inherently there is a limitation of looking at stimulus related changes with engagement, as even for passing viewing stimuli the animals are in general still required to fixate (as visual cortex has a retinotopic organization), and fixation is already engaging. Still it would be worth training subjects in a stimulus dependent task and compare the visual response to stimuli in a passive viewing task and a stimulus relevant task and look for engagement differential representation.

More probably, our results reflect arousal, as Pisauro et al. 2016. Once more we did not have classical measures of arousal as EEG or pupilometry. That said in a future study aiming at disambiguate if the effects we observed here could be related to arousal, it could be relevant to record activity changes in the thalamus (in particular corticothalamic and lemniscal projections, for a review see Castro-Alamancos 2004). An interesting study in humans, which aimed at relating variability in perception to variability in baseline BOLD activity, found those to be related (Boly et al. 2007). Interestingly in this study, increases in thalamic baseline activity facilitated perception. When recording electrophysiology, one would expect the periods in which the animals were less engaged in the task to be associated with bursts of activity in thalamus (for a review see Llinás & Steriade 2006). In the experiments aforesaid (Otazu et al. 2009), they observed an increase in spontaneous activity in the engaged condition relative to the passive listening one, but no changes in thalamus's burstiness. Bursting episodes during awake states are rare (Woody et al. 2003), only some of the cycles of sleep do exhibit them (Llinás & Steriade 2006), which puts into question if this might be the better metric to assert no relation to arousal. Potentially, recordings of locus coeruleus could more definitive disambiguate a role for arousal (for a review see Aston-Jones & Cohen 2005).

We used a simple behavior; and different experiments would be required to try to disambiguate if we were observing a prevailing contribution of arousal or not. Still, the pursuit of such research would be relevant, as there is evi-

dence that endogenous and exogenous hemodynamic responses interact differently than similar changes in electrophysiology (He 2013). In this study by He in 2013, she looked at two different conditions: resting state with eyes open while fixating on a cross and under similar illumination conditions and with the same cross, subjects were asked to detect of diming of the fixation cross. The results indicated a more complex interplay between hemodynamics and underlying electrophysiology, where a more complex relationship between endogenous and exogenous contributions to fMRI BOLD activity is present; as variability in the evoked activity is influenced by baseline activity with a negative correlation. Similar idea had been also presented in a prior study (Boly et al. 2007), where they observed that higher BOLD fMRI prestimulus activity was associated with lower stimulus perception. It remains to be understood what are the mechanisms underlying these hemodynamic endogenous changes and if they serve a behavioral role.

Studies that point into different observations than the ones reported here should be mentioned. A study looking among other things at the difference in cerebral blood flow (CBF, as measured by arterial spin labeling imaging) reported that between the conditions: engaged in a task or at rest (rest here defined as alert with eyes open, not performing a task) CBF decreased from task to rest condition, in occipital cortex, which contains V1, (Pfefferbaum et al. 2011). It could be argued that a 'rest' condition can still be 'engaging' and different from the disengagement or arousal reductions that we think represent changes in our signal. It would be hard to reproduce their 'rest' condition with monkeys, Pfefferbaum and colleagues worked with humans.

Finally, in the context of stimulus related changes in the hemodynamic response it has been shown in the lab that those changes are best predicted by changes in neuronal firing rates, compared against LFPs (Lima et al. 2014). Local changes in firing rates are not the drivers of changes in the endogenous hemodynamic response, as noted by the modest correlation between firing rate changes and performance. Still these behavioral fluctuations should be affecting even early sensory areas. Our hemodynamic signal is

able to track some of the changes in brain states. These come accompanied by changes in intra-cortical correlations, heart rate, and quiescence. Finally it remains open what the best neural correlate for endogenous changes in hemodynamic response might be.

4.6 Acknowledgments

We would like to thank Eric DeWitt for the fruitful discussions.

5 General Discussion

Neuroimaging is both extremely useful and also a rather complex methodology to interpret. In this thesis the aim was to further explore neuroimaging in the context of behavior. We divided the work presented here into two broad parts. The first, aimed at addressing the relationship between stimuli--related hemodynamic responses and underlying neural activity, in early sensory areas (Chapter 2). The second aimed at exploring the representation of behavior-related endogenous responses in the hemodynamic response, and also neurally, as well, in early sensory areas (Chapters 3 and 4).
The work presented here does not close any of the lingering questions in the neuroimaging field. It nevertheless succeeds in bringing more attention to the question of how to analyze responses happening at different time scales, and coming from different sources. Is repeating trials multiple times and averaging their responses the best way to capture task relevant features?

5.1 Exogenous responses in V1

In Chapter 2 we discussed how stimulus-related and task-related components can be distinguished in the neuroimaging signal when looking at early sensory areas. We observed that in a periodic task there was a stimulus--related contribution to the hemodynamic response and a task-related component. Moreover these two components added linearly to give the resulting hemodynamic response. This relationship though simple did not have to be like this, we could have found evidence of interaction between the stimulus and task components. Finally, the relationship between the hemodynamic response and underlying neuronal activity has also been subject of significant debate (for a review see: Logothetis & Wandell 2004). The prevailing idea has been that the hemodynamic response mostly reflects metabolic demand, and that it is better tracked by LFP activity. There is evidence in this direction (e. g., Logothetis et al. 2001, Niessing et al. 2005, Goense &

Logothetis 2008). The work presented here suggests also that spiking activity is well correlated with the stimulus related hemodynamic response. More recent work from the lab showed that for the same task (where were included several of the same datasets presented on Chapter 2) spiking is a better predictor of the stimulus related hemodynamic response than LFP (Lima et al. 2014). Thus we have good evidence that exogenous hemodynamic responses in V1 are linearly related to changes in local spiking activity. Therefore deconvolving the stimulus-related hemodynamic response with an HRF provides a good estimate of underlying neural activity, particularly relevant for fMRI studies. This also suggests that the hemodynamic response is tightly linked to spiking activity and presynaptic activity into a sensory area, as anyway observed in different experiments (Gurden et al. 2006, Lee et al. 2010, Scott & Murphy 2012, Kahn et al. 2013). Finally, to the neuroimaging community, this reinforces the importance of appropriate task design: aiming at estimating task non-relevant contributions (in our case, we were interested in characterizing stimulus representation) in order to separate those from stimulus-related components that will have a linear relationship to underlying local neural activity, as least in early sensory areas. The question of what the neuronal nature of endogenous hemodynamic responses is remains unanswered.

5.2 Endogenous responses in V1

In Chapter 3 we aimed at characterizing behavior aspects of the previously described task-related hemodynamic signal (Sirotin & Das 2009). In the original publication this signal had been characterized as present in V1 in a periodic fixation task, and with a time course matching that of the trial duration. We investigated this issue further by manipulating trial duration and fixation duration. The hemodynamic response tends to track the duration of the trials, but its time course points to a trial initiation response. As we saw that alternation between two schedule regimes did not produce significant

changes for a large portion of time into long trials, when compared to short ones. Then we looked at the effect of fixation duration. The task-related response keeps tracking the total duration of the trial, but longer fixations tend to be associated with higher task-related response amplitudes and also slower in the peaking time. Taken together, this suggests that the hemodynamic task-related response is influenced by the duration of trials. Importantly it might be triggered by initiation of a trial, but modulated by the time the animal is required to hold fixation. These are rather specific features associated with the specific fixation task we used.

We used a different task, not reliant on fixation to address this question. We used a task that used auditory stimuli as cues and motor response and output. First, we observed a robust task-related response in V1 for this task, with comparable magnitudes. We then looked at the time course of such responses between the two task types and found great similarity between those. Moreover, it should be once more pointed out that we have used two slightly different versions the auditory/motor task, with similar results on both. It is worth noting that the two variations differ significantly in their event sequence. One task was designed to emulate, as much as possible, the fixation task, both in its event sequence (trials were presented automatically to the animal that could engage on them or not), and timing. The other task variation was different: the animal initiated the trials, and there was a hiatus of several seconds between trial start and the auditory cue coming on, and finally reward. It is still remarkable the similarity in the time course between this auditory/motor task and the fixation task. This suggests that there is a potential role for initiating a trial (engaging in the task) as a triggering signal for the resulting hemodynamic task-related activity.

We also looked at the effects of reward/motivation to completing trials, and observed that reward amount increased the probability of initiating a trial and it increased the magnitude of the task-related hemodynamic changes. We observed as well a slower trend on the hemodynamic signal. This trend had the unexpected property of decreasing as one goes into a block of high

reward (and increasing when progressing into a low reward block). Apart from these changes, we have not found significant changes in the shape of the temporal profiles of high or low reward trials.

Previous work in the lab (Sirotin et al. 2012) had already pointed out that the starkest difference lay between initiated or non-initiated trials. At some level this is trivial: it a *task*-related signal; no task, no signal. But the question remains; what in the task triggers this signal? Is it effort? Is it reward? Is it expectation? Is it something else? Understanding the behavior or such signal might help hint at what mechanisms underlie it.

In the final chapter, Chapter 4, we explored further the idea of engagement or arousal and its influence on the hemodynamic response. We noticed that the slow changes in the hemodynamic response had significant amplitude and they tended to increase as engagement in the task decreases, similarly to the observations by Pisauro and colleagues (Pisauro et al. 2016). Our work here aimed at further confirming the non-local origin of these hemodynamic changes. We looked at several correlations between the different measurements, and in particular we noticed a non-linear relationship between heart-rate and hemodynamic responses; as if there were two distinct coupling modes operating in two different time scales. This observation might be particularly relevant when considering how to discount heart-rate from the fMRI signals (for some discussion about heart rate contributions to BOLD fMRI and how to account for those see Chang et al. 2009).

In summary, there is a task-related signal; it is present in V1 for visual tasks as well as for an auditory/motor tasks, it is more global than a modality specific signal; it is present in initiated trials independently if trials were rewarded or not; and there is a slower (trial length) signal that tracks probably task engagement or arousal. It would be relevant to explore the role of neuromodulation, with this evidence we suggest it would be relevant to look at norepinephrine in particular.

5.3 Future directions

5.3.1 Locus coeruleus – noradrenergic system

Norepinephrine (NA) and locus coeruleus (LC) activation are an extremely interesting system for further speculation of a neuromodulatory contribution to the hemodynamic signal related to task engagement. The work by Aston-Jones and colleagues showing the two modes of activation of LC, tonic and phasic, and its relationship to behavior is rather relevant (for a review see Aston-Jones & Cohen 2005). Tonic discharge associated with global changes in task disengagement and performance, and phasic changes associated to outcome and task relevant features like reward related targets (e.g. Aston-Jones et al. 1994, Usher et al. 1999). Moreover, more recent work by Gold and colleagues (Kalwani et al. 2014, Joshi et al. 2016) where they observed that LC (phasic) activation was related to 'active' actions differently than to withholded ones. Even though these two conditions differ in the actions the subject had to perform both lead to a rewarded outcome; suggesting that LC phasic activation encodes goal-directed actions more than solely reward.

It would be extremely interesting to record activity directly from LC in both the fixation task and the auditory/motor task, and, simultaneously, observe not only LC activity changes during this task, but also how LC responses when the animal goes into low performing periods as we observed in Chapter 4. Neuroimaging of such an area with OIIS is not possible given its location in the brain. The use of fMRI techniques can be challenging given the location of LC, its small size or the fact that brainstem experiences significant pulsation. The use of appropriate coils could aid in this task, but with the disadvantage that it could be hard to resolve the whole brain. Finally, to my understanding, the exact pattern of activation/deactivation associated with the known electrophysiological responses of LC is not well characterized in neuroimaging. Moreover, MRI techniques are not ideally posed when looking at slow changes (in the scale of several seconds or

minutes) in response given limitation in maintaining the magnetic field in the scanner. Ideally, experiments involving LC would use electrophysiology.
Alternatively, pharmacology could be used while recording the same hemodynamic responses with OIIS, in the same tasks we used before. Does inactivation of NA receptors influence the hemodynamic response? Visual cortex receives LC innervations (e.g. Kosofsky et al. 1984). As a note, initial research on NA modulation in visual cortex was associated with visual plasticity (for a brief review, see Sillito 1986). More recent work with systemic inhibition of NA transporters has been linked to changes in the 'default mode network' (DMN, on resting state fMRI and the DMN see Biswal et al. 1997, Raichle et al. 2001, respectively) (Minzenberg et al. 2011). In rodents, NA was shown to have a role in astroglial responses (Paukert et al. 2014). In these experiments they have looked at astrocytic Ca^{2+} activity in visual cortex. This activity had low baseline levels, but paring of a visual stimulus with periods of locomotion (where NA in visual cortex is elevated), consistently increased astrocytic Ca^{2+} activity. In the context of hemodynamic responses, these results are very interesting. In a nutshell, NA modulation into visual cortex is a promising avenue to pursue following the work presented in this thesis.

5.3.2 Neural basis of neuroimaging

The work presented in this thesis sheds light on the interpretation of neuroimaging signals. Most questions pertaining to it, however, still remain. In the introduction there was an effort of bringing to light the unknown nature of the definitive mechanisms underlying the hemodynamic response. The use of intrinsic signal optical imaging allowed the presentation of results in this thesis. Moving forward there are several research questions that might be better addressed with the use of other experimental techniques.
To understand and distinguish metabolic and vascular contributions to the resulting hemodynamic signal it would be relevant to use techniques where

those would be separated. Of particular interest are metabolic measures that can have a more direct relationship with underlying neuronal activity. We propose that a technique which shares similarities with intrinsic signal optical imaging would be relevant to advance our understanding of neuro-imaging: autofluorescence imaging, specifically, flavoprotein fluorescence imaging. It is based on changes with oxidative respiration in mitochondria of molecular species that fluoresce differently in their oxidized and reduced form (Chance et al. 1979). These are even more interesting because they fluoresce in the visible spectrum. Not only have such techniques been used successfully in rodents (e.g. Shibuki et al. 2003) as they have previously been used in the lab (Sirotin & Das 2010b). This technique similarly to OIIS does not require the use of any agent like dyes or contrast to record the response. This represents an advantage, as those are often toxic and require injection/ application. It would be interesting to repeat all experiments with both OIIS and autofluorescence imaging. Of particular relevance would be to compare the relationship between the two imaging methods of exogenous and endogenous contributions to the hemodynamic response. Is the hemodynamic-metabolic coupling preserved for exogenous and endogenous signals?

I have devoted little attention to the electrophysiological recordings in the collected data. We consistently collected MUA data, but its relationship with the hemodynamic response was not extremely informative, other than, reinforcing that the endogenous responses do not have their origin in V1. This information is relevant and valuable per se, in my opinion it absolutely states the importance of looking into other brain regions. However it contributes to the understanding of neurovascular coupling in a limited way. It would be relevant to do more granular analysis of the electrophysiological data, which could potentially bring to light more information.

References

Aitken, P.G., Fayuk, D., Somjen, G.G. & Turner, D. a, 1999. Use of intrinsic optical signals to monitor physiological changes in brain tissue slices. *Methods (San Diego, Calif.)*, 18(2), pp.91–103.

Albrecht, D.G. & Hamilton, D.B., 1982. Striate cortex of monkey and cat: contrast response function. *Journal of neurophysiology*, 48(1), pp.217–37.

Arieli, A., Grinvald, A. & Slovin, H., 2002. Dural substitute for long-term imaging of cortical activity in behaving monkeys and its clinical implications. *Journal of Neuroscience Methods*, 114(2), pp.119–133.

Arieli, A., Shoham, D., Hildesheim, R. & Grinvald, A., 1995. Coherent spatiotemporal patterns of ongoing activity revealed by real-time optical imaging coupled with single-unit recording in the cat visual cortex. *Journal of neurophysiology*, 73(5), pp.2072–2093.

Arsenault, J.T., Nelissen, K., Jarraya, B. & Vanduffel, W., 2013. Dopaminergic Reward Signals Selectively Decrease fMRI Activity in Primate Visual Cortex. *Neuron*, 77(6), pp.1174–1186.

Aston-Jones, G. & Cohen, J.D., 2005. An Integrative Theory of Locus Coeruleus-Norepinephrine Function: Adaptive Gain and Optimal Performance. *Annual Review of Neuroscience*, 28(1), pp.403–450.

Aston-Jones, G., Rajkowski, J., Kubiak, P. & Alexinsky, T., 1994. Locus coeruleus neurons in monkey are selectively activated by attended cues in a vigilance task. *The Journal of neuroscience : the official journal of the Society for Neuroscience*, 14(July), pp.4467–4480.

Attwell, D., Buchan, A.M., Charpak, S., Lauritzen, M., Macvicar, B. a & Newman, E. a, 2010. Glial and neuronal control of brain blood flow. *Nature*, 468(7321), pp.232–43.

Attwell, D. & Laughlin, S.B., 2001. An energy budget for signaling in the grey matter of the brain. *Journal of Cerebral Blood Flow and Metabolism*, 21(10), pp.1133–1145.

Bashinski, H.S. & Bacharach, V.R., 1980. Enhancement of perceptual sensitivity as the result of selectively attending to spatial locations. *Perception & psychophysics*, 28(3), pp.241–248.

Birn, R.M., Smith, M.A., Jones, T.B. & Bandettini, P.A., 2008. The respiration response function: The temporal dynamics of fMRI signal fluctuations related to changes in respiration. *NeuroImage*, 40(2), pp.644–654.

Biswal, B.B., Van Kylen, J. & Hyde, J.S., 1997. Simultaneous assessment of flow and BOLD signals in resting-state functional connectivity maps. *NMR in biomedicine*, 10(4-5), pp.165–170.

Boly, M., Balteau, E., Schnakers, C., Degueldre, C., Moonen, G., Luxen, A., Phillips, C., Peigneux, P., Maquet, P. & Laureys, S., 2007. Baseline brain activity fluctuations predict somatosensory perception in humans.

Proceedings of the National Academy of Sciences of the United States of America, 104(29), pp.12187–92.
Bonhoeffer, T. & Grinvald, A., 1991. Iso-orientation domains in cat visual cortex are arranged in pinwheel-like patterns. *Nature*, 353(6343), pp.429–431.
Bonhoeffer, T. & Grinvald, A., 1996. Optical Imaging Based on Intrinsic Signals. In N. Pouratian & A. W. Toga, eds. *Brain mapping: The methods*. pp. 55–97.
Boynton, G.M., 2011. Spikes, BOLD, Attention, and Awareness: A comparison of electrophysiological and fMRI signals in V1. *Journal of Vision*, 11(5), pp.12–12.
Boynton, G.M., Demb, J.B., Glover, G.H. & Heeger, D.J., 1999. Neuronal basis of contrast discrimination. *Vision Research*, 39(2), pp.257–269.
Boynton, G.M., Engel, S., Glover, G.H. & Heeger, D.J., 1996. Linear systems analysis of functional magnetic resonance imaging in human V1. *The Journal of neuroscience : the official journal of the Society for Neuroscience*, 16(13), pp.4207–4221.
Buckner, R.L., Goodman, J., Burock, M., Rotte, M., Koutstaal, W., Schacter, D., Rosen, B. & Dale, A.M., 1998. Functional-anatomic correlates of object priming in humans revealed by rapid presentation event-related fMRI. *Neuron*, 20(2), pp.285–96.
Cardoso, M.M.B., Sirotin, Y.B., Lima, B., Glushenkova, E. & Das, A., 2012. The neuroimaging signal is a linear sum of neurally distinct stimulus- and task-related components. *Nature Neuroscience*, 15(9), pp.1298–1306.
Castro-Alamancos, M.A., 2004. Dynamics of sensory thalamocortical synaptic networks during information processing states. *Progress in Neurobiology*, 74(4), pp.213–247.
Chaigneau, E., Oheim, M., Audinat, E. & Charpak, S., 2003. Two-photon imaging of capillary blood flow in olfactory bulb glomeruli. *Proceedings of the National Academy of Sciences of the United States of America*, 100(22), pp.13081–6.
Chaigneau, E., Tiret, P., Lecoq, J., Ducros, M., Knöpfel, T. & Charpak, S., 2007. The relationship between blood flow and neuronal activity in the rodent olfactory bulb. *The Journal of neuroscience : the official journal of the Society for Neuroscience*, 27(24), pp.6452–6460.
Chance, B., Schoener, B., Oshino, R., Itshak, F. & Nakase, Y., 1979. Oxidation-reduction ratio studies of mitochondria in freeze-trapped samples. NADH and flavoprotein fluorescence signals. *Journal of Biological Chemistry*, 254(11), pp.4764–4771.
Chang, C., Cunningham, J.P. & Glover, G.H., 2009. Influence of heart rate on the BOLD signal: The cardiac response function. *NeuroImage*, 44(3), pp.857–869.
Chen, B.R., Bouchard, M.B., McCaslin, A.F.H., Burgess, S.A. & Hillman, E.M.C., 2011. High-speed vascular dynamics of the hemodynamic response. *NeuroImage*, 54(2), pp.1021–1030.

Cheng, K., Waggoner, R. a & Tanaka, K., 2001. Human ocular dominance columns as revealed by high-field functional magnetic resonance imaging. *Neuron*, 32(2), pp.359–374.
Cohen, L.B., Keynes, R.D. & Hille, B., 1968. Light Scattering and Birefringence Changes during Nerve Activity. *Nature*, 218, pp.438–441.
Cohen, M.R. & Kohn, A., 2011. Measuring and interpreting neuronal correlations. *Nature neuroscience*, 14(7), pp.811–9.
Cohen, M.R. & Maunsell, J.H.R., 2009. Attention improves performance primarily by reducing interneuronal correlations. *Nature neuroscience*, 12(12), pp.1594–600.
Cohen, M.S., 1997. Parametric analysis of fMRI data using linear systems methods. *NeuroImage*, 6(2), pp.93–103.
Corbetta, M., Miezin, F.M., Dobmeyer, S., Shulman, G.L. & Petersen, S.E., 1990. Attentional modulation of neural processing of shape, color, and velocity in humans. *Science*, 248(4962), pp.1556–1559.
Crochet, S. & Petersen, C.C.H., 2006. Correlating whisker behavior with membrane potential in barrel cortex of awake mice. *Nature neuroscience*, 9(5), pp.608–610.
Dale, A.M. & Buckner, R.L., 1997. Selective Averaging of Rapidly Presented Individual Trials Using fMRI. *Hum. Brain. Mapp.*, 5, pp.329–340.
Das, A. & Sirotin, Y.B., 2011. What could underlie the trial-related signal? A response to the commentaries by Drs. Kleinschmidt and Muller, and Drs. Handwerker and Bandettini. *NeuroImage*, 55(4), pp.1413–1418.
Davies, D.R. & Krkovic, A., 1965. Skin-Conductance, Alpha-Activity, and Vigilance. *The American Journal of Psychology*, 78(2), pp.304–306.
Devor, A., Dunn, A.K., Andermann, M.L., Ulbert, I., Boas, D.A. & Dale, A.M., 2003. Coupling of total hemoglobin concentration, oxygenation, and neural activity in rat somatosensory cortex. *Neuron*, 39(2), pp.353–9.
Devor, A., Tian, P., Nishimura, N., Teng, I.C., Hillman, E.M.C., Narayanan, S.N., Ulbert, I., Boas, D.A., Kleinfeld, D. & Dale, A.M., 2007. Suppressed Neuronal Activity and Concurrent Arteriolar Vasoconstriction May Explain Negative Blood Oxygenation Level-Dependent Signal. *Journal of Neuroscience*, 27(16), pp.4452–4459.
Donner, T.H., Sagi, D., Bonneh, Y.S. & Heeger, D.J., 2008. Opposite neural signatures of motion-induced blindness in human dorsal and ventral visual cortex. *The Journal of neuroscience : the official journal of the Society for Neuroscience*, 28(41), pp.10298–310.
Elkhetali, A.S., Vaden, R.J., Pool, S.M. & Visscher, K.M., 2015. Early visual cortex reflects initiation and maintenance of task set. *NeuroImage*, 107, pp.277–288.
Engel, S.A., Zhang, X. & Wandell, B.A., 1997. Colour tuning in human visual cortex measured with functional magnetic resonance imaging. *Nature*, 388(6637), pp.68–71.
Engelmann, J.B., Damaraju, E., Padmala, S. & Pessoa, L., 2009. Combined effects of attention and motivation on visual task performance: transient and sustained motivational effects. *Frontiers in human neuroscience*,

3(March), p.4.
Fox, M.D., Snyder, A.Z., Zacks, J.M. & Raichle, M.E., 2006. Coherent spontaneous activity accounts for trial-to-trial variability in human evoked brain responses. *Nature Neuroscience*, 9(1), pp.23–25.
Friston, K.J., Jezzard, P. & Turner, R., 1994. Analysis of functional MRI time-series. *Human Brain Mapping*, 1(2), pp.153–171.
Fukuda, M., Moon, C., Wang, P. & Kim, S., 2006. Mapping Iso-Orientation Columns by Contrast Agent- Enhanced Functional Magnetic Resonance Imaging : Reproducibility , Specificity , and Evaluation by Optical Imaging of Intrinsic Signal. *The Journal of neuroscience*, 26(46), pp.11821–11832.
Gandhi, S.P., Heeger, D.J. & Boynton, G.M., 1999. Spatial attention affects brain activity in human primary. *Proceedings of the National Academy of Science USA*, 96(March), pp.3314–3319.
Gardner, J.L., Sun, P., Waggoner, R.A., Ueno, K., Tanaka, K. & Cheng, K., 2005. Contrast adaptation and representation in human early visual cortex. *Neuron*, 47, pp.607–620.
Glover, G.H., 1999. Deconvolution of impulse response in event-related BOLD fMRI. *NeuroImage*, 9(4), pp.416–429.
Goense, J.B.M. & Logothetis, N.K., 2008. Neurophysiology of the BOLD fMRI signal in awake monkeys. *Current biology : CB*, 18(9), pp.631–40.
Griffis, J.C., Elkhetali, A.S., Vaden, R.J. & Visscher, K.M., 2015. Distinct Effects of Trial-Driven and Task Set-Related Control in Primary Visual Cortex. *NeuroImage*, 120, pp.285–297.
Grill-Spector, K. & Malach, R., 2001. fMR-adaptation: a tool for studying the functional properties of human cortical neurons. *Acta psychologica*, 107(1-3), pp.293–321.
Grinvald, A., Lieke, E.E., Frostig, R.D., Gilbert, C.D. & Wiesel, T.N., 1986. Functional architecture of cortex revealed by optical imaging of intrinsic signals. *Nature*, 324(6095), pp.361–364.
Grinvald, A., Shoham, D., Shmuel, A., Glaser, D., Vanzetta, I., Shtoyerman, E., Slovin, H., Hildesheim, R. & Arieli, A., 1999. In-vivo optical imaging of cortical architecture and dynamics. *Modern techniques in*, (January).
Gurden, H., Uchida, N. & Mainen, Z.F., 2006. Sensory-Evoked Intrinsic Optical Signals in the Olfactory Bulb Are Coupled to Glutamate Release and Uptake. *Neuron*, 52(2), pp.335–345.
He, B.J., 2013. Spontaneous and Task-Evoked Brain Activity Negatively Interact. *Journal of Neuroscience*, 33(11), pp.4672–4682.
Heeger, D.J., Huk, A.C., Geisler, W.S. & Albrecht, D.G., 2000. Spikes versus BOLD: what does neuroimaging tell us about neuronal activity? *Nature Neuroscience*, 3(7), pp.631–633.
Heeger, D.J. & Ress, D., 2002. What does fMRI tell us about neuronal activity? *Nature Reviews Neuroscience*, 3(February), pp.142–151.
Hubel, D.H. & Wiesel, T.N., 1968. Receptive Fields and Functional Architecture of monkey striate cortex. *Journal of Physiology*, 195, pp.215–243.

Iadecola, C. & Nedergaard, M., 2007. Glial regulation of the cerebral microvasculature. *Nature neuroscience*, 10(11), pp.1369–76.
Jack, A.I., Shulman, G.L., Snyder, A.Z., McAvoy, M. & Corbetta, M., 2006. Separate Modulations of Human V1 Associated with Spatial Attention and Task Structure. *Neuron*, 51(1), pp.135–147.
Jezzard, P., Heineman, F., Taylor, J., DesPres, D., Wen, H., Balaban, R.S. & Turner, R., 1994. Comparison of EPI gradient-echo contrast changes in cat brain caused by respiratory challenges with direct simultaneous evaluation of cerebral oxygenation via a cranial window. *NMR in biomedicine*, 7(1-2), pp.35–44.
Josephs, O., Turner, R. & Friston, K.J., 1997. Event-related fMRI. *Human Brain Mapping*, 5(4), pp.243–248.
Joshi, S., Li, Y., Kalwani, R.M. & Gold, J.I., 2016. Relationships between Pupil Diameter and Neuronal Activity in the Locus Coeruleus , Colliculi , and Cingulate Cortex Article Relationships between Pupil Diameter and Neuronal Activity in the Locus Coeruleus , Colliculi , and Cingulate Cortex. *Neuron*, 89(1), pp.1–14.
Kahn, I., Desai, M., Knoblich, U., Bernstein, J., Henninger, M., Graybiel, A.M., Boyden, E.S., Buckner, R.L. & Moore, C.I., 2011. Characterization of the Functional MRI Response Temporal Linearity via Optical Control of Neocortical Pyramidal Neurons. *J Neurosci*, 31(42), pp.15086–15091.
Kahn, I., Knoblich, U., Desai, M., Bernstein, J., Graybiel, A.M., Boyden, E.S., Buckner, R.L. & Moore, C.I., 2013. Optogenetic drive of neocortical pyramidal neurons generates fMRI signals that are correlated with spiking activity. *Brain research*, 1511, pp.33–45.
Kalatsky, V.A. & Stryker, M.P., 2003. New paradigm for optical imaging: temporally encoded maps of intrinsic signal. *Neuron*, 38(4), pp.529–45.
Kalwani, R.M., Joshi, S. & Gold, J.I., 2014. Phasic Activation of Individual Neurons in the Locus Ceruleus/Subceruleus Complex of Monkeys Reflects Rewarded Decisions to Go But Not Stop. *Journal of Neuroscience*, 34(41), pp.13656–13669.
Kasischke, K.A., Vishwasrao, H.D., Fisher, P.J., Zipfel, W.R. & Webb, W.W., 2004. Neural activity triggers neuronal oxidative metabolism followed by astrocytic glycolysis. *Science*, 305(5680), pp.99–103.
Kastner, S., Pinsk, M. a., De Weerd, P., Desimone, R. & Ungerleider, L.G., 1999. Increased activity in human visual cortex during directed attention in the absence of visual stimulation. *Neuron*, 22(4), pp.751–761.
Kennerley, A.J., Berwick, J., Martindale, J., Johnston, D., Zheng, Y. & Mayhew, J.E., 2009. Refinement of optical imaging spectroscopy algorithms using concurrent BOLD and CBV fMRI. *NeuroImage*, 47(4), pp.1608–1619.
Knapen, T., Roelfsema, P., Vanduffel, W., Arsenault, J.T. & Donner, T.H., 2012. A negative fMRI response to reward in human visual cortex. In *Society for Neuroscience*. New Orleans, LA.

Kosofsky, B.E., Molliver, M.E., Morrison, J.H. & Foote, S.L., 1984. The serotonin and norepinephrine innervation of primary visual cortex in the cynomolgus monkey (Macaca fascicularis). *The Journal of comparative neurology*, 230(2), pp.168–78.

Krimer, L.S., Muly, E.C.I., Williams, G. V & Goldman-Rakic, P.S., 1998. Dopaminergic regulation of cerebral cortical microcirculation. *Nature neuroscience*, 1(4), pp.286–289.

Lacey, B.C. & Lacey, J.I., 1970. Some autonomic-central nervous system interrelationships. In P. Black, ed. *Physiological Correlates of Emotion*. New York and London: Academic Press, pp. 205–227.

Lacey, B.C. & Lacey, J.I., 1978. Two-way communication between the heart and the brain: Significance of time within the cardiac cycle. *American Psychologist*, 33(2), pp.99–113.

Lacroix, A., Toussay, X., Anenberg, E., Lecrux, C., Ferreirós, N., Karagiannis, A., Plaisier, F., Chausson, P., Jarlier, F., Burgess, S.A., Hillman, E.M.C., Tegeder, I., Murphy, T.H., Hamel, E. & Cauli, B., 2015. COX-2-Derived Prostaglandin E2 Produced by Pyramidal Neurons Contributes to Neurovascular Coupling in the Rodent Cerebral Cortex. *The Journal of neuroscience : the official journal of the Society for Neuroscience*, 35(34), pp.11791–810.

Larsson, J., Landy, M.S. & Heeger, D.J., 2006. Orientation-selective adaptation to first-and second-order patterns in human visual cortex. *Journal of Neurophysiology*, 95, pp.862–881.

Laughlin, S.B., de Ruyter van Steveninck, R.R. & Anderson, J.C., 1998. The metabolic cost of neural information. *Nature neuroscience*, 1(1), pp.36–41.

Lee, J.H., Durand, R., Gradinaru, V., Zhang, F., Goshen, I., Kim, D.-S., Fenno, L.E., Ramakrishnan, C. & Deisseroth, K., 2010. Global and local fMRI signals driven by neurons defined optogenetically by type and wiring. *Nature*, 465(7299), pp.788–792.

Lima, B., Cardoso, M.M.B., Sirotin, Y.B. & Das, A., 2014. Stimulus-Related Neuroimaging in Task-Engaged Subjects Is Best Predicted by Concurrent Spiking. *Journal of Neuroscience*, 34(42), pp.13878–13891.

Lima, B., Singer, W. & Neuenschwander, S., 2011. Gamma Responses Correlate with Temporal Expectation in Monkey Primary Visual Cortex. *Journal of Neuroscience*, 31(44), pp.15919–15931.

Livingstone, M.S. & Hubel, D.H., 1981. Effects of sleep and arousal on the processing of visual information in the cat. *Journal of Chemical Information and Modeling*, 291(5816), pp.554–61.

Llinás, R.R. & Steriade, M., 2006. Bursting of thalamic neurons and states of vigilance. *Journal of Neurophysiology*, 95(6), pp.3297–308.

Logothetis, N.K., 2008. What we can do and what we cannot do with fMRI. *Nature*, 453(7197), pp.869–878.

Logothetis, N.K., Pauls, J., Augath, M., Trinath, T. & Oeltermann, A., 2001. Neurophysiological investigation of the basis of the fMRI signal. *Nature*, 412(6843), pp.150–7.

Logothetis, N.K. & Wandell, B.A., 2004. Interpreting the BOLD Signal. *Annual Review of Physiology*, 66(1), pp.735–769.
Lu, H.D. & Roe, A.W., 2007. Optical imaging of contrast response in Macaque monkey V1 and V2. *Cerebral Cortex*, 17(11), pp.2675–2695.
Lucas, B.D. & Kanade, T., 1981. An iterative image registration technique with an application to stereo vision. *Proceedings of the 7th international joint Conference on Artificial Intelligence*, pp.674–679.
Luck, S.J., Chelazzi, L., Hillyard, S.A. & Desimone, R., 1997. Neural mechanisms of spatial selective attention in areas V1, V2, and V4 of macaque visual cortex. *Journal of neurophysiology*, 77(1), pp.24–42.
Madsen, M.T., 1992. A simplified formulation of the gamma variate function. *Physics in Medicine and Biology*, 37(7), pp.1597–1600.
Maier, A., Wilke, M., Aura, C., Zhu, C., Ye, F.Q. & Leopold, D.A., 2008. Divergence of fMRI and neural signals in V1 during perceptual suppression in the awake monkey. *Nature Neuroscience*, 11(10), pp.1193–1200.
Malmstrom, E.J., Opton, E. & Lazarus, R.S., 1965. Heart rate measurement and the correlation of indices of arousal. *Psychosomatic medicine*, 27(6), pp.546–556.
Mandeville, J.B., Jenkins, B.G., Kosofsky, B.E., Moskowitz, M.A., Rosen, B.R. & Marota, J.J.A., 2001. Regional sensitivity and coupling of BOLD, and CBV changes during stimulation of rat brain. *Magnetic Resonance in Medicine*, 45(3), pp.443–447.
Martin, C., Berwick, J., Johnston, D., Zheng, Y., Martindale, J., Port, M., Redgrave, P. & Mayhew, J.E., 2002. Optical imaging spectroscopy in the unanaesthetised rat. *Journal of neuroscience methods*, 120(1), pp.25–34.
Matsuda, K., Nagami, T., Kawano, K. & Yamane, S., 2000. A new system for measuring eye position on a personal computer. *Soc. Neurosci. Abstr*, 26, p.744.2.
Mayhew, J.E.W., Askew, S., Zheng, Y., Porrill, J., Westby, G.W.M., Redgrave, P., Rector, D.M. & Harper, R.M., 1996. Cerebral vasomotion: a 0.1-Hz oscillation in reflected light imaging of neural activity. *NeuroImage*, 4(3 Pt 1), pp.183–93.
Meister, M. & Bonhoeffer, T., 2001. Tuning and topography in an odor map on the rat olfactory bulb. *The Journal of neuroscience : the official journal of the Society for Neuroscience*, 21(4), pp.1351–1360.
Meng, M., Remus, D.A. & Tong, F., 2005. Filling-in of visual phantoms in the human brain. *Nature Neuroscience*, 8(9), pp.1248–1254.
Millett, D., 2001. Hans Berger: From Psychic Energy to the EEG. *Perspectives in Biology and Medicine*, 44(4), pp.522–542.
Minzenberg, M.J., Yoon, J.H. & Carter, C.S., 2011. Modafinil modulation of the default mode network. *Psychopharmacology*, 215(1), pp.23–31.
Mitra, P.P. & Bokil, H., 2008. *Observed brain dynamics.*, New York: Oxford University Press.
Moore, B., Cox, M.A., Dougherty, K., Young, M.S. & Maier, A., 2014.

Resting state correlations in visual cortex reflect fluctuations of cortical arousal. *Society for Neuroscience*, p.8.
Moran, J. & Desimone, R., 1985. Selective attention gates visual processing in the extrastriate cortex. *Science (New York, N.Y.)*, 229(4715), pp.782–784.
Mukamel, R., Gelbard, H., Arieli, A., Hasson, U., Fried, I. & Malach, R., 2005. Coupling Between Neuronal Firing, Field Potentials, and fMRI in Human Auditory Cortex. *Science*, 309(5736), pp.951–954.
Nemoto, M., Sheth, S.A., Guiou, M., Pouratian, N., Chen, J.W.Y. & Toga, A.W., 2004. Functional Signal- and Paradigm-Dependent Linear Relationships between Synaptic Activity and Hemodynamic Responses in Rat Somatosensory Cortex. *Journal of Neuroscience*, 24(15), pp.3850–3861.
Niessing, J., Ebisch, B., Schmidt, K.E., Niessing, M., Singer, W. & Galuske, R. a W., 2005. Hemodynamic signals correlate tightly with synchronized gamma oscillations. *Science*, 309(5736), pp.948–51.
O'Connell, M.N., Barczak, A., Ross, D., McGinnis, T., Schroeder, C.E. & Lakatos, P., 2015. Multi-Scale Entrainment of Coupled Neuronal Oscillations in Primary Auditory Cortex. *Frontiers in human neuroscience*, 9(December), p.655.
Ogawa, S., Lee, T.M., Kay, A.R. & Tank, D.W., 1990. Brain magnetic resonance imaging with contrast dependent on blood oxygenation. *Proc. Natl. Acad. Sci. USA*, 87(24), pp.9868–72.
Otazu, G.H., Tai, L.-H., Yang, Y. & Zador, A.M., 2009. Engaging in an auditory task suppresses responses in auditory cortex. *Nature neuroscience*, 12(5), pp.646–54.
Paukert, M., Agarwal, A., Cha, J., Doze, V.A., Kang, J.U. & Bergles, D.E., 2014. Norepinephrine controls astroglial responsiveness to local circuit activity. *Neuron*, 82(6), pp.1263–1270.
Pestilli, F., Carrasco, M., Heeger, D.J. & Gardner, J.L., 2011. Attentional Enhancement via Selection and Pooling of Early Sensory Responses in Human Visual Cortex. *Neuron*, 72(5), pp.832–846.
Pfefferbaum, A., Chanraud, S., Pitel, A.L., Muller-Oehring, E., Shankaranarayanan, A., Alsop, D.C., Rohlfing, T. & Sullivan, E. V, 2011. Cerebral blood flow in posterior cortical nodes of the default mode network decreases with task engagement but remains higher than in most brain regions. *Cerebral Cortex*, 21(1), pp.233–244.
Pisauro, M.A., Benucci, A. & Carandini, M., 2016. Local and global contributions to hemodynamic activity in mouse cortex. *Journal of neurophysiology*.
Prichard, J., Rothman, D., Novotny, E., Petroff, O., Kuwabara, T., Avison, M., Howseman, A., Hanstock, C. & Shulman, R., 1991. Lactate rise detected by 1H NMR in human visual cortex during physiologic stimulation. *Proceedings of the National Academy of Sciences of the United States of America*, 88, pp.5829–31.
Raichle, M.E., 1979. Quantitative in vivo autoradiography with positron

emission tomography. *Brain Research Reviews*, 1, pp.47–68.
Raichle, M.E., MacLeod, A.M., Snyder, A.Z., Powers, W.J., Gusnard, D.A. & Shulman, G.L., 2001. A default mode of brain function. *Proceedings of the National Academy of Sciences of the United States of America*, 98(2), pp.676–82.
Raichle, M.E. & Shepherd, G.M., 2014. *Angelo Mosso's Circulation of blood in the human brain.*, Oxford University Press.
Rees, G., Friston, K.J. & Koch, C., 2000. A direct quantitative relationship between the functional properties of human and macaque V5. *Nature neuroscience*, 3(7), pp.716–23.
Reimer, J., Froudarakis, E., Cadwell, C.R., Yatsenko, D., Denfield, G.H. & Tolias, A.S., 2014. Pupil Fluctuations Track Fast Switching of Cortical States during Quiet Wakefulness. *Neuron*, 84(2), pp.355–362.
Ress, D., Backus, B.T. & Heeger, D.J., 2000. Activity in primary visual cortex predicts performance in a visual detection task. *Nature neuroscience*, 3(9), pp.940–5.
Ress, D. & Heeger, D.J., 2003. Neuronal correlates of perception in early visual cortex. *Nature neuroscience*, 6(4), pp.414–20.
Ress, D., Thompson, J.K., Rokers, B., Khan, R.K. & Huk, A.C., 2009. A model for transient oxygen delivery in cerebral cortex. *Frontiers in neuroenergetics*, 1(June), p.3.
Ritchie, J.M., 1967. The oxygen consumption of mammalian non-myelinated nerve fibres at rest and during activity. *J Physiol*, 188(3), pp.309–329.
Saltzberg, B., Lustick, L.S. & Heath, R.G., 1971. Detection of focal depth spiking in the scalp EEG of monkeys. *Electroencephalography and Clinical Neurophysiology*, 31, pp.327–333.
Scott, N.A. & Murphy, T.H., 2012. Hemodynamic responses evoked by neuronal stimulation via channelrhodopsin-2 can be independent of intracortical glutamatergic synaptic transmission. *PLoS ONE*, 7(1), pp.1–10.
Serences, J.T., 2008. Value-Based Modulations in Human Visual Cortex. *Neuron*, 60(6), pp.1169–1181.
Serences, J.T., Yantis, S., Culberson, A. & Awh, E., 2004. Preparatory Activity in Visual Cortex Indexes Distractor Suppression During Covert Spatial Orienting. *The Journal of Neurophysiology*, 92, pp.3538–3545.
Sheth, S.A., Nemoto, M., Guiou, M., Walker, M.A., Pouratian, N. & Toga, A.W., 2004. Linear and nonlinear relationships between neuronal activity, oxygen metabolism, and hemodynamic responses. *Neuron*, 42(2), pp.347–55.
Shibuki, K., Hishida, R., Murakami, H., Kudoh, M., Kawaguchi, T., Watanabe, M., Watanabe, S., Kouuchi, T. & Tanaka, R., 2003. Dynamic imaging of somatosensory cortical activity in the rat visualized by flavoprotein autofluorescence. *The Journal of physiology*, 549(Pt 3), pp.919–27.
Shtoyerman, E., Arieli, A., Slovin, H., Vanzetta, I. & Grinvald, A., 2000. Long-term optical imaging and spectroscopy reveal mechanisms

underlying the intrinsic signal and stability of cortical maps in V1 of behaving monkeys. *The Journal of neuroscience : the official journal of the Society for Neuroscience*, 20(21), pp.8111–8121.
Shuler, M.G.H. & Bear, M.F., 2006. Reward timing in the primary visual cortex. *Science*, 311(5767), pp.1606–1609.
Shulman, G.L., Mcavoy, M.P., Cowan, M.C., Astafiev, S. V, Tansy, A.P., Avossa, G. & Corbetta, M., 2003. Quantitative Analysis of Attention and Detection Signals During Visual Search. *Journal of Neurophysiology*, (August 2003), pp.3384–3397.
Sillito, A.M., 1986. Cholinergic input and plasticity? *Nature*, 320, pp.109–110.
Silver, M.A., Ress, D. & Heeger, D.J., 2007. Neural correlates of sustained spatial attention in human early visual cortex. *Journal of neurophysiology*, 97(1), pp.229–37.
Sirotin, Y.B., Cardoso, M., Lima, B. & Das, A., 2012. Spatial homogeneity and task-synchrony of the trial-related hemodynamic signal. *NeuroImage*, 59(3), pp.2783–2797.
Sirotin, Y.B. & Das, A., 2009. Anticipatory haemodynamic signals in sensory cortex not predicted by local neuronal activity. *Nature*, 457(7228), pp.475–479.
Sirotin, Y.B. & Das, A., 2010a. How Well does Local Neuronal Activity Predict Cortical Hemodynamics? In *CoSYNE*. COSYNE.
Sirotin, Y.B. & Das, A., 2010b. Spatial Relationship between Flavoprotein Fluorescence and the Hemodynamic Response in the Primary Visual Cortex of Alert Macaque Monkeys. *Frontiers in neuroenergetics*, 2(June), p.6.
Sirotin, Y.B., Hillman, E.M.C., Bordier, C. & Das, A., 2009. Spatiotemporal precision and hemodynamic mechanism of optical point spreads in alert primates. *Proc. Natl. Acad. Sci. USA*, 106(43), pp.6–11.
Sokoloff, L., Reivich, M., Kennedy, C., Des Rosiers, M.H., Patlak, C.S., Pettigrew, K.D., Sakurada, O. & Shinohara, M., 1977. The [14 C] deoxyglucose method for the measurement of local cerebral glucose utilization: theory, procedure, and normal values in the conscious and anesthetized albino rat. *Journal of Neurochemistry*, 28, pp.897–916.
Somers, D.C., Dale, A.M., Seiffert, A.E. & Tootell, R.B.H., 1999. Functional MRI reveals spatially specific attentional modulation in human primary visual cortex. *Proceedings of the National Academy of Sciences of the United States of America*, 96(4), pp.1663–8.
Sylvester, C.M., Shulman, G.L., Jack, A.I. & Corbetta, M., 2007. Asymmetry of anticipatory activity in visual cortex predicts the locus of attention and perception. *The Journal of neuroscience : the official journal of the Society for Neuroscience*, 27(52), pp.14424–33.
Thomson, D.J., 1982. Spectrum estimation and harmonic analysis. *Proceedings of the IEEE*, 70(9), pp.1055–1096.
Tootell, R.B.H., Hadjikhani, N., Hall, E.K., Marrett, S., Vanduffel, W., Vaughan, J.T. & Dale, A.M., 1998. The retinotopy of visual spatial

attention. *Neuron*, 21(6), pp.1409–22.
Usher, M., Cohen, J.D., Servan-Schreiber, D., Rajkowski, J. & Aston-Jones, G., 1999. The Role of Locus Coeruleus in the Regulation of Cognitive Performance. *Science*, 283(5401), pp.549–554.
Vinck, M., Batista-Brito, R., Knoblich, U. & Cardin, J.A., 2015. Arousal and Locomotion Make Distinct Contributions to Cortical Activity Patterns and Visual Encoding. *Neuron*, 86(3), pp.740–754.
Weber, B., Burger, C., Wyss, M.T., von Schulthess, G.K., Scheffold, F. & Buck, A., 2004. Optical imaging of the spatiotemporal dynamics of cerebral blood flow and oxidative metabolism in the rat barrel cortex. *The European journal of neuroscience*, 20(10), pp.2664–70.
Woody, C.D., Gruen, E. & Wang, X.F., 2003. Electrical properties affecting discharge of units of the mid and posterolateral thalamus of conscious cats. *Neuroscience*, 122(2), pp.531–539.
Zhao, F., Welsh, D., Williams, M., Coimbra, A., Urban, M.O., Hargreaves, R., Evelhoch, J. & Williams, D.S., 2012. fMRI of pain processing in the brain: a within-animal comparative study of BOLD vs. CBV and noxious electrical vs. noxious mechanical stimulation in rat. *NeuroImage*, 59(2), pp.1168–79.
Zijlstra, W.G. & Buursma, A., 1997. Spectrophotometry of Hemoglobin : Absorption Spectra of Bovine Oxyhemoglobin , Deoxyhemoglobin , Carboxyhemoglobin , and Methemoglobin. *Comparative Biochemistry and Physiology*, 118(4), pp.743–749.

ITQB-UNL | Av. da República, 2780-157 Oeiras, Portugal
Tel (+351) 214 469 100 | Fax (+351) 214 411 277

www.itqb.unl.pt